UNIVERSITY OF SOUTHAMPTON

The Dynamical Controls on the Antarctic Circumpolar Current with the use of General Circulation Models

Anita Grezio

Submitted for the Degree of Doctor of Philosophy

School of Ocean and Earth Sciences

May 2002

UNIVERSITY OF SOUTHAMPTON

ABSTRACT

FACULTY OF SCIENCE

School of Ocean and Earth Sciences

Doctor of Philosophy

The Dynamical Controls on the Antarctic Circumpolar Current, with the use of General Circulation Models

by Anita GREZIO

Three general circulation models (FRAM, OCCAM and POP) are used in order to investigate the dynamics of the Antarctic Circumpolar Current (ACC) at the Drake Passage latitudes (ACCB) where the ACC is unbounded. In these models bottom form stress balances the wind stress in the momentum budgets. In the vorticity budgets the main balance is between wind curl and bottom pressure torque in FRAM and OCCAM. In the higher resolution model (POP) the non linear advection is one of the main terms. Whereas standing eddies mainly decelerate the flow in the ACCB, transient eddies play a different role in the three models. In the upper levels transient eddies accelerate the flow in POP and FRAM, but decelerate the flow in OCCAM. The behaviour of standing and transient eddies changes throughout the water column in the ACCB and eddies have a dragging effect on the flow below the levels where the topography starts to obstruct the flow. The crucial role of topography is investigated using a set of numerical experiment. In the coarse version of OCCAM Kerguelen Plateau is lowered and the Drake Passage Region and the Antarctic-Pacific Ridge are removed. Results from the analysis in the ACCB indicate that changing topography has a local effect. The complete investigation of the ACC dynamics is extended to the ACC Path (ACCP). The vorticity budgets show that the Drake Passage Region affects all of the ACC flow. Removing Drake Passage reduces the contribution of the bottom pressure torque to the vorticity balance and the region of Sverdrup-like balance is extended. The key role for all the ACC is played by the Drake Passage but not from other topographic features.

Acknowledgements

I wish to thank my supervisor Dr. Neil Wells for his guidance which allowed me to have the freedom of exploring the subject of my thesis and learning during this research. I also wish to thank Prof. Jochem Marotzke and Dr. Kelvin Richards for the helpful advices and discussions during our advisory panel meetings. Moreover, I am very grateful to Prof. Jochem Marotzke for the encouragement during the period of the OCCAM runs.

Special thanks to Dr. Vladimir Ivchenko and Dr. David Webb for the valuable suggestions and helpful discussions on the general circulation models and the Southern Ocean dynamics.

I wish to express my thanks to Prof. Peter Killworth, Dr. Jeff Blundel and Dr. Paolo Cipollini for the discussions on the planetary waves and the ACC dynamics.

My gratitude goes also to Mrs. Beverly deCuevas and Dr. Andrew Coward for their precious support using OCCAM and FRAM models, and to Dr. Robert Malone for providing the POP model data.

All the words that I have in my mind seem to be inadequate to thank my friends in Southampton and Alessio. They were wonderful in trying to keep me smiling during the dark moments of the PhD student's life.

Finally, I am most grateful to the European Union, who funded my PhD project and my training with a TMR Marie Curie Grant (Nr ERBFMBICT972863).

Contents

List of Tables

List of Figures

List of Abbreviations

AABW	Antarctic Bottom Water
ACC	Antarctic Circumpolar Current
ACCB	Antarctic Circumpolar Belt
ACCP	Antarctic Circumpolar Path
CDW	Circumpolar Deep Water
ECMWF	European Centre for Medium Range Weather Forecasting
FRAM	Fine Resolution Antarctic Model
GM	Gent and McWilliams (1990) parameterization
KE	Kinetic Energy
H-R	Hellerman and Rosenstein (1983)
NADW	North Atlantic Deep Water
OCCAM	Ocean and Climate Circulation Advanced Model
OGCMs	Ocean General Circulation Models
PE	Primitive Equation
POP	Parallel Ocean Program
QG	Quasi-Geostrophic
RHSM	Right Hand Side of Momentum
RHSV	Right Hand Side of Vorticity

Chapter 1

Introduction

1.1 Motivation

The Antarctic Circumpolar Current (ACC) connects the three major oceans and dynamical and thermodynamical balances in the ACC are linked to the global ocean circulation. This interbasin connection occurs in the belt where the ACC flows zonally with no continental barriers (Antarctic Circumpolar Belt - ACCB) at the Drake Passage latitudes.

One of the main questions about the ACC dynamics is how the strong input of momentum at the surface is transferred downward and dissipated. Model investigations without topography considering a standard diffusive momentum parameterisation and bottom friction give unreasonable volume transport at the Drake Passage (Hidaka and Tsuchiya (1953), Gill (1968)). In these cases eddy coefficients should be two orders of magnitude bigger than the observed values in the Southern Ocean in order to fit the model transport to the observed transport. On the other hand, the large effect of the topography on the ACC was argued

since 1951 by Munk and Palmén. They affirmed that the momentum input at the surface is transferred down the water column by turbulent interchange of momentum from the surface layer to the layers beneath and removed by bottom form stress. Bottom form stress is considered the main sink of momentum in the ACC and it is induced by the pressure exerted by the submarine ridges against the deep flow.

Quasi-Geostrophic models (QG models) have been largely employed in the ACC dynamics investigations in order to explore a circumpolar current in a zonal channel on the β-plane with eddies and topographic constraints (McWilliams et al. (1978), McWilliams and Chow (1981), Wolff and Olbers (1989) and Wolff et al. (1991)). QG models pointed out that eddies transferred momentum downward through the action of the interfacial form stress and were dissipated by bottom form stress. Bottom topography increased momentum dissipation through bottom form stress and reduced the total transport in the channel with respect to the flat bottom case.

However, QG models do not resolve adequately topography because they cannot represent steep topography and a realistic amplitude of topography compared with the total ocean depth. Moreover, QG models do not consider the outcropping of isopycnic surfaces in the Southern Ocean.

On the contrary, Primitive Equation models (PE models) do not have those problems but their resolution has to be able to display topographic forms and eddies (Killworth and Nanneh (1994)).

Recently, Stevens and Ivchenko (1997) have demonstrated that the vertical penetration of momentum is achieved through the action of the interfacial form stress, which is provided by eddies, in a PE model (FRAM). However, the role of eddies

on the horizontal redistribution of zonal momentum is still controversial both in observations and in models. In QG models eddies are acting to accelerate the jet centre and decelerate the wings (McWilliams et al. (1978), McWilliams and Chow (1981), Treguier and McWilliams (1990), Wolff et al. (1991) and Marshall et al. (1993)). In FRAM transient eddies accelerated the flow in a zonal analysis (Stevens and Ivchenko (1997)) as it was for QG models but transient eddies decelerated the flow in streamwise co-ordinates (Ivchenko et al. (1996)). In a recent observational study Hughes and Ash (2001) found that the strongest jets in the ACC are not accelerated but decelerated by eddies in satellite altimeter measurements, in contradiction to Morrow et al. (1992). Moreover, Hughes and Ash (2001) found that the continuous presence of fronts from satellite altimeter measurements is not reproduced by ACC models. They indicate that inadequate resolution and representation of topography can be the cause of the poor representation of eddy activity in these models.

It is well known that the ACC is the strongest current in the world having a volume transport of about 126 Sv through the Drake Passage (Whitworth and Peterson (1985)). The strongest winds in the world blow over the Southern Ocean at the Drake Passage latitudes and they are three orders of magnitude larger than the mid latitude winds (Gille et al. (2001)). However, the ACC dynamics in this region is still not fully understood. Part of the ACC flows in the unique rotating channel in the global ocean. The traditional Sverdrup theory and geostrophy which are valid in all oceans do not hold there. More investigations are required on the ACC dynamics using models.

1.2 Aim and Objectives

The aim of this research is to understand the main mechanisms that control the ACC dynamics with the use of OGCMs. The scientific questions addressed in this study are:

- What are the dynamical controls on the ACC dynamics?
- What is the role of topography in the ACC dynamics?

In particular we investigate the role of eddies and non-linear terms in the dynamical budgets in the barrier-free belt around the Antarctica (ACCB), whether eddies accelerate or decelerate the flow in the ACCB as a whole, what is their variation across the zonal belt and what is their variation with the depth. Moreover, we investigate how increasing model resolution can affect the volume transport, momentum and vorticity budgets in the ACCB. The investigation is carried out using a set of PE models (FRAM, OCCAM 1/4 and POP). FRAM, OCCAM 1/4 and POP are OGCMs which are able to display eddies. They are different not only because of resolution but also because of forcing and topography. Consequently, the three models represent differently the ACC volume transport and the ACC flow.

The model comparison in the ACCB outlines the importance of topography in the ACC. Only a narrow part of the ACC flows in a belt and in order to investigate the role of topography in the ACC a set of numerical experiments needs to be performed with a coarse model. A complete investigation of the ACC dynamics is carried out in the ACCP. The ACCP is the region in the Southern Ocean which is between the streamfunctions passing through the Drake Passage.

Chapter 2

Dynamics of the ACC

2.1 Introduction

The vastness of the Southern Ocean and the hard atmospheric and oceanic conditions there have made the ocean models one of the most powerful way to study the complexity of the ACC dynamics.

2.2 Studies of the ACC dynamics using models

Coarse resolution models and one-layer models can give a rough but interesting view of the ACC main flow and the effect of the Drake Passage on the flow. Gill and Bryan (1971) investigated the extension and the friction parameters of the zone downstream the Drake Passage. In their model they explored the importance of the Drake Passage threshold on the ACC transport and the importance of the horizontal density gradient West and East of the Drake Passage. They found that

the presence of the Drake Passage sill reduced the ACC volume transport but the horizontal density gradients at the Drake Passage accelerated the ACC flow. Many authors examined barotropic circulation in rotating channels with simple topography. Krupitsky and Cane (1994) focused their work on f/H isolines that are blocked by zonal walls in a zonal channel. It is well known that streamlines of the zonal current tend to follow lines of constant f/H. If the topography was small enough, then there were closed f/H isolines encircling Antarctica and a rather large transport. If the f/H isolines were blocked by zonal walls then the zonal transport was proportional to the bottom topographic wave length and inversely proportional to the topographic height. The momentum input was balanced by bottom form stress. Wang and Huang (1995) tried to quantify a parameter called potential vorticity resistance. It was introduced to quantify the degree by which the ridge impedes the through-channel flow. This parameter represents the minimum amount of potential vorticity that a fluid particle has to exchange with its environment in order to cross the ridge. The transport decreased with the increase of this parameter. The parameter was also related to the height of a ridge and they indicated that the Drake passage plays a central role in the circumpolar ocean while other topographic features play a secondary role. In his model Klinck (1986) concluded that the lateral boundaries of the Southern Ocean cause the flow to act more like an inviscid Sverdrup flow rather than like the strongly viscous flow considered by Hidaka and Tsuchiya (1953).

From recent studies it has been noted that the ACC flow has an equivalent barotropic character. Killworth (1992) found that the mean flow and the eddy kinetic energy are self-similar in the vertical in the FRAM model. Ivchenko et al. (1999) compared FRAM with an Equivalent Barotropic model and they showed

that the transport streamfunction patterns were similar in both models.

QG models have been largely employed in the ACC dynamics investigations. QG models were mainly directed to explore a circumpolar current in a zonal channel on the β-plane with eddies and topographic constraints. McWilliams et al. (1978), McWilliams and Chow (1981), Wolff and Olbers (1989) and Wolff et al. (1991) allowed dynamical flow instabilities that created eddies in their models. Eddies transferred momentum downward and were dissipated by bottom form stress. Bottom topography increased momentum dissipation through bottom form stress and reduced the total transport in the channel with respect to the flat bottom case. In all cases bottom friction presented small values. Johnson and Bryden (1989) studied the interfacial form drag that causes a vertical flux of zonal momentum from the upper layers to the lower layers. The importance of the interfacial form drag was pointed out also by Olbers and Wubber (1991), Olbers (1998) and Stevens and Ivchenko (1997) using PE models.

2.3 The role of eddies in the ACC

Eddies play a crucial role in the dynamics of the Southern Ocean. They transfer momentum downward and heat from the Equator to the Pole. Eddies in the Southern Ocean have typical velocities of 30 cm s^{-1} or greater at the surface and length scales of 30-100 km. In the Southern Ocean eddies are coherent formations from the surface to the bottom. Bryden and Heath (1985) found energetic eddies of 20 cm s^{-1} at 1000 m with time scales of 20-50 days. To the south east of New Zealand the eddies extended vertically to 5000 m and propagated south-eastward

at about 12 cm s^{-1}. The related eddy kinetic energy decreases from 169 cm^2 s^{-2} at 1000 m to 30 cm^{-2} s^{-2} at 4000 m.

These energetic eddies are produced by fluctuations of the mean flow, mostly in the Sub-Antarctic Front and in the Polar Front which are eddy generating regions over their entire length. A large amount of mesoscale variability in the ACC is related with the zonation, but the higher mesoscale variability is associated with areas of major topographic relief. The maximum eddy kinetic energy is found to correspond to major topographic features (Patterson (1985)). The eddy kinetic energy is mainly due to the fluctuations of the geostrophic flow having periods less than one month.

Johnson and Bryden (1989) found that the wind driven zonal momentum is carried down by eddy processes to a depth, where it can be removed by bottom pressure differences across ridges. In this model the eddy form drag results from a poleward transport of the heat by eddies originating from the baroclinically unstable current. McWilliams et al. (1978) considered eddies generated by baroclinic instability of the mean flow. Eddies intensified the mean jet and transferred down mean zonal momentum through the eddy standing and transient interfacial form stress. The major sink was bottom form stress rather than bottom friction in presence of a large topographic barrier. Turbulent eddies were in phase at all depths and the westward propagation was due primarily to advection by zonal jet. Eddies acted to spatially concentrate and accelerate the mean jet, with the greatest effect in the shallowest layer (McWilliams and Chow (1981)).

Realistic topography in the Maquarie Ridge region was added by Wolff et al. (1991) in a QG model. This case summed up the previous cases, in particular the interfacial form drag was mainly caused by standing eddies and the jet

intensification by transient eddies. Wolff et al. (1992) found that the main balance in momentum was between the wind stress and the bottom form stress. A strong contribution was carried out also by the divergence of Reynolds stress (standing more than transient). Marshall et al. (1993) found that transient eddies transferred potential vorticity northward across the time mean axis of the ACC. Treguier and McWilliams (1990) examined the statistics of the eddies in particular their penetration and correlation with the topographic field, finding a correlation between the interfacial form drag and the bottom form stress. In that case standing eddies rather than transient eddies transferred momentum downward. Stevens and Ivchenko (1997) found that the standing and transient eddies redistribute zonal momentum horizontally, decelerating the flow in some regions but accelerating it in others. Also isopycnal analysis (Killworth and Nanneh (1994)) has shown that eddies transport eastward momentum from the upper layers to the lower layers.

It seems clear that eddies are the mechanism that transfers the wind stress momentum from the surface to the bottom. However, their role is controversial. Standing eddies decelerate the main flow in a zonal analysis. The transient eddies accelerate the flow in zonal analysis (Stevens and Ivchenko (1997)) and decelerate it in streamwise co-ordinates of PE models (Ivchenko et al. (1996)). Hence, more investigations are necessary using PE models.

2.4 The role of topography in the ACC

In a QG model with the topography and the eddies McWilliams et al. (1978) and McWilliams and Chow (1981) found that the wind stress was source of eastward momentum, interfacial form drag was a sink for the upper layer and a source for the lower layer. In the depth integrated momentum budget calculated by McWilliams et al. (1978) the wind stress was the source and the bottom form stress was the sink.

Wolff and Olbers (1989) performed a set of experiments changing the bottom stress parameter and topography. They also calculated the depth integrated momentum budget and they found that the main sink was the bottom stress only when: a) the topography was far from the latitudes of highest winds or b) the frictional parameter was very high. In the other cases the input of the eastward momentum by the wind stress into the upper layer was transferred to the lower layer by the interfacial form drag, which was set by eddies, and dissipated by the bottom form stress against the topography. The divergence of horizontal Reynolds stresses redistributed zonal momentum in the horizontal direction. Also Treguier and McWilliams (1990) found that in a flat bottom case the bottom stress was the only efficient sink of eastward momentum. When topography was present the bottom form stress was the sink in the momentum budget and largely decreased the zonal transport. Large scale topography (of the scale of forcing) provides largest bottom form stress. Topographic scales larger than the internal Rossby radius affected the whole water column and in this case the interfaces were deformed by standing eddies. Standing eddies replaced transient eddies in transferring momentum downward. Even low topography (about 200 m) generated large bottom

form stress and replaced bottom stress in the momentum budget in that QG model. In the seamount case flow went around the seamount but in the ridge case the flow was blocked. Also a meridional ridge affected the transport more than a seamount of limited latitudinal extension.

In FRAM Killworth and Nanneh (1994) calculated the momentum budget along the isopycnic surfaces. In this analysis the form drag varied with the depth and increased with the density in a roughly linear fashion until the bottom was reached.

2.5 ACC Volume transport at the Drake Passage

The volume transport of the ACC at the Drake Passage was monitored during ISOS Experiment in the 1980's and the observed values are 126 $\pm$ 10 Sv. Recently, Cunningham (2001) pointed out that the ISOS measurements underestimate the error and the ACC volume transport is 134 $\pm$ 27 Sv. A minimum transport is reached in Winter (June-July) and a second minimum in Summer (January) is evident in most years. Two higher values are reached in Spring (October) and Autumn (April-May). Whitworth (1983) calculated that the 70% of net transport is due to the baroclinic component of the velocity but the higher frequency fluctuations occur in the barotropic mode. The fluctuations in the transport come from shifts of the Sub-Antarctic Front. When warm water flow extends to the North part of the Drake Passage the Sub-Antarctic Front moves southward and the transport increases. Whitworth and Peterson (1985) found that transport fluctuations, which approached 50% of the mean transport, occurred over intervals of

less than a month. In addition, the changes in transport through the Drake Passage over a period of order a month or less appear to be forced also by changes in the circumpolar averaged wind stress, rather than the local wind stress. Analysis by Wearn and Baker (1980) argue that the ACC transport through the Drake Passage represents the entire circumpolar system. Those wind-driven fluctuations in the ACC are barotropic and the circumpolar averaged current lags the zonally averaged wind stress by 9 days. Clarke (1982) indicates that significant wind driven fluctuations in the strength of the baroclinic ACC can only occur with periods of 70 years.

Stommel (1957) observed that only a narrow band of the ACC flows in a zonal channel and the ACC connects all oceans but it is not a completely zonal current. The ACC shifts northward by 10 degrees in the western South Atlantic Ocean. In fact, it flows in a channel only at the Drake Passage latitudes. He suggested that most of the flow in Southern Ocean is dominated by a Sverdrup dynamics. He explained that the viscous dissipation takes place in a western boundary current that exists along land boundary and in the Southern Ocean the principal dissipation occurs downstream the Drake Passage along the South America coast. In this region the water turns northward, as a western boundary current, before flowing east again near 40 S. Baker (1982) affirmed that in this region the water going northward balances the water driven southward at 55 S in the sector which excludes the Drake Passage region (between 40 W and 70 W). He calculated the Sverdrup balance using the available observed wind curl (Taylor (1978)) and velocity values (Gordon et al. (1978)) at 55 S in the sector. He found an agreement in these analysis and concluded that the southward open ocean geostrophic flow balances the transport through the Drake Passage but with a large error in his

calculations.

The problem of a sverdrupian ACC flow depending on the wind curl at the northern latitude of the ACCB following Stommel (1957) and Baker (1982) provoked a debate by Warren et al. (1996), Hughes (1997), Warren et al. (1997), Olbers (1998) and Warren et al. (1998). Recently Gnanadesikan and Hallberg (2000) and Gent et al. (2001) addressed the problem on what sets the mean transport through the Drake Passage. Gnanadesikan and Hallberg (2000) analysed the dependence of the ACC transport on the wind stress within the latitudes of Drake Passage and on the wind curl at the northern and southern latitudes of the ACCB. They conclude that increasing the strength of the winds can change the thermodynamic balances and increase the ACC transport. On the other hand, they did not find any evidence that the ACC transport is affected by changing wind curl. Gent et al. (2001) find that eddy activity and southward velocities in the intermediate layers (layers below the Ekman layer and above topography) are two important factors in setting the ACC transport. When the parameterised magnitude of eddy activity in their model was doubled then the ACC transport decreased about 30%. The intermediate layers were the most effective at accelerating the ACC and a small increase in southward velocity produced an increase in the strength of the ACC. Moreover, they considered the thermohaline circulation effects and indicated that an increase in the overturning of 1 Sv causes an increase of ACC transport of 7 Sv. From their study Drake Passage transport is not set solely by Sverdrup transport at the South Antarctic tip for two reasons. Firstly, in their model not all the flow through Drake Passage turns north as the Malvinas Current. Secondly, the ACC flow is blocked only by the bottom in the region where there is lack of land boundaries.

Gille et al. (2001) show using observational data that ACC transport and wind forcing are coherent over a broad range of frequencies. In contrast, ACC transport lags wind curl suggesting that the ocean response is not governed by simple sverdrup dynamics.

Chapter 3

FRAM, OCCAM and POP models

3.1 Introduction

The following sections present the OGCMs used in this study. They are different because of resolution, forcing and boundary conditions and the main characteristic of the models are summarised in Table 3.1. They are based on the Primitive Equations of the motion:

$$\frac{\partial \mathbf{u}}{\partial t} + (\mathbf{u} \cdot \nabla)\mathbf{u} + w\frac{\partial \mathbf{u}}{\partial z} + f\mathbf{k} \times \mathbf{u} = -\frac{1}{\rho_0}\nabla p + \mathbf{d_u} + \mathbf{f_u} \tag{3.1}$$

$$\frac{\partial S}{\partial t} + (\mathbf{u} \cdot \nabla)S + w\frac{\partial S}{\partial z} = d_S + f_S \tag{3.2}$$

$$\frac{\partial T}{\partial t} + (\mathbf{u} \cdot \nabla)T + w\frac{\partial T}{\partial z} = d_T + f_T \tag{3.3}$$

$$\rho g = -\frac{\partial p}{\partial z} \tag{3.4}$$

$$\nabla \cdot \mathbf{u} + \frac{\partial w}{\partial z} = 0 \tag{3.5}$$

$$\rho = \rho(T, S, p) \tag{3.6}$$

where $\mathbf{u}$ is horizontal velocity vector (u, v) and w vertical velocity, t is the time, z is depth, f is the Coriolis parameter ($f = 2\Omega \sin\varphi$, φ is the latitude and Ω is the speed of angular rotation of the Earth), p is pressure, $\mathbf{d_u}$ represents the horizontal mixing of momentum and $\mathbf{f_u}$ represents the vertical mixing of momentum, ρ_0 is the reference density, S and T are salinity and temperature, ∇ is the horizontal gradient operator, d_S and d_T represents the horizontal diffusivity of tracers and f_S and f_T represents the vertical diffusivity of tracers.

The term $\mathbf{d_u} = (d^\lambda, d^\varphi)$ has the following expression $d^\lambda = A_m(\nabla^2 u + (1 - \tan^2\varphi)\, u/a^2 - 2v_\lambda \tan\varphi/a^2\cos\varphi)$ and $d^\phi = A_m(\nabla^2 v + (1 - \tan^2\varphi)v/a^2 + 2u_\lambda \tan\varphi/a^2\cos\varphi)$, where A_m is the horizontal viscosity coefficient.

The term $\mathbf{f_u} = (f^\lambda, f^\varphi)$ has the following expression $f^\lambda = K_m \frac{\partial^2 u}{\partial z^2}$ and $f^\varphi = K_m \frac{\partial^2 v}{\partial z^2}$ where K_m is the vertical viscosity coefficient.

A_h is the horizontal diffusivity coefficient in $d_S = A_h \nabla^2 S$ and $d_T = A_h \nabla^2 T$.

K_h is the vertical diffusivity coefficient in $f_S = K_h \frac{\partial^2 S}{\partial z^2}$ and $f_T = K_h \frac{\partial^2 T}{\partial z^2}$.

3.2 Fine Resolution Antarctic Model (FRAM)

Fine Resolution Antarctic Model (FRAM) is based on the Geophysical Fluid Dynamics Laboratory Model using Bryan-Cox-Semtner code (Bryan (1969), Semtner (1974), Cox (1984)). It is an eddy-permitting model of the Southern Ocean covering the region from 78 S to 23 S (FRAM-Group (1991)). The horizontal resolution is 0.5 long. $\times$ 0.25 lat. and at 60 S the grid size is 27.8 $\times$ 27.8 km. The vertical resolution is 32 levels and the depth levels span from 20 m at the surface to 230 m at the bottom level. The topography dataset is DBDB5. The formulation of barotropic-mode equation (rigid lid condition) is applied. In order to increase the numerical stability the bottom topography is smoothed at 1 degree. The northern boundary is an open boundary (Stevens (1990) and Stevens (1991)) which uses the Sverdrup balance to specify the stream function. Horizontal mixing of momentum and tracers are obtained by a combination of harmonical and biharmonical operators. The horizontal mixing coefficient of momentum was $2 \times 10^2 m^2 s^{-1}$. The bottom friction is quadratic in the last 6 years run. The model was initialised as a cold ($2^o C$), saline (36.69 ppu), motionless fluid, and the temperature and salinity fields dynamically relaxed to the Levitus (1982) data. During the first 2 years and 160 days, the relaxation time scales are 180 days for the top 140 m and 540 days for the deeper levels. From that time up to 6 years the time scale is 360 days throughout; after 6 years the model ran freely from relaxation terms for a total time of integration of 16 years. The model forcing is the annual mean wind field Hellerman and Rosenstein (1983) (H-R). The total transport at the Drake Passage was 184 Sv calculated over the last 6 years of model integration.

3.3 Ocean Circulation and Climate Advanced Model (OCCAM)

The Ocean Circulation and Climate Advanced Model (OCCAM) is a modified version of the Modular Ocean Model (MOM) for parallel calculation which includes an explicit free surface scheme (Webb et al. (1997)). This global model uses a Pacanowski and Philander vertical mixing parameterization (Pacanowski and Philander (1981)). A free-surface model provides more accurate solution to the governing equations and the development of external gravity waves. Also this method reduces the global communication otherwise required by a rigid-lid model and permits the use of a varying number of processors. The number of processors depends on the resolution of OCCAM. OCCAM is available in several versions using different horizontal resolutions. The OCCAM versions used in this study have 1/4 degree and 1 degree horizontal resolution. The 36 vertical levels vary from 20 m near the surface to 255 m at a depth of 5500 m. Topography is obtained from DBDB5/ETOPO5 dataset at the model resolution with important sills and straits modified according to more recent data (Thompson (1995)). The land boundary conditions are no slip and the bottom friction is quadratic. This model combines two grids. The first grid uses geographical co-ordinates for all oceans except in the North Atlantic and the Arctic, and a second, 90 degrees rotated grid, covers the area from the Bering Strait to the Equator in order to exclude the singularity in the North Pole. The two grids meet ortogonally at the equator in the Atlantic where longitude lines of the first grid become the pseudo-latitude lines of the second grid. The model uses a Laplacian operator to represent the horizontal mixing of momentum and tracers. The velocity field

was initialised to zero. The model potential temperature and salinity fields were relaxed to Levitus et al. (1994) data using a time scale of 30 days at the surface layer and 360 days at all others levels. In OCCAM the forcing supplied is the ECMWF monthly average wind stress climatology from the years 1986 to 1988 inclusive.

3.3.1 OCCAM 1/4 × 1/4

The first version of OCCAM (here and after OCCAM 1/4) has a standard latitude-longitude grid of 1/4 degree resolution (Webb et al. (1997)). The horizontal resolution in the Southern Ocean is 13.9 × 27.8 km at 60 S. The model uses a Laplacian operator to represent the horizontal mixing of momentum. The horizontal mixing coefficient was $2 \times 10^2 m^2 s^{-1}$. In OCCAM 1/4 the total transport at the Drake Passage was 152 Sv.

3.3.2 OCCAM 1 × 1

The OCCAM 1 x 1 differs from the other OCCAM versions only for the horizontal resolution. In this coarse version of OCCAM the horizontal resolution is 55.6 × 111.2 km at 60 S. The wind field is ECMWF as it is in the higher resolution OCCAM run. In a coarse resolution model eddies needed to be parameterised in order to give a realistic representation of the large scale flow. Two numerical experiments have been performed considering two eddy parameterisations in the model. In the first run a conventional parameterisation of momentum and tracers

was given. In the second run Gent P.R. and McWilliams J.C. (1990) parameterisation eddies (GM parameterisation) was applied.

• **OCCAM 1 × 1 using a standard parameterization of momentum and tracers.**

The conventional parameterisation of momentum and tracers presents two numerical problems: *1)* representation of subgrid scale processes and *2)* limitation of the model time integration.

1) Two constrains on the horizontal viscosity coefficient of momentum A_m are considered in order to restrict the value of A_m: cell Reynolds number criterion and viscous boundary layer criterion.

Bryan et al. (1975) indicated the cell Reynolds number $A_m \geq U_{max}\Delta x/2$. In this case the typical maximum velocities are considered the advective velocities in the upper ocean (order of magnitude $1ms^{-1}$). The viscous boundary layer criterion is $A_m \geq \beta(\sqrt{3}\Delta x/\pi)^3$ (Munk (1950)). Then the chosen value for A_m was $10^4 m^2 s^{-1}$.

2) The effect of the conventional parameterisation of momentun and tracers in coarse resolution models is a downward motion in the interior of the ocean and an intense upwelling in the western boundary layer of the subtropical gyre in the North Atlantic (Boning et al. (1995)). This strong upwelling in midlatitudes reduces the amount of deep water which is carried from the subpolar North Atlantic toward the low latitude and the equator. The progressive deepening of thermocline leads to a significantly lower than observed overturning circulation with the increasing of the model time integration. In order to prevent an erosion of the stratification in the Southern Ocean the model time integration was no longer than 10 years in OCCAM 1 x 1.

• **OCCAM 1 × 1 using Gent and McWilliams (1990) parameterization.**

This parameterization (Gent P.R. and McWilliams J.C. (1990)) is based on two fundamental assumptions: *1)* density is conserved following a fluid particle under mesoscale activities and *2)* tracer properties mix along isopycnal surfaces rather than across them. The dynamical effects of eddies are represented using an along isopycnal diffusion of tracers and an adiabatic down-gradient diffusion of layer thickness. The tracer equation in the Primitive Equation have the following expression for the potential temperature:

$$\frac{\partial \theta}{\partial t} + ((\mathbf{u} + \mathbf{u}*) \cdot \nabla)\theta + (w + w*)\frac{\partial \theta}{\partial z} = R(k_I, \theta) + (k_V \theta_z)_z \qquad (3.7)$$

where R is a diffusion operator along the isopycnal surfaces with the isopycnal tracer diffusion coefficient k_I and k_V is the cross-isopycnal diffusion coefficient. In this equation the effective advection velocity is the sum of the mean velocity $(\mathbf{u}, w)$ and the eddy-induced transport velocity $(\mathbf{u}*, w*)$. The eddy induced transport velocity is nondivergent and is defined by $\mathbf{u}* = (k_I \nabla \rho / \rho_z)_z$ and $w* = -\nabla \cdot (k_I \nabla \rho / \rho_z)$, where $k_I = 10^2 m^2 s^{-1}$. An analogous equation for the salinity completes the set of equations.

The GM parameterization has the advantage of flattening the isopycnal slope maintaining the vertical stratification and reducing the spurious along-coordinate mixing. Danabasoglu et al. (1994) and Danabasoglu and McWilliams (1995) compared the case of conventional parameterisation of momentum and tracers with the case of GM parameterisation implemented for a global model. In the first case they found an unrealistic extensive upwelling near 60 S that weakens the

density stratification and enhances convection. In the second case the upwelling was weaker and there was much less convection. Moreover, in the standard parameterization case all oceans were warmer than observed by about 2^oC at 1000 m depth and by about 1^oC in the deeper levels. The GM parameterization improved the global distribution of potential temperature and gave northward heat transport in the North Atlantic consistent with the estimate values (about 1 PW). However, this parameterization gives unrealistic representation of the flow in frontal regions where baroclinic instability is not the major process. Also the globally averaged potential temperature is colder (3.3^oC) than the climatology (3.6^oC) (Danabasoglu et al. (1994)). Moreover, if the thickness diffusivity is not tuned adequately the abyssal water properties may not be realistic (England and Rahmstorf (1999)).

3.4 Parallel Ocean Program Model (POP)

POP is a global high-resolution numerical model (Smith et al. (1992), Smith et al. (1993) and Dukowicz and Smith (1994)) that extends the MOM simulations performed by Semtner and Chervin (1988) and Semtner and Chervin (1992). It is adapted to parallel calculation and it uses an implicit free-surface formulation of the barotropic mode (Dukowicz and Smith (1994)). It covers the whole ocean from 77 S to 77 N using a Mercator grid (Maltrud et al. (1998)). The horizontal resolution varies with the latitude using a constant zonal size of the grid which is equal to about 0.28 degree. The meridional grid size spans from about 6.8 km at 77 N or S to 31.25 km at the Equator. The horizontal grid size is 15.6 $\times$

15.5 km at 60 S. There are 20 depth levels and they are spaced from 25 m at the top to 550 m at the bottom. The POP topography is the global topography available at NCAR (National Center for Atmospheric Research). The horizontal mixing of momentum and tracers is accomplished using biharmonic operators with viscosity and diffusivity varying as the cube of the grid length. At the bottom boundary there is a quadratic bottom friction. In this study the third run of POP experiments was used. The output used in this study was initialised from the final state of the previous experiments. The surface heat fluxes are based on Barnier et al. (1995) formulation in the third run but the sea surface temperature values were restored to 2^oC with 1 month timescale in areas covered by sea ice. The surface salinity was restored to the monthly Levitus (1982) climatology. At the high latitudes temperatures and salinity were relaxed to the annual Levitus (1982) climatology in the top 2 km with a relaxation time scale of 3 years. The wind stress is the 3-day average ECMWF from 1985-1995. In POP the total volume transport at the Drake Passage was 134 Sv.

	FRAM	**OCCAM 1/4**	**POP**
Geographic coverage	24°S-79°S	global	global
Grid	spherical	spherical	Mercator grid
Horizontal resolution lon. × lat.(degrees)	0.5 × 0.25	0.25 × 0.25	0.28 × 0.14 (at 60S)
Vertical resolution top-bottom levels	32 levels 21m - 233m	36 levels 20m - 255m	20 levels 25m - 550m
Initialization	-2°C,36.69‰ zero velocities	Levitus 1994 zero velocities and free surface height	from Semtner and Chervin's run
Time integration	16 model years	12 model years	11 model years
Surface condition	rigid lid	free surface explicit	free surface implicit
Boundary condition	zero velocity, S and T gradients	zero velocity, S and T gradients	from Semtner and Chervin's run
Bottom drag coefficient	quadratic 1×10^{-3}	quadratic 1×10^{-3}	quadratic 1.225×10^{-3}
Topography	smoothed 1×1 resolution	non-smoothed model resolution	non-smoothed model resolution
Forcing	H-R annual mean 1993	ECMWF 3 years mean 1986-88	ECMWF 10 years mean 1985-95
Volume Transport at Drake Passage South-Australia	184 Sv 184 Sv	152 Sv 165 Sv	134 Sv 139 Sv

Table 3.1: *Main characteristics of FRAM, OCCAM 1/4 and POP models*

Chapter 4

Dynamical Controls on the ACC in OGCMs

4.1 Introduction

Three OGCMs (FRAM, OCCAM 1/4 and POP) are used in order to investigate the ACC dynamics at the Drake Passage latitudes (ACCB : 63.5 S - 55 S), where the ACC flows with no continental barriers. In order to describe the ACCB dynamics all factors are considered in the Primitive Equations. The comparison between FRAM, OCCAM 1/4 and POP allows the understanding of the effects of improved topography representation, higher resolution and different wind field on the ACC flow. These are general circulation models, which are able to display eddies and they are different not only because of resolution but also because of forcing and topography. Consequently, they represent differently the ACC flow and ACC volume transport (Figure 4.1 and Figure 4.2).

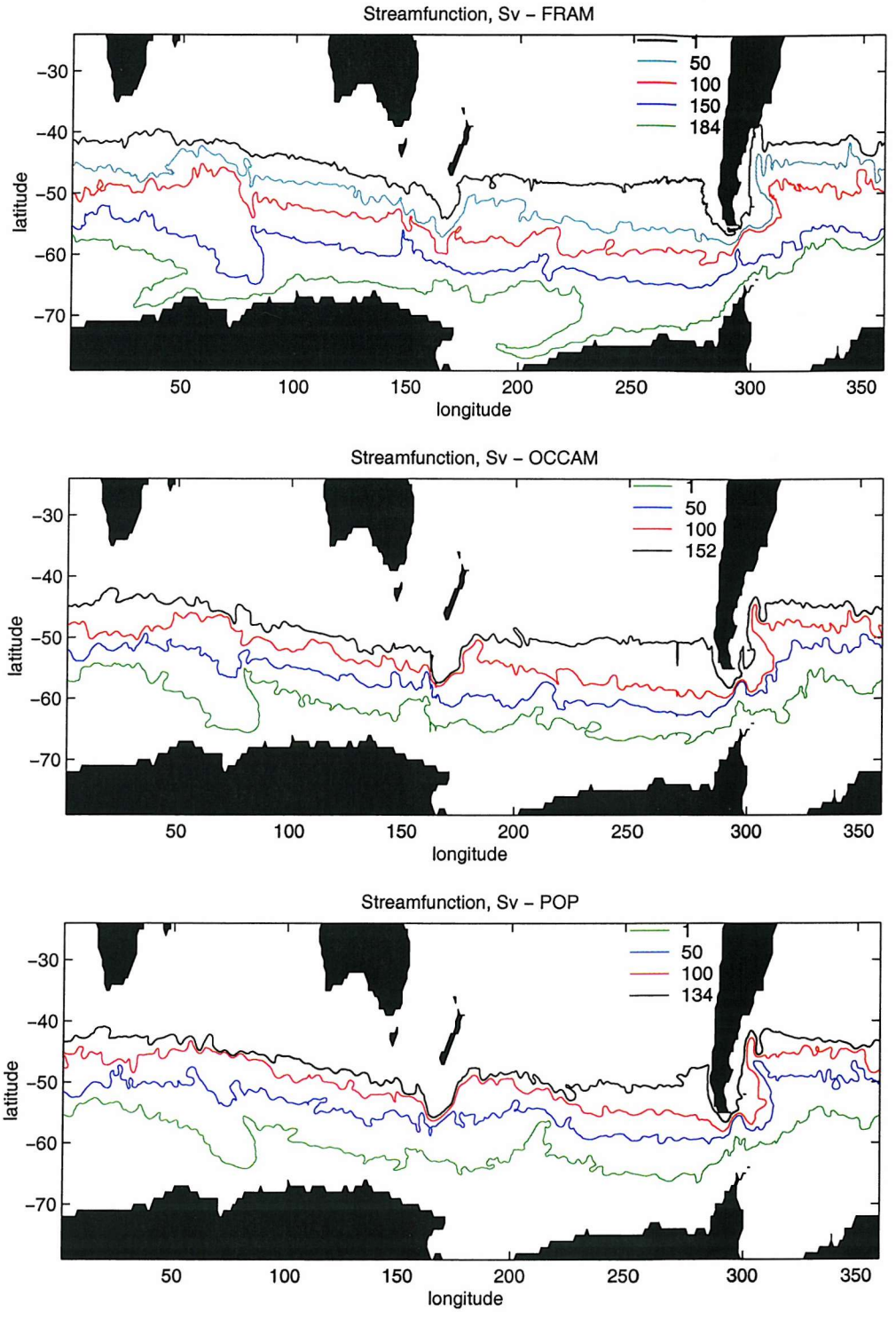

Figure 4.1: *Time mean streamfunctions (Sv) in FRAM, OCCAM 1/4 and POP*

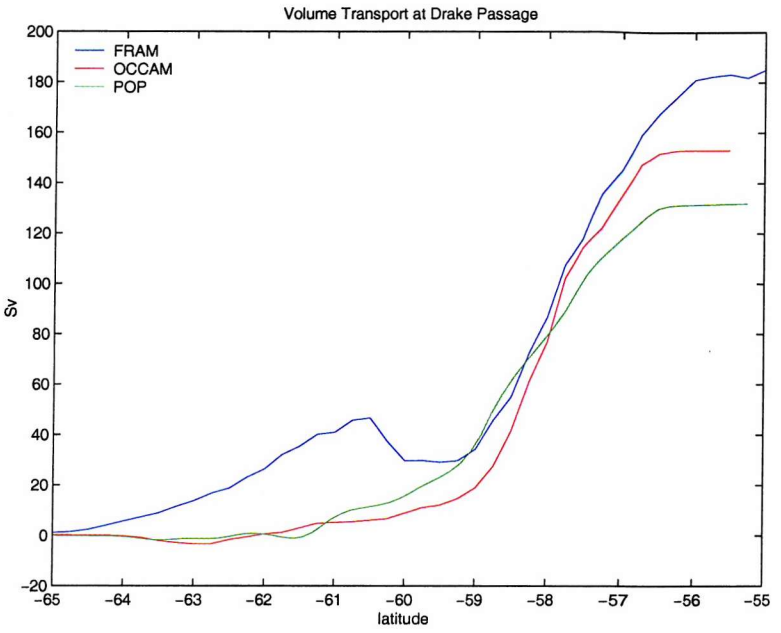

Figure 4.2: *Accumulated time mean volume transport in FRAM, OCCAM 1/4 and POP across Drake Passage*

4.2 Momentum Budgets

The zonal character of the ACC suggests to focus the following momentum analysis on the eastward component of the motion (Appendix A.1).

4.2.1 Time mean zonally averaged depth integrated momentum budget

In order to describe the ACCB dynamics all terms are considered in the primitive equations (Coriolis term, momentum flux divergence, bottom form stress, horizontal mixing, wind stress, bottom form stress).The Right hand side (RHSM)

represents the total rate of change of momentum and it is calculated as a residual from the other terms in OCCAM 1/4. RHSM is considered zero in POP assuming a steady state following Maltrud et al. (1998), who affirmed that in the last 5 year of POP integration the model was in a state of quasi-equilibrium. The assumption of steady state was made in order to calculate the bottom form stress as a residual because these values were not available. The hypothesis of steady state does not compromise the following analysis on the leading terms in the momentum budgets. Without this hypothesis the RHSM value is expected to be at least one order of magnitude less than the leading terms in POP, as it is in FRAM and OCCAM 1/4.

The zonal momentum budget is a standard diagnostic in a zonal open channel. The time mean zonally averaged depth integrated momentum budget in the ACCB in FRAM was calculated by Stevens and Ivchenko (1997). In that case the time mean was over the last 6 years of the 16-years FRAM run. The time mean zonally averaged depth integrated momentum balance was calculated in OCCAM 1/4 and POP in the ACCB and then compared with FRAM. The time mean is over 4 years of OCCAM 1/4 model run (from year 8 to year 12) and over the last 5 years of POP model integration.

In OCCAM 1/4 and POP the leading terms in the budgets are bottom form stress and wind stress while the other terms are small (Table 4.1). Also in FRAM the balance was mainly between wind stress (about $70 \times 10^{-3} Nm^{-2}$) and bottom form stress (about $-65 \times 10^{-3} Nm^{-2}$) and the contribution to the budget from the other terms was small.

The balances in the three models present important differences. The values of the leading terms are almost double in OCCAM 1/4 compared to FRAM and

$\times 10^{-3} Nm^{-2}$	**OCCAM 1/4**	**POP**
Coriolis term	- 2.510	3.280
momentum flux divergence	- 0.843	- 6.877
bottom form stress	-122.035	- 89.636
horizontal mixing	0.017	0.019
wind stress	117.733	93.493
bottom stress	- 0.298	- 0.279
RHSM	- 7.936	0.000

Table 4.1: *Time mean area averaged depth integrated momentum budget in OCCAM 1/4 and POP in the ACCB*

significantly higher than those in POP.

It is well known that H-R and ECMWF wind fields are different in the Southern Ocean (Glowienka-Hense et al. (1992)). The ECMWF eastward wind stress component is stronger than the H-R eastward wind stress component in all sectors of the Southern Ocean, in particular in the Southern Indian Ocean. In the ACCB the zonally averaged wind stress is twice as strong in OCCAM 1/4 than in FRAM. However in POP the ECMWF zonally averaged wind stress is lower than in OCCAM 1/4 by about 21%. This difference is due to a different method of calculating the wind stress in the two models. The OCCAM 1/4 wind stress is the Siefridt and Barnier (1993) climatology. This monthly climatology was corrected using Killworth (1996)'s linear interpolation in time. The POP wind stress climatology is obtained by averaging the wind field over 3 days.

Over the ACCB the wind stress is balanced mainly by bottom form stress in

OCCAM 1/4 and POP (Figure 4.3) and the contribution from the momentum flux divergence is small compared to the two leading terms (Figure 4.3 and Figure 4.4). The eastward wind stress is a source for the momentum at the surface and increases almost linearly northward through the ACCB. The main sink of momentum is the bottom form stress, which decreases northward balancing the wind stress. The bottom form stress presents oscillations which are mainly in opposite phase to the latitudinal variations of the momentum flux divergence. This kind of modulation is more clearly pronounced in POP, which is the model with the highest horizontal resolution. In this case the retarding effect on the flow due to the bottom form stress is affected by eddy activity in the model.

4.2.2 Time mean zonally averaged momentum balance level by level

The vertical time mean zonally averaged momentum balance in the ACCB is investigated level by level in OCCAM 1/4 (Figure 4.5). The levels are grouped in seven parts and integrated on the depth corresponding to the sum of depths of each group. The criterion for grouping these levels was that the main terms in the budget had the same order of magnitude. In this way it is possible to identify at which depths the bottom form stress acts in order to balance the wind stress in the ACCB.

The vertical momentum balance has a different structure in OCCAM 1/4 when compared to FRAM (Stevens and Ivchenko (1997)).

In OCCAM 1/4 the Ekman balance takes place in the *surface levels* (0-41 m),

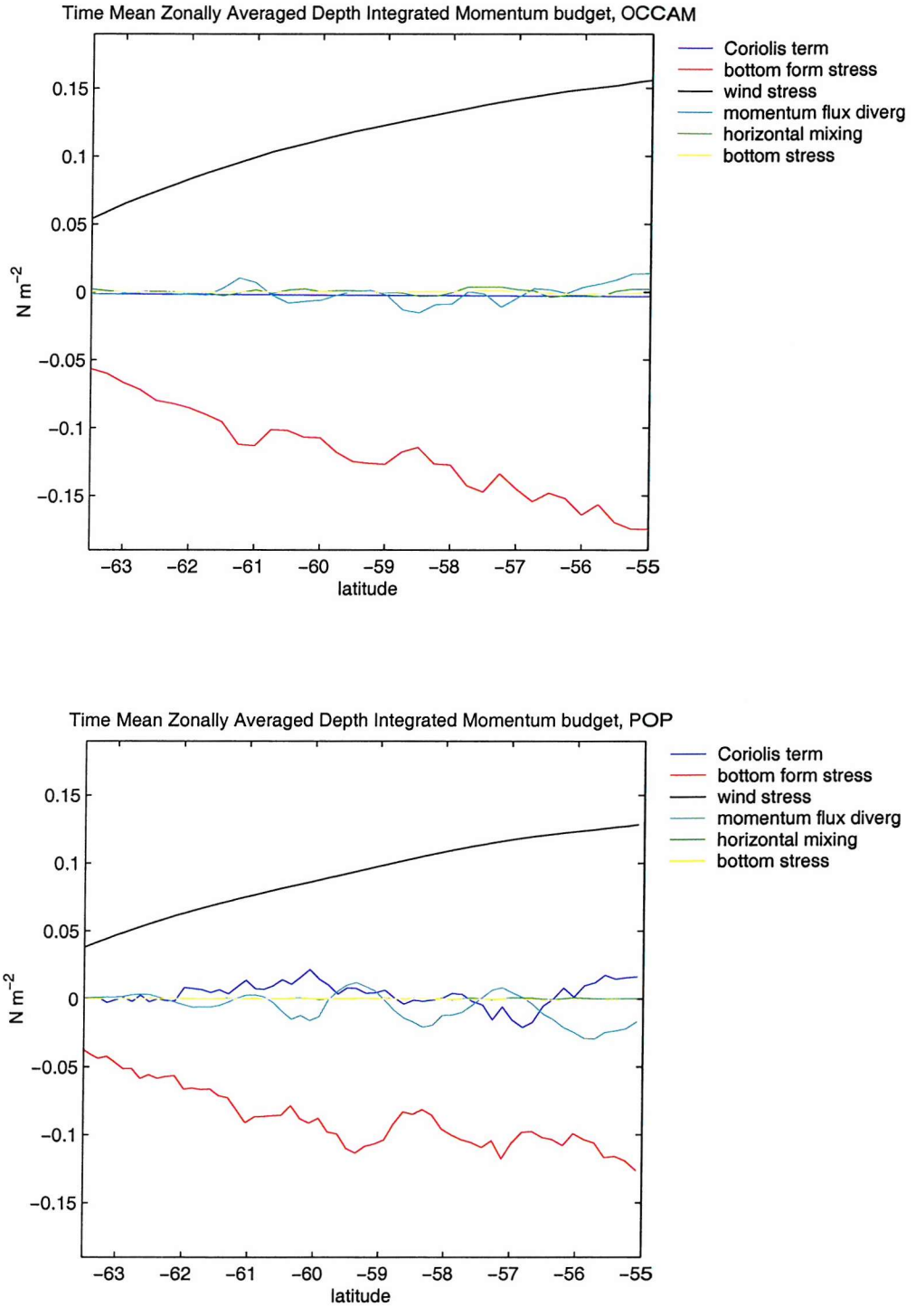

Figure 4.3: *Time mean zonally averaged depth integrated momentum budget in OCCAM 1/4 and POP in the ACCB*

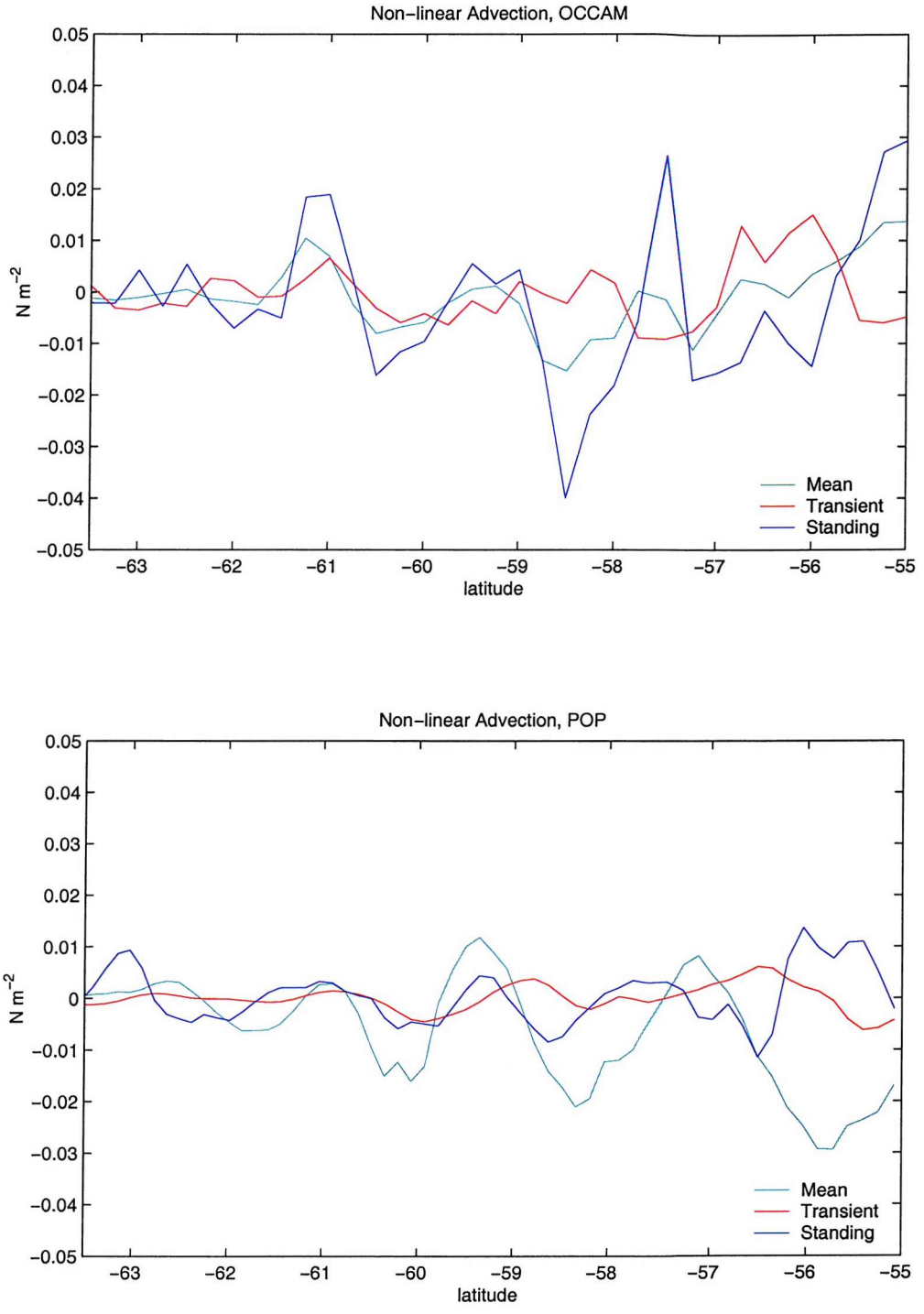

Figure 4.4: *Mean, transient and standing contributions to the time mean zonally averaged depth integrated momentum flux divergence term in the momentum budget in OCCAM 1/4 and POP in the ACCB*

whereas in FRAM the balance between vertical mixing of momentum and the Coriolis term is confined to the upper 21 m.

The *intermediate levels* are complete zonal levels not interrupted by topography. In the intermediate levels the balance is between the momentum flux divergence and the Coriolis term. Under the assumption of geostrophic balance along a line of constant latitude and constant depth in the barrier-free belt there is no meridional circulation. The balance between momentum flux divergence and Coriolis term indicates that this assumption is not valid in the intermediate levels and a meridional motion of water masses can occur due to eddies. In OCCAM 1/4 this balance occurs between 41 m and 323 m. The bottom form stress appears to be important in the depth range of 323-1419 m at the southern boundary of the ACCB because of the slope of the Antarctic Peninsula. At these depths the barrier-free flow is confined between 60 S and 57 S. The OCCAM 1/4 balance in the intermediate levels is consistent with FRAM results above topography. However in FRAM the intermediate levels span a wider range of depths (between 21 m and 2056 m).

At the *deep levels* the bottom form stress has the same order of magnitude of the wind stress in the first level. In OCCAM 1/4 bottom form stress is significantly higher between 1419 m and 3722 m and between 3722 m and 4989 m because of the topographic features (Kerguelen Plateau, southern part of the Campbell Plateau, Indian Ridge, South-Pacific Ridge and Scotia Arc). In the deep levels the southward-flowing deep currents are associated with pressure differences across topography. Stevens and Ivchenko (1997) found that in FRAM the balance between pressure gradients and southern flow was confined to the depth range of 2056-3874 m.

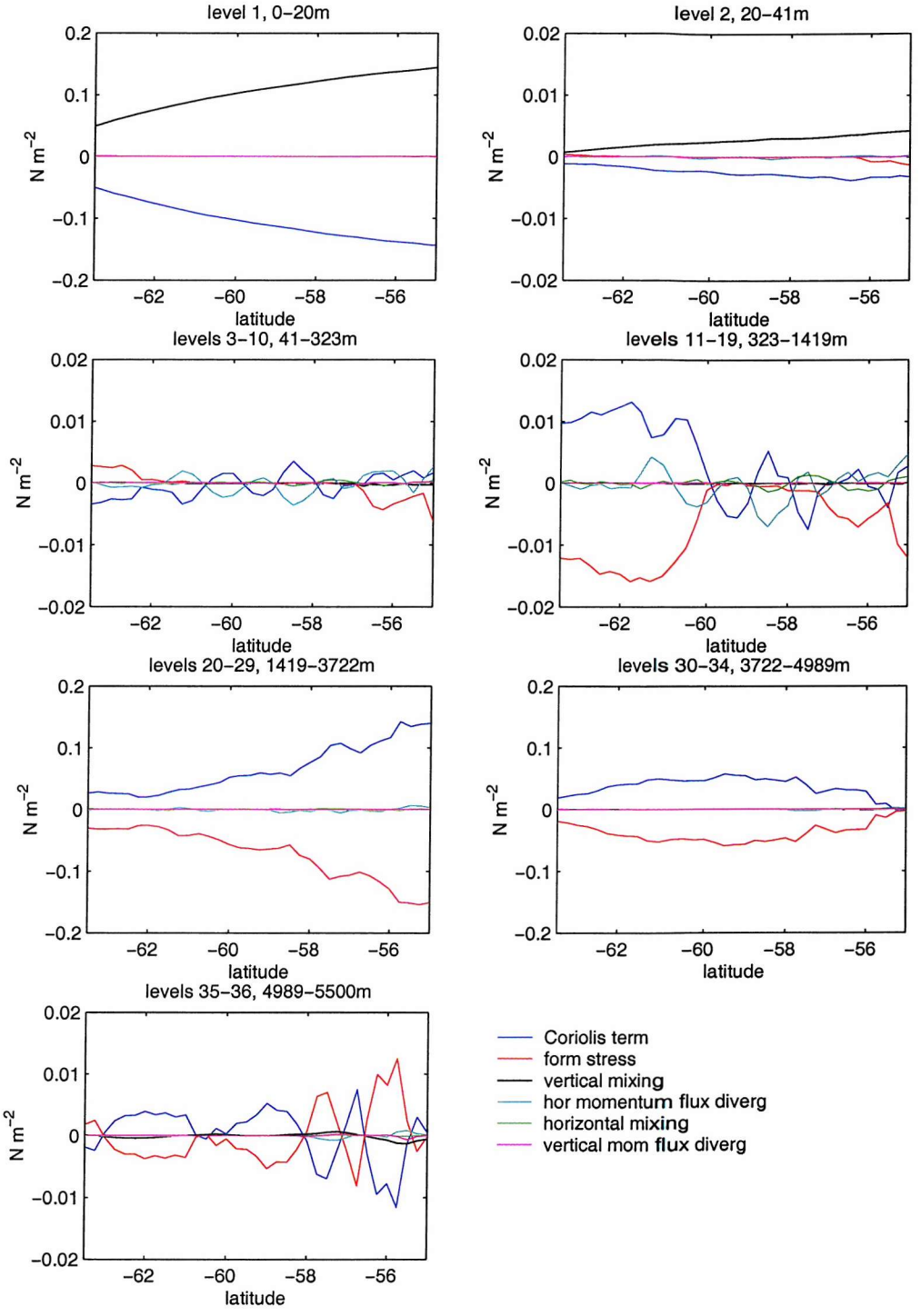

Figure 4.5: *Time mean zonally averaged momentum budget level by level in OCCAM 1/4 in the ACCB*

In the *very deep levels* the bottom form stress is one order of magnitude less than the deep levels. In FRAM those levels were between 3874 m and 5499 m. In FRAM the Coriolis term was negative in the ACCB indicating the presence of a northward flow and the bottom form stress was positive providing an acceleration to the flow. The problem of overestimated velocities in the South Atlantic has been pointed out recently also by Stevens and Stevens (1999). Unlike FRAM, in OCCAM 1/4 the very deep levels are between 4989 m and 5500 m. There is no northward flow in the ACCB in these levels and the bottom form stress is not acting to accelerate the flow. It is positive only between 58 S and 58.5 S and between 57.5 S and 56.7 S whilst elsewhere it is negative and therefore acts as a drag.

4.3 Reynolds Stresses

The Reynolds stress $\overline{[uv]}_{zonal}$ can be decomposed in to

$$\overline{[uv]}_{zonal} = \overline{[u]}_{zonal}\overline{[v]}_{zonal} + [u^*v^*]_{zonal} + \overline{[u'v']}_{zonal} \tag{4.1}$$

where u and v are separated in $u' = u - \overline{u}$, $v' = v - \overline{v}$ and $u^* = \overline{u} - \overline{[u]}_{zonal}$, $v^* = \overline{v} - \overline{[v]}_{zonal}$. The overbar indicates the time mean over 4 years in OCCAM 1/4 and over 5 years in POP. The first term on the right hand side is the mean overturning term, the second term is the standing eddy contribution to the Reynolds stresses and it represents the departure of the time mean flow from the zonal mean flow, the third term is the transient eddy contribution to the Reynolds stresses and it is due to the variations in time of the flow.

Both OCCAM 1/4 and POP show transient and standing Reynolds stresses decreasing from the surface to the bottom, with standing Reynolds stresses in OC-

CAM 1/4 greater than those in POP (Figure 4.6). At the surface the transient Reynolds stresses have comparable values (2.5 $\times 10^{-4} m^2 s^{-2}$ in OCCAM 1/4 and 1.7 $\times 10^{-4} m^2 s^{-2}$ in POP) whereas standing Reynolds stresses are double those in OCCAM 1/4 (7.9 $\times 10^{-4} m^2 s^{-2}$) than POP (3.7 $\times 10^{-4} m^2 s^{-2}$). In OCCAM 1/4 and POP the greatest part of the eddy activity is above the major topographic structures in the ACCB (above 2000 m). FRAM standing Reynolds stresses were calculated by Stevens and Ivchenko (1997). They were comparable to POP at the surface and mainly concentrated in the upper levels (above 2000 m). FRAM transient Reynolds stresses were one order of magnitude less than standing Reynolds stresses at the surface and negative and they showed that the poleward transfer of eastward momentum concentrated momentum into the ACCB flow.

Most interesting are the transient and standing components of the area averaged momentum flux divergence on the RHSM of the momentum equation

$$-\frac{\rho_0}{a\cos\varphi}\frac{\partial\overline{u'u'}}{\partial\lambda}-\frac{\rho_0}{a\cos\varphi}\frac{\partial\overline{u'v'}\cos\varphi}{\partial\varphi} \tag{4.2}$$

and

$$-\frac{\rho_0}{a\cos\varphi}\frac{\partial u^*u^*}{\partial\lambda}-\frac{\rho_0}{a\cos\varphi}\frac{\partial u^*v^*\cos\varphi}{\partial\varphi}. \tag{4.3}$$

These terms represent also the Reynolds stresses divergence. The momentum flux divergence was calculated in OCCAM 1/4 and POP in the ACCB (Figure 4.7). Positive values of momentum flux divergence in Figure 4.7 indicate that the flow is being accelerated by eddies. Transient eddies act in order to accelerate the flow at the surface and in the upper 1000 m in POP. A small deceleration of the flow occurs in the deepest levels. OCCAM 1/4 shows an opposite behaviour to POP at the surface and in the upper 1000 m depth where the transient eddies

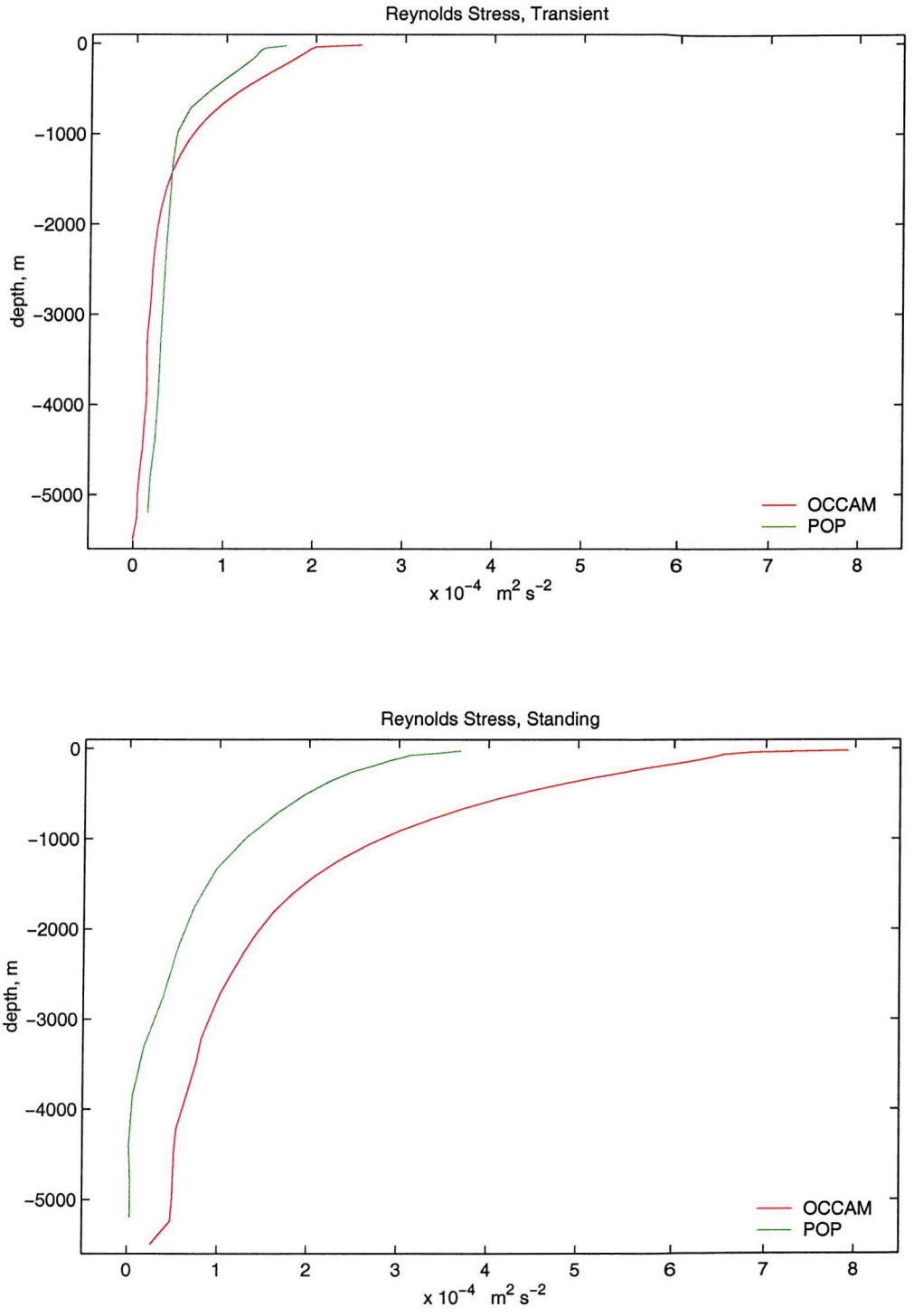

Figure 4.6: *Area averaged Reynolds stresses in OCCAM 1/4 and POP in the ACCB*

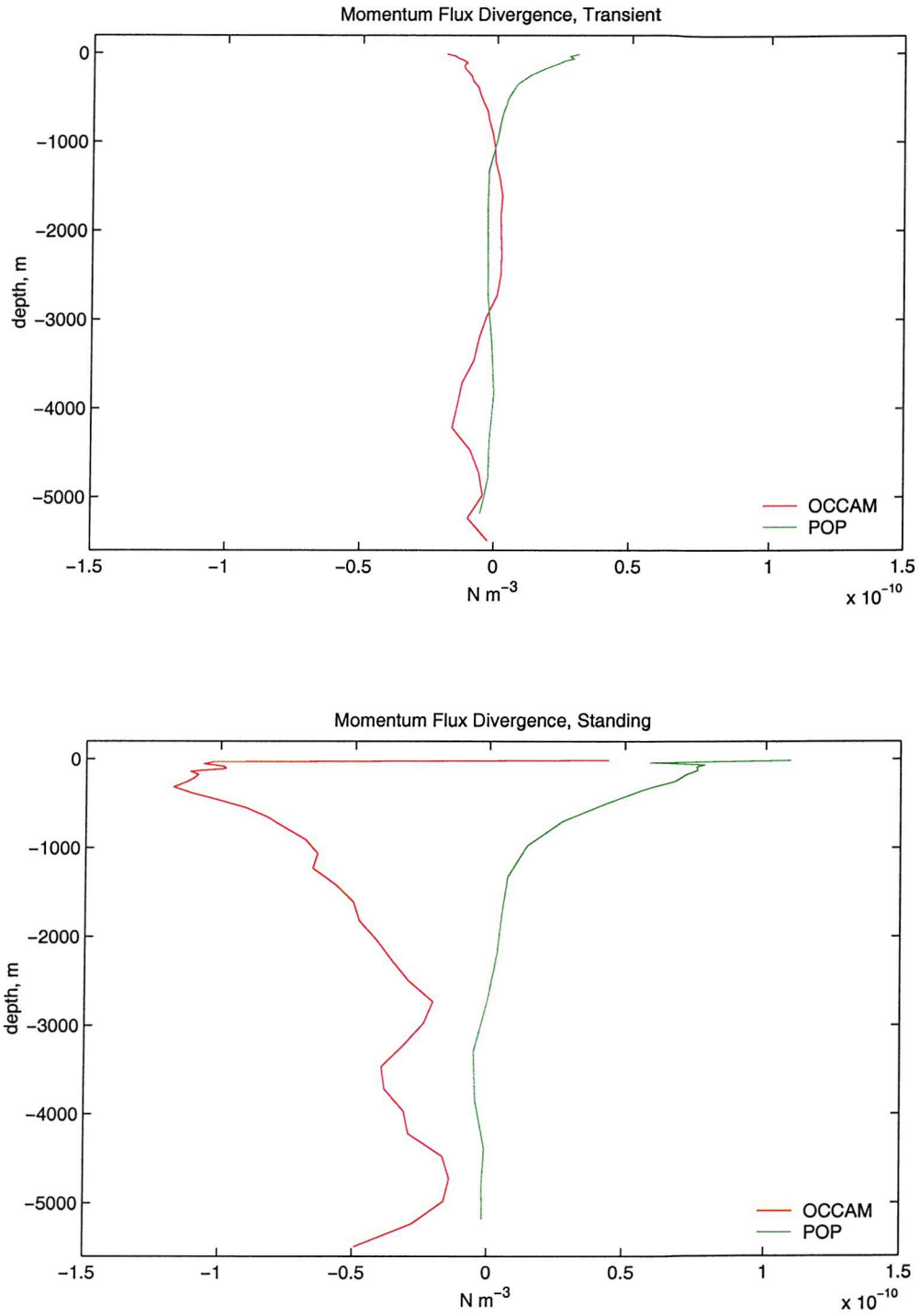

Figure 4.7: *Area averaged momentum flux divergence in OCCAM 1/4 and POP in the ACCB*

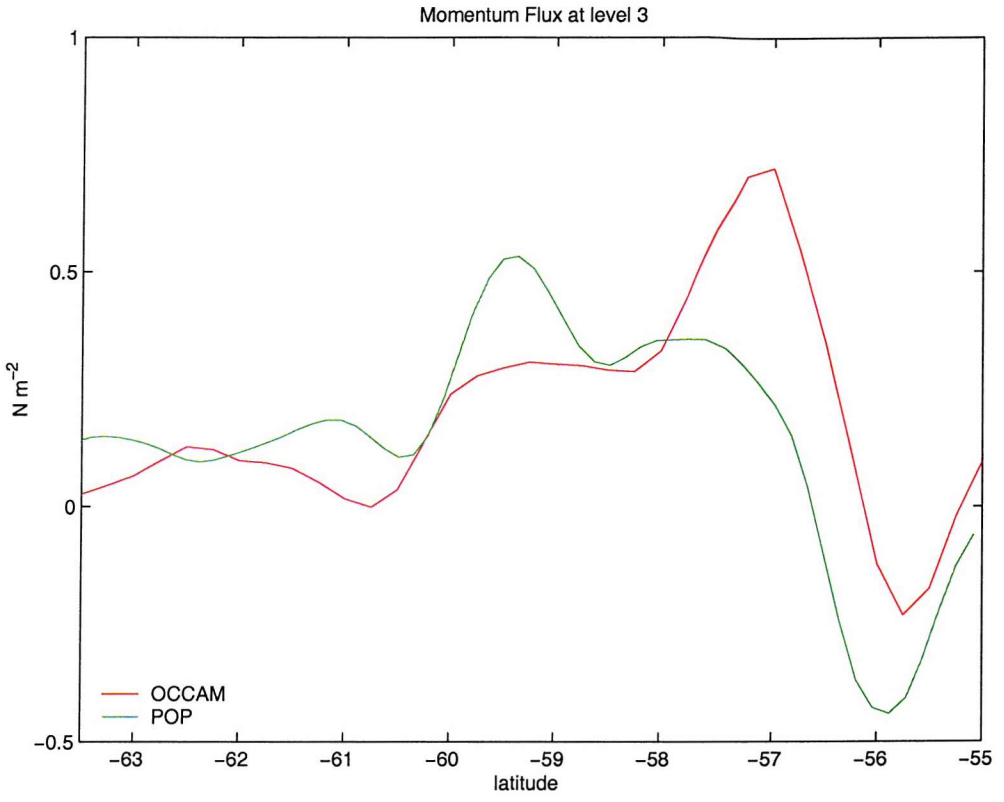

Figure 4.8: *Zonally averaged transient momentum flux at level 3 in OCCAM 1/4 (64 m) and POP (75 m) in the ACCB*

decelerate the flow, in agreement with Hughes and Ash (2001)'s observations. A small acceleration of the flow occurs between 1000 m and 2737 m, but at depths greater than 2737 m transient eddies continue to decelerate the flow. Hence, in OCCAM 1/4 transient eddies tend to decelerate the mean flow, whereas in POP transient eddies accelerate the flow. The transient components of the momentum flux divergence are different in the ACCB because of the geographical representation of the momentum flux in the two models (Figure 4.8). In the upper levels OCCAM 1/4 momentum flux shows a peak in the northern part of the ACCB (57

S) whereas in POP the highest value of momentum flux occur at 59.5 S. In OCCAM 1/4 and POP standing eddies act to accelerate the flow in both models at the surface. However, immediately below the Ekman layer OCCAM 1/4 presents a strong standing eddy activity which decelerates the flow. POP standing eddies start to decelerate the mean flow below 2200 m. Regarding FRAM, Stevens and Ivchenko (1997) concluded that transient eddies were a forcing factor in the momentum balance and standing eddies a dragging factor in the ACCB at all depths.

4.4 Kinetic Energy

The role of eddies has been investigated in the kinetic energy field in the ACCB. The zonally averaged Kinetic Energy (KE) in POP shows that the highest contribution to the total KE comes from the transient eddies and the lowest from the standing eddies (Figure 4.9 and Figure 4.10). In OCCAM 1/4 the eddy KE contribution to the total energy is lower than the standing contribution (Figure 4.9 and Figure 4.10) as it was in FRAM (Best et al. (1999)). FRAM was able to reproduce the general distribution of eddy KE in the ACC but it failed to estimate the observed eddy KE because of the low resolution and showed eddy KE values lower than about 25% of observational estimates (Stevens and Killworth (1992)). Despite the fact that the OCCAM 1/4 and POP present similar depth averaged eddy KE (Table 4.2), the KE due to the transient eddies is remarkably different in the two models at the surface in the ACCB (Figure 4.11). The POP top layer eddy KE is in agreement with the TOPEX estimation (Best et al. (1999)) whereas in OCCAM 1/4 it is 32% of that in POP. Transient KE in POP

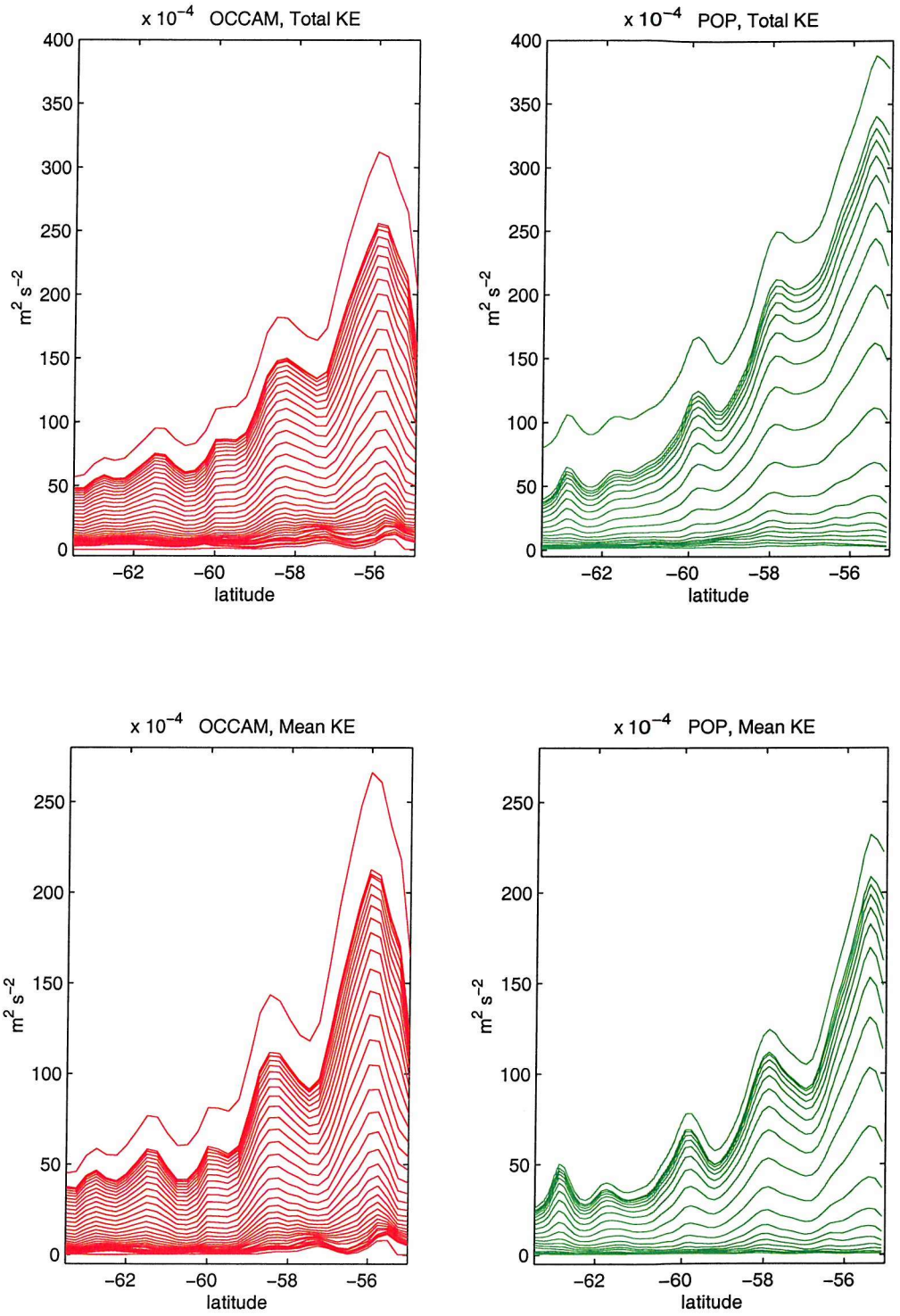

Figure 4.9: *Zonally averaged total and mean KE for each level in OCCAM 1/4 and POP in the ACCB*

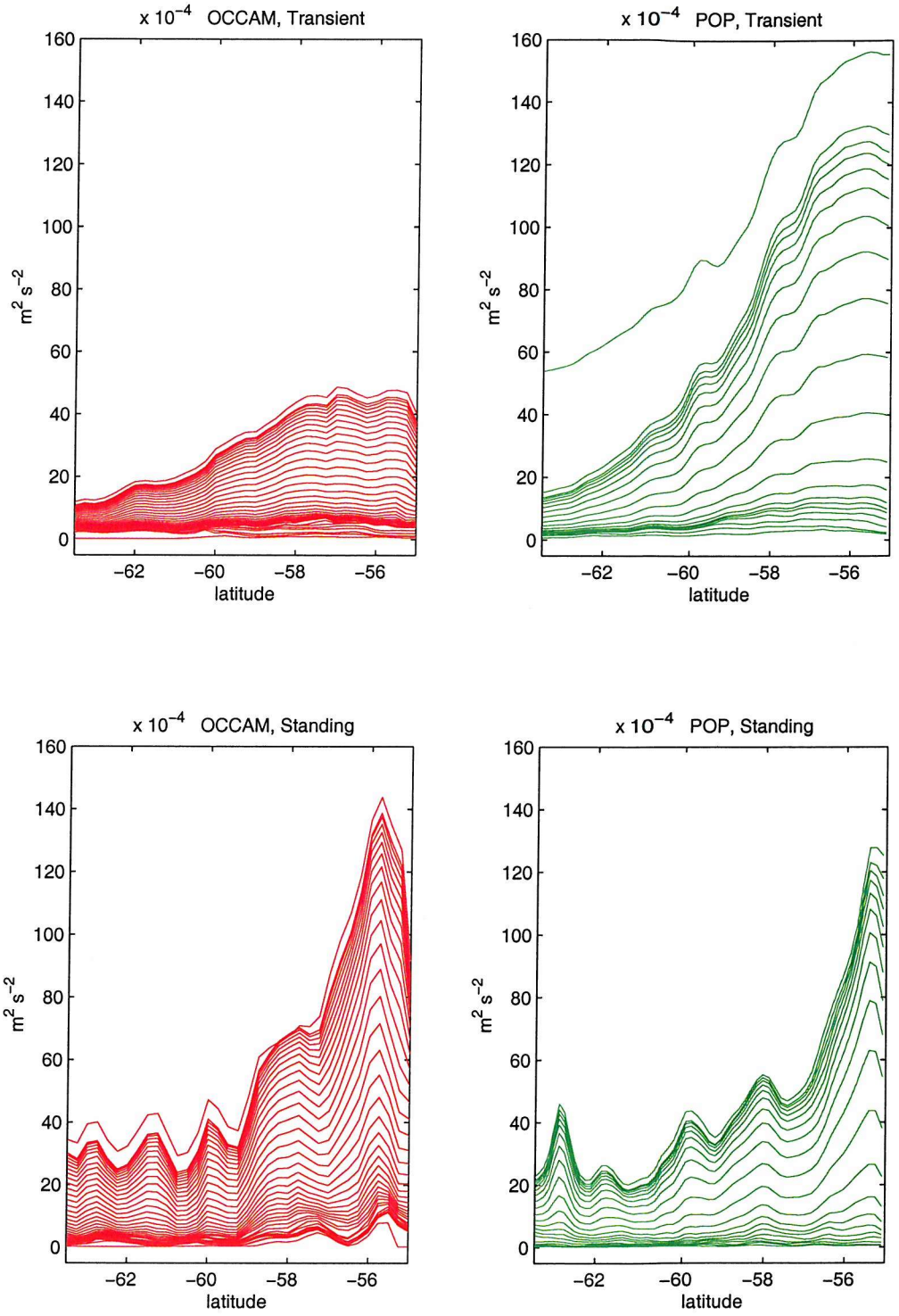

Figure 4.10: *Zonally averaged transient and standing KE for each level in OCCAM 1/4 and POP in the ACCB*

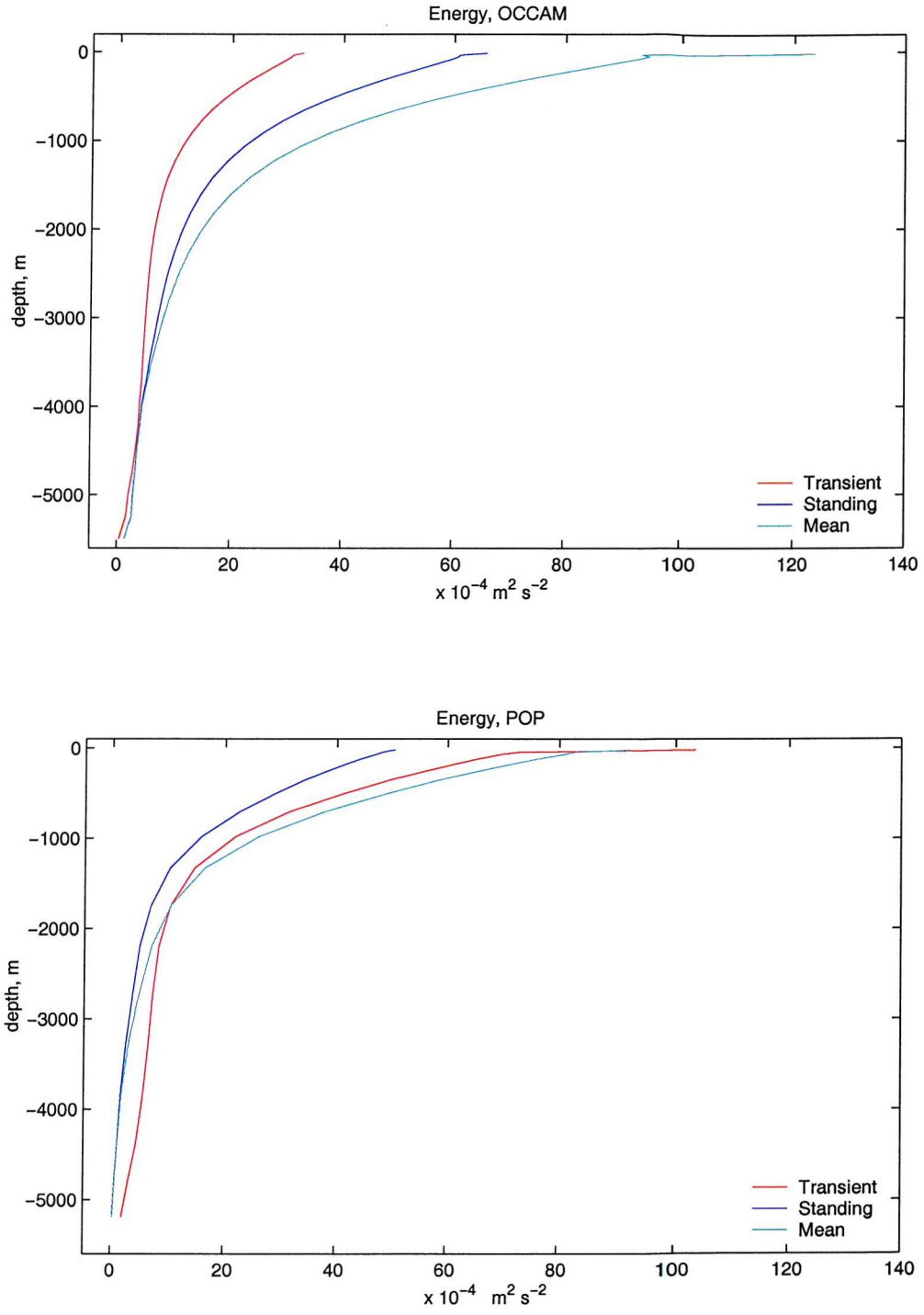

Figure 4.11: *Area averaged mean, transient and standing KE in OCCAM 1/4 and POP in the ACCB*

$\times 10^{-4} m^2 s^{-2}$	**OCCAM 1/4**	**POP**
transient eddy KE at the surface	32.78	103.25
transient eddy KE depth averaged	9.54	12.91
standing eddy KE at the surface	65.86	50.55
standing eddy KE depth averaged	17.08	7.83

Table 4.2: *Transient eddy KE and standing eddy KE in OCCAM 1/4 and POP in the ACCB*

is concentrated in the upper part of the water column and it decreases rapidly to reach 10% of the surface value at 2000 m. The greatest values of KE are in the levels above topographic structures. At levels deeper than 2000 m the transient and standing KE values are similar in OCCAM 1/4 and POP, indicating that at the deepest levels the KE values are not strongly affected by resolution.

Beckmann et al. (1994) pointed out that for a realistic simulation of eddy KE in a numerical model the grid spacing should be smaller than the local internal Rossby radius. The local internal Rossby radius R has been calculated in OCCAM 1/4 and POP

$$R = \int_{-H}^{h} N(z) dz / \pi f \tag{4.4}$$

where $N^2(z) = -g/\rho_0 \frac{\partial \rho_\sigma}{\partial z}$ is the buoyancy frequency, the potential density ρ_σ is referred to level 1 in the two models). Both OCCAM and POP do not fully resolve the internal Rossby radius in the ACCB (Table 4.3).

Energy can be lost by the mean field through the instability processes (barotropic and baroclinic processes). The transfer of energy from the mean horizontal flow

km	**OCCAM 1/4**	**POP**
Rossby radius		
at 55 S	12.3	11.6
at 59 S	10.1	9.0
at 63.5 S	7.6	6.4
Horizontal resolution dx × dy		
at 55 S	15.9 × 27.8	17.8 × 17.9
at 59 S	14.3 × 27.8	16.0 × 16.1
at 63.5 S	12.4 × 27.8	13.9 × 13.9

Table 4.3: *Internal Rossby radius and horizontal resolution in OCCAM 1/4 and POP in the ACCB*

to the transient and standing eddy flow

$$-\frac{\overline{u'v'}}{a}\frac{\partial \overline{u}}{\partial \varphi} \tag{4.5}$$

and

$$-\frac{u^*v^*}{a}\frac{\partial \overline{u}}{\partial \varphi} \tag{4.6}$$

has been calculated in OCCAM 1/4 and POP in each level following Best et al. (1999), Ivchenko et al. (1997), Boning and Budich (1992). In Figure 4.12 positive values indicate an energy transfer from mean KE to eddy KE and negative values an energy transfer from eddy KE to mean KE. In OCCAM 1/4 in the upper levels ($\leq$ 779 m) the energy transfer due to transient eddies is negative indicating that eddies transfer KE to the mean flow. This could be a baroclinic instability, which is triggered by topography (Best et al. (1999), Ivchenko et al. (1997), Johnson and Bryden (1989)). However, at the deepest levels KE is transferred from the

mean flow to the eddy flow (barotropic instability). The barotropic instability can be interpreted as the work of Reynolds stresses on the mean flow. In this case Reynolds stresses extract energy from the horizontal shear decelerating the zonal flow. Between 2737 m and 3722 m the energy transfers due to transient eddies suggest that the instability becomes baroclinic again. In POP the barotropic instability is concentrated in the upper 2750 m. Below 2750 m the sign of energy transfer due to transient eddies changes indicating a baroclinic instability.

4.5 Vorticity Budgets

In order to explore the non-sverdrup character of the ACC flow all terms in the vorticity budgets were calculated (Appendix A.2).

4.5.1 Time mean area averaged depth integrated vorticity budget

The time mean depth integrated vorticity budget was calculated in FRAM, OCCAM 1/4 and POP (Appendix A.2) in the ACCB. In FRAM the time mean is over 6 years, in OCCAM 1/4 the time mean involves the 4 years averaged data set and in POP it is over 5 years. All components in the budgets were area averaged over the ACCB. The leading terms in the budgets (Table 4.4) are wind curl and bottom pressure torque, whilst non-linear advection is a major term only in the highest resolution model. In OCCAM 1/4 wind curl and bottom pressure torque values are almost double those in FRAM. POP and OCCAM 1/4 bottom pres-

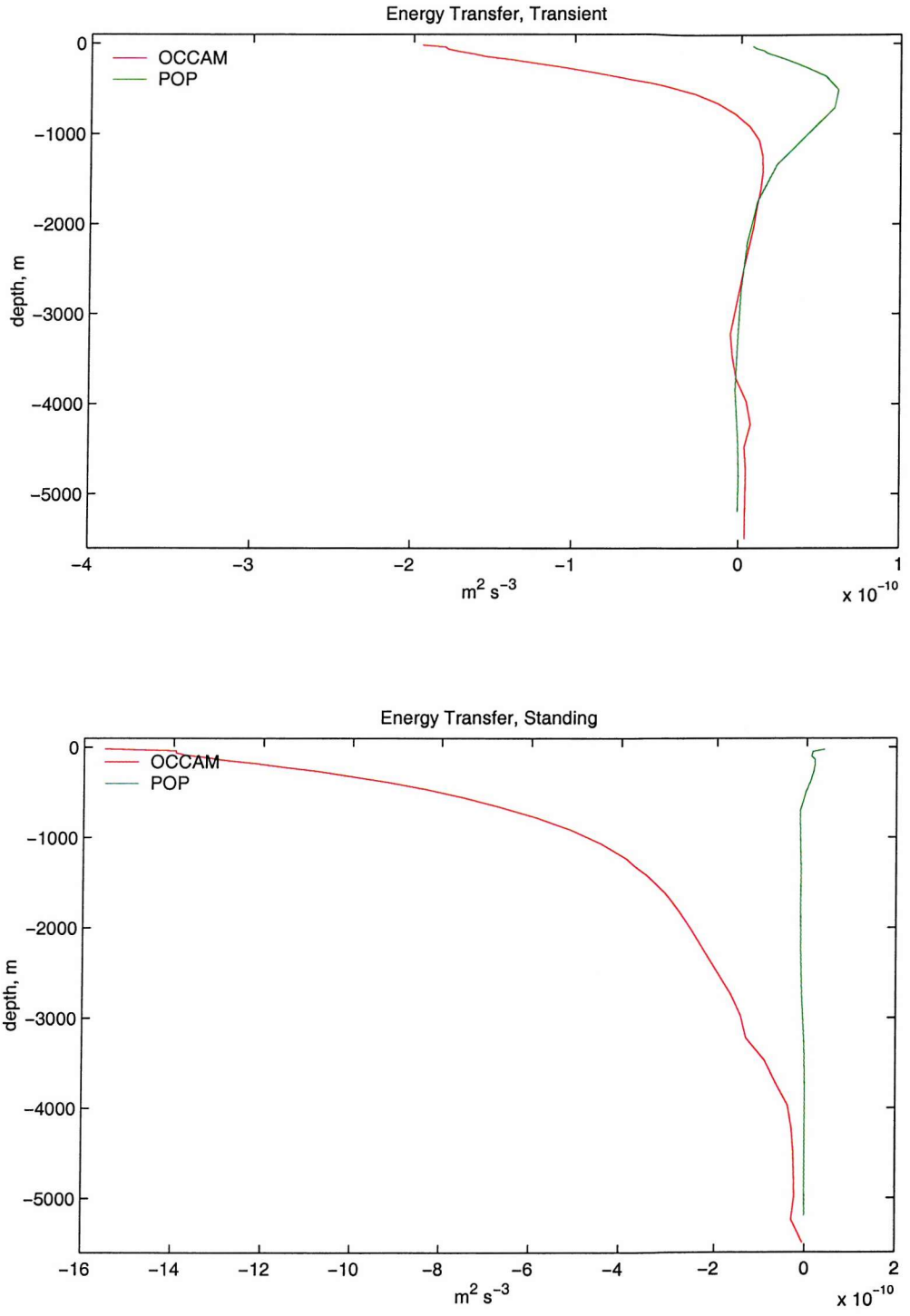

Figure 4.12: *Area averaged transient and standing energy transfer in OCCAM 1/4 and POP in the ACCB (values* < 0*, baroclinic instability - values* > 0*, barotropic instability)*

$\times 10^{-12} ms^{-2}$	**FRAM**	**OCCAM 1/4**	**POP**
planetary vorticity	0.000	2.644	- 3.405
non-linear advection	- 5.684	- 15.360	- 56.116
bottom pressure torque	81.956	153.625	152.788
lateral friction	0.729	- 4.794	0.047
wind curl	- 79.320	-134.278	- 94.088
bottom friction	0.970	0.661	0.774
RHSV	- 1.349	2.498	0.000

Table 4.4: *Time mean area averaged depth integrated vorticity budget in FRAM, OCCAM 1/4 and POP in the ACCB*

sure torque are similar. Non-linear advection increases considerably in the POP budget and it is more than three times higher than the non-linear advection in OCCAM 1/4. There are differences between the wind fields used in OCCAM 1/4 and POP, though both models use ECMWF wind field.

FRAM planetary vorticity is coincident to βV and it is called beta term (Wells and de Cuevas (1995)). Due to the rigid lid condition this term is zero when integrated around a latitude circle and it does not make any contribution to the budget. In OCCAM 1/4 and POP that condition is replaced by a free surface. A mass flux through the free surface is possible and a contribution of this term to the budget is not necessarily zero.

Bottom friction was small in the three PE models. The total rate of change of vorticity (RHSV) is calculated like a residual of the other terms in the balances in OCCAM 1/4 and FRAM. In POP we made the assumption that the model

was in a steady state (RHSV=0) and bottom pressure torque was calculated as a residual. With bottom pressure torque calculated as a residual in POP it is not possible to use the RHSV as a check for the others term, in particular for the non linear advection.

The accumulation of each term in the vorticity budgets was calculated in FRAM, OCCAM 1/4 and POP in the eastward direction from the Greenwich meridian. This analysis allows a large scale view of the ACC dynamics in the ACCB (Wells and de Cuevas (1995)) and displays longitudinal variations of each term of the budgets (Figure 4.13). In FRAM the accumulated balance is mainly between the beta term, wind curl and bottom pressure torque. A main balance between wind curl and beta term (Sverdrup balance) is reached almost everywhere except in the Drake Passage region (290-340 E). Non-linear advection is not a leading term in the ACCB.

In OCCAM the main accumulated balance remains between the planetary vorticity, bottom pressure torque and wind curl. Beta term and planetary vorticity describe similarly the ACC flow in the belt. However, the eastern part of the Weddell Sea (40-80 E) is the only region where the planetary vorticity and the wind curl balance. Except for this region, a Sverdrup-like balance is never reached. OCCAM 1/4 bottom pressure torque is higher than that in FRAM even far from the Drake Passage region. This term compensates in OCCAM the stronger wind curl. Non-linear advection has the highest values downstream of the South-East Indian Ridge, in the South Pacific sector and across the Drake Passage in the ACCB.

Conversely to FRAM and OCCAM 1/4, in POP non-linear advection is one of the leading terms in the accumulated balance, in particular downstream of the

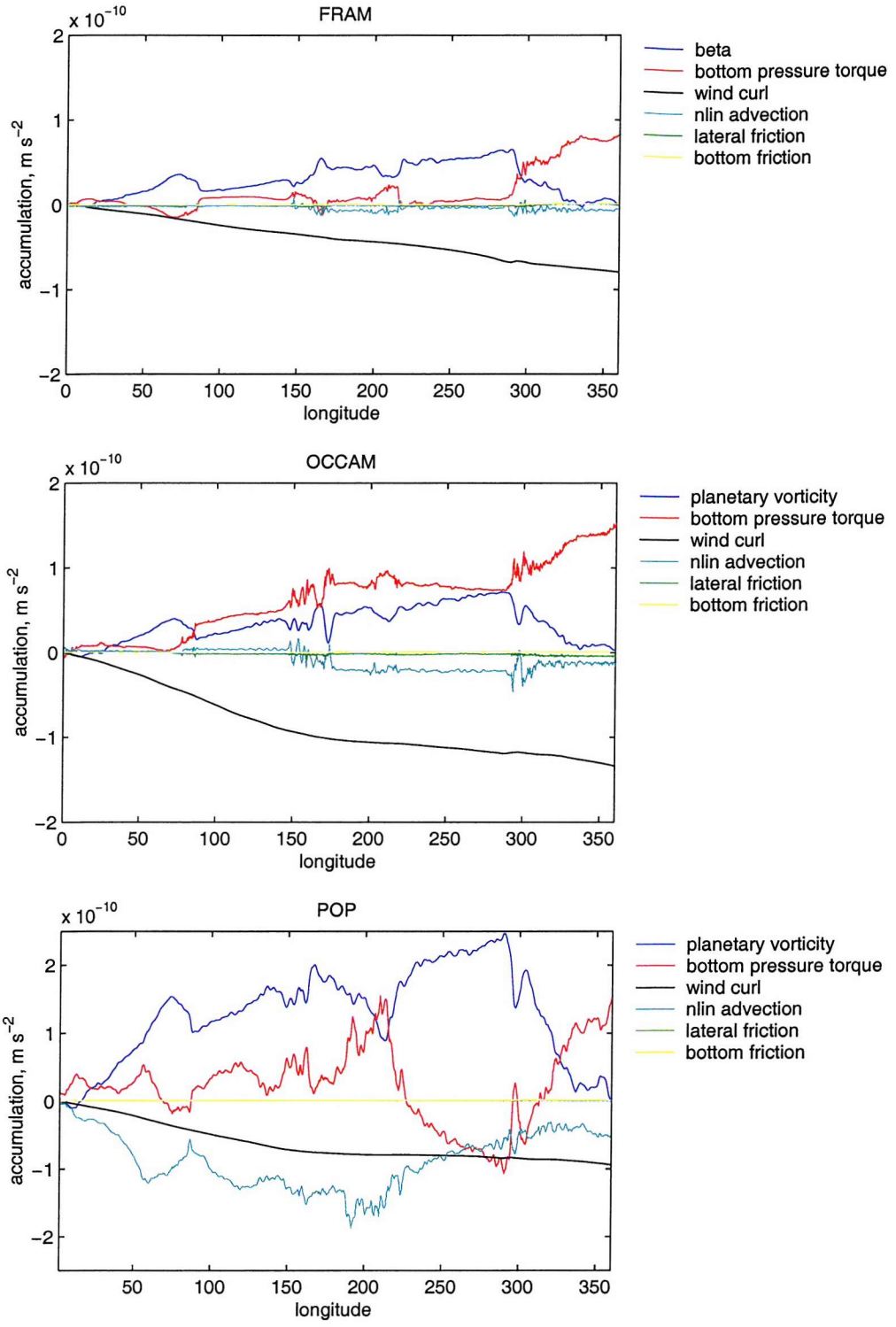

Figure 4.13: *Accumulated time mean area averaged depth integrated vorticity budgets in FRAM, OCCAM 1/4 and POP in the ACCB*

Drake Passage and above the Maquarie Ridge and the South Pacific Ridge. The accumulated planetary vorticity in POP has higher values compared to FRAM and OCCAM 1/4 and it is also anticorrelated to the bottom pressure torque. Bottom pressure torque presents peaks when the flow is over the most important topographic features (South-East Indian Ridge, Maquarie Ridge, South Pacific Ridge and Drake Passage). In contrast to FRAM and OCCAM 1/4, POP bottom pressure torque is negative in the South Atlantic Basin and in the South Pacific Basin. The other terms are small in POP as it is for the other two models.
The comparison of the area averaged values of bottom pressure torque and non-linear advection in the ACCB in the three models (Figure 4.14 and Figure 4.15) shows that all the models have the strongest signals in correspondence with the major topographic features that the ACC flow crosses.

4.5.2 Time mean area averaged vorticity budget level by level

The time mean area averaged vorticity budget for each level was calculated in the ACCB in OCCAM 1/4. The vorticity balance level by level is plotted in Figure 4.16. The balance in the Ekman layer is between planetary vorticity and wind curl. The flow in the *surface levels* is northward. At the *deep levels* the negative planetary vorticity term can be related to the deep currents flowing southward and associated with the pressure differences across the major topographic ridges. At these levels the southward flow balances the northward flow of the surface. At *very deep levels* the balance is between the same two terms but the direction

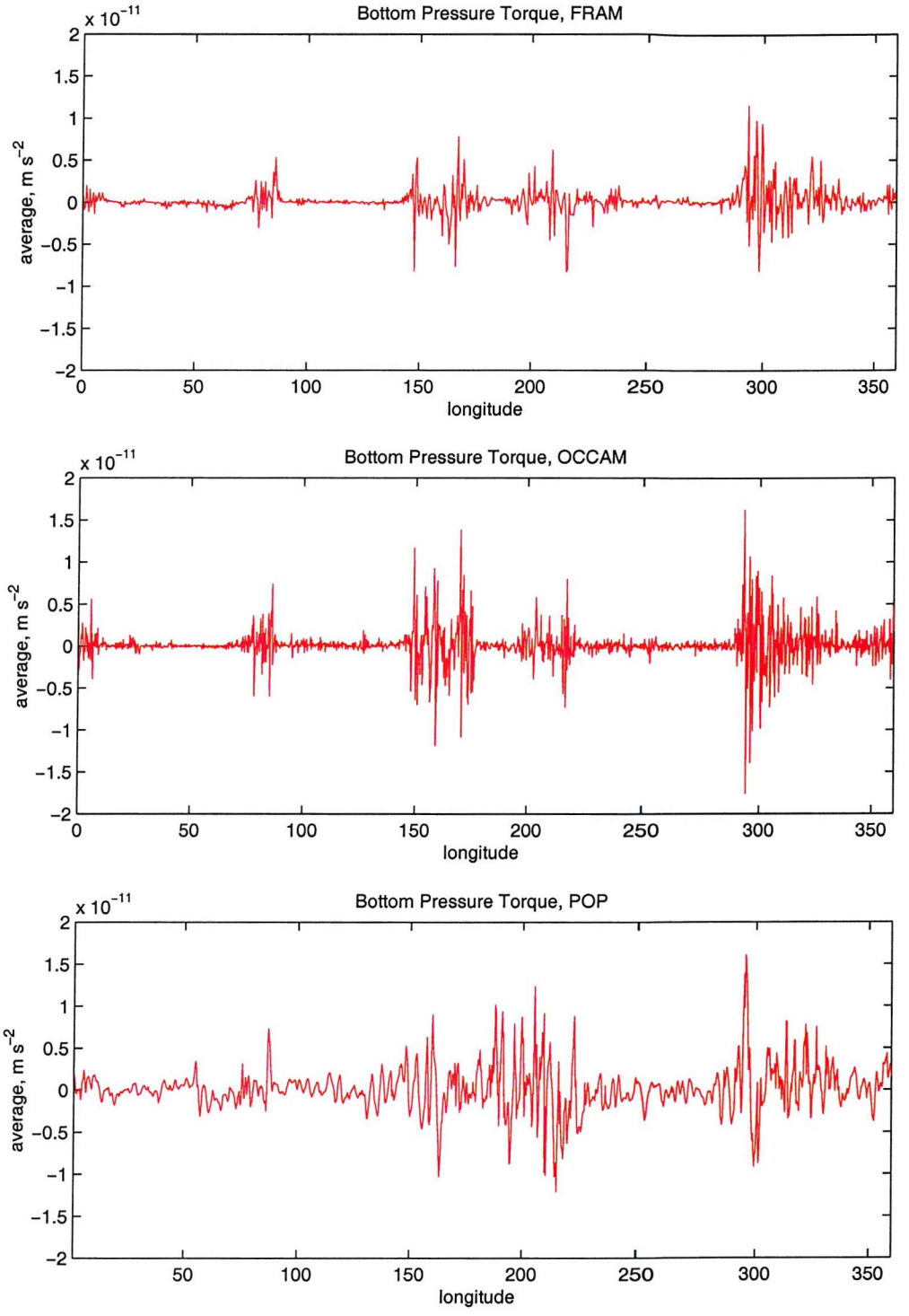

Figure 4.14: *Time mean meridionally averaged depth integrated bottom pressure torque in FRAM, OCCAM 1/4 and POP in the ACCB*

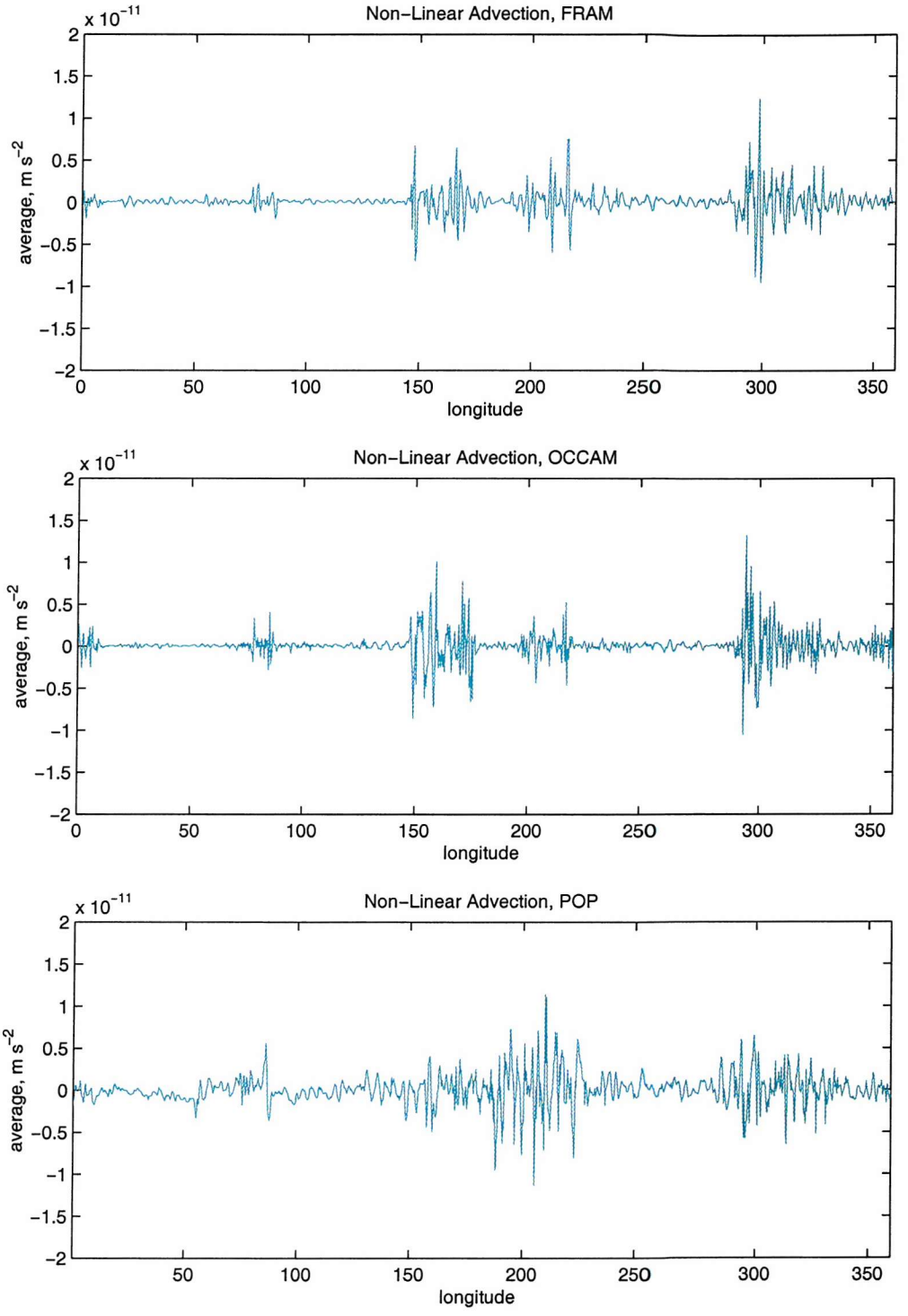

Figure 4.15: *Time mean meridionally averaged depth integrated non-linear advection in FRAM, OCCAM 1/4 and POP in the ACCB*

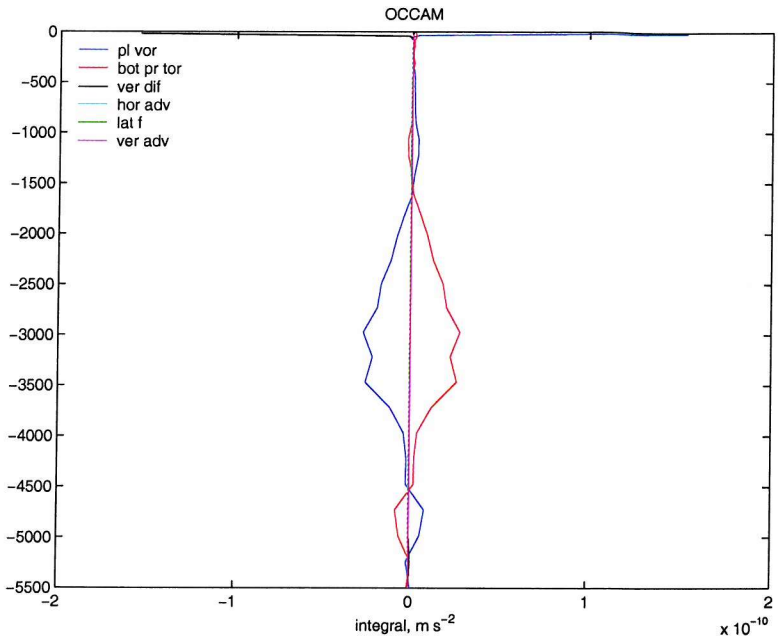

Figure 4.16: *Time mean area averaged vorticity budget level by level in OCCAM 1/4 in the ACCB*

of the flow is the opposite. This can be associated with a northward flow of the AABW. In order to see the contributions of southward and northward current in each basin the level by level analysis is split in four parts (Figure 4.17). In each region the main balance is similar to the Figure 4.16. However, in the region between the Indian Ridge and the South Pacific Ridge in the upper layers the wind curl is less intense than in other basins. The greatest contribution to the northward flow in the deep levels occur in the South-East Pacific Sector (between Indian Ridge and South Pacific Ridge) and in the South-West Pacific Sector (between South Pacific Ridge and Drake Passage).

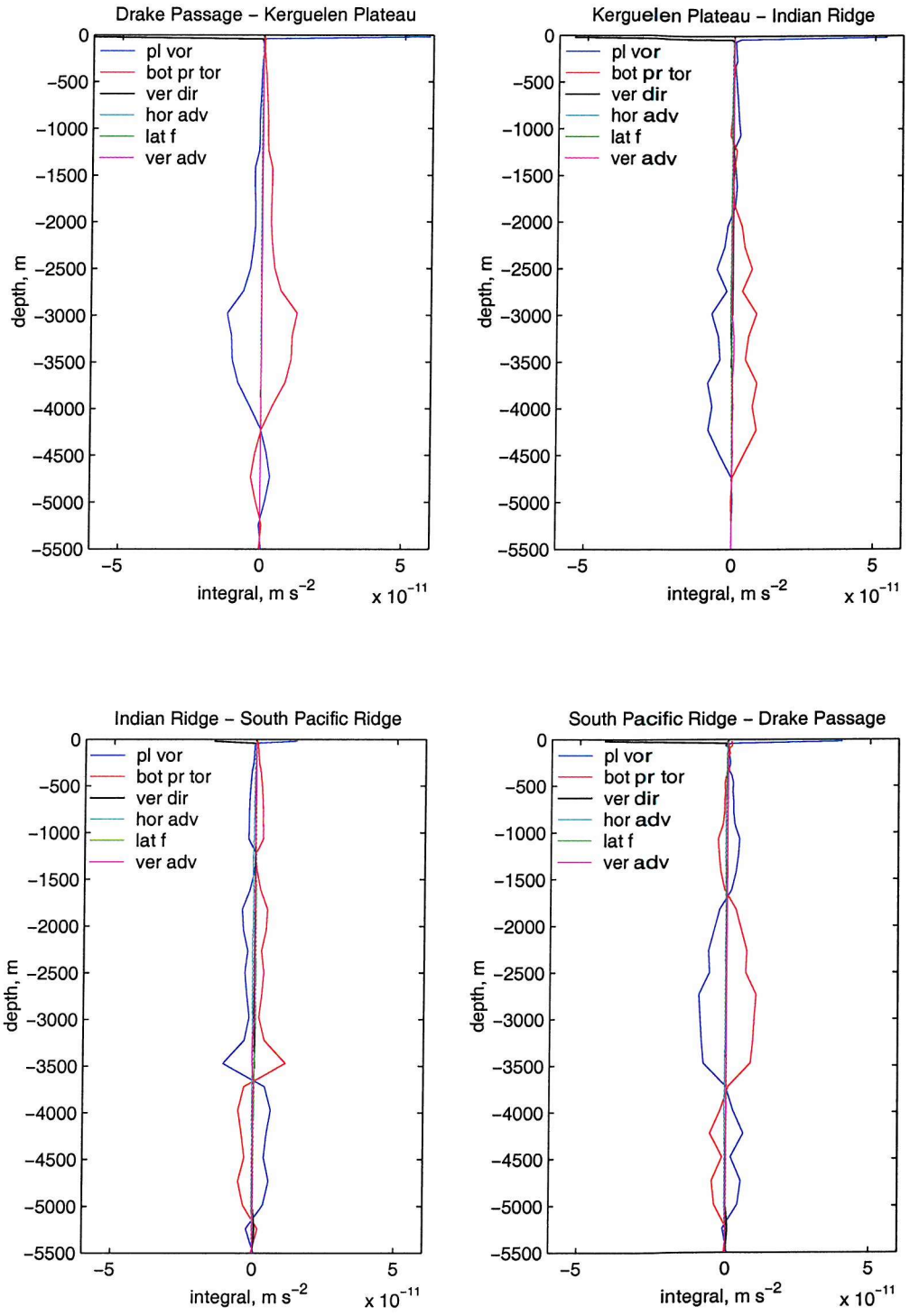

Figure 4.17: *Time mean area averaged vorticity budget level by level in OCCAM 1/4 in the ACCB in the South Atlantic Sector, South Indian Sector, South-East Pacific Sector and South-West Pacific Sector*

4.6 ACC volume transport

Cunningham (2001) states that the error in Drake Passage transport gives an ACC volume transport in a range between 107 and 161 Sv in a review of volume transport estimates at Drake Passage by Whitworth (1980), Whitworth (1983), Whitworth and Peterson (1985). Both OCCAM 1/4 and POP models presents volume transport in acceptable ranges, whilst FRAM overestimate the absolute ACC transport. At the Drake Passage 125 Sv is above 2500 m and 9 Sv below 2500 m with an error between ±27 Sv (Cunningham (2001)). The overestimated absolute transport in FRAM comes from the barotropic mode and the averaged FRAM baroclinic transport relative to 2500 m is in a range of 83-98 Sv at the Drake Passage (Grose et al. (1995)). The volume transports above 2500 m in OCCAM and POP are respectively 137.9 Sv and 116.1 Sv.

Recent works indicate that the ACC volume transport is not set by the wind curl in the Southern Ocean (Gnanadesikan and Hallberg (2000)), Gent et al. (2001) and Gille et al. (2001)). The simple idea of a Sverdrup balance linking the ACC volume transport to the wind curl is investigated in OGCMs. In order to quantify the non-sverdrup flow far from the Drake Passage region in the ACCB we use two approaches.

Firstly, we simply calculated the ACC volume transport from the Sverdrup balance

$$V = \frac{1}{\beta \rho_0} \mathbf{k} \cdot (\nabla \times \tau) \tag{4.7}$$

using the time mean velocity and wind curl fields in FRAM, OCCAM 1/4 and POP. In this case the sector is the portion of the parallel between 320 E and 290 E at 55 S which excludes the Drake Passage region (Table 4.5). In FRAM, OCCAM

Sv	**FRAM**	**OCCAM 1/4**	**POP**
V	126.1	124.7	101.6
$\frac{1}{\beta\rho_0}\mathbf{k}\cdot(\nabla\times\tau)$	122.4	121.8	64.8
Volume transport at the Drake Passage	184	152	134

Table 4.5: *Volume transport in the sector (320 E -290 E) at 55 S in FRAM, OCCAM 1/4 and POP*

1/4 and POP the total volume transport at the Drake Passage is not determined by the wind curl as suggested by Stommel (1957) and Baker (1982). Moreover, Baker's calculations were affected by large error (30 %). The wind curl values in OCCAM 1/4 and FRAM are surprisingly similar to the meridional volume transport at 55 S. However, the variations with latitude of H-R and ECMWF wind curl indicates this is a fortuitous case at 55 S. Furthermore, the POP values prove that the two terms are not in Sverdrup balance.

Secondly, we calculated the time mean area averaged depth integrated vorticity budget in FRAM, OCCAM 1/4 and POP. In order to have a more complete analysis the sector in this case is taken as a portion of the the ACCB between 320 E and 290 E (Table 4.6). The main differences between these three models is the wind forcing. H-R wind field is weaker than ECMWF wind field, but the resulting ACC transport at Drake Passage is 1/3 more than expected in FRAM. In FRAM the major terms in the sector are planetary vorticity and wind curl. In the models with higher resolution and stronger wind curl the Sverdrup balance clearly does not hold far from the Drake Passage region, confirming the results from the previous section.

$\times 10^{-12} ms^{-2}$	**FRAM**	**OCCAM 1/4**	**POP**
planetary vorticity	51.219	49.219	62.432
non-linear advection	- 6.690	- 27.526	- 73.676
bottom pressure torque	37.187	127.196	102.438
lateral friction	- 1.690	- 3.837	- 0.274
wind curl	- 81.832	-143.859	- 91.122
bottom friction	- 0.001	0.972	0.202
RHSV	- 1.807	2.165	0.000

Table 4.6: *Time mean area averaged depth integrated vorticity budget in the sector (320 E - 290 E) in FRAM, OCCAM 1/4 and POP in the ACCB*

4.7 Summary

In this chapter the ACC dynamics is investigated in the ACCB. The source of momentum in the ACCB is the wind stress at the surface and the sink of momentum is the bottom form stress at the bottom in OGCMs. Bottom form stress is more active in the deep levels where the pressure gradients acts in order to retard the flow. The role of transient eddies presents contradictory behaviour in FRAM, OCCAM 1/4 and POP models. The transient eddies accelerate the flow in the upper levels in FRAM and POP and decelerate the flow in OCCAM 1/4. This contradiction is due to the different representation of the momentum flux in the models. However, all the OGCMs show that the eddy activity is more intense in the upper levels. Standing eddies mainly decelerate the flow and

transient eddies decelerate the flow at levels where the topography blocks the flow in the models with higher resolution (OCCAM 1/4 and POP). The vorticity budgets show a main balance between bottom pressure torque and wind curl in all the OGCMs. However, in the higher resolution models there is no Sverdrup dynamics applicable to the regions far from the Drake Passage. The bottom pressure torque and the non-linear advection are significant terms also in the other regions where topographic features are present. Finally, the analysis of the ACC volume transport in the sector between 320 E and 290 E establishes that the volume transport through the Drake Passage is not determined by the wind curl.

Chapter 5

Effects of eddy mixing parameterization on the ACC dynamics

5.1 Introduction

In the previous chapter the importance of resolution in OGCMs was investigated in order to understand the effects of eddies on the ACCB dynamics. An ocean model able to resolve the eddies and the internal Rossby radius of deformation should have a horizontal resolution of the order of magnitude of a few km, a vertical resolution of greater than 40 levels and a time integration of thousands of years to reach an equilibrium state (Bryan et al. (1998)). This ideal situation is not possible with present computer resources. If a number of numerical experiments are required, as it was planned in this research for the investigations of the topographic effects on the ACC dynamics, the use of a coarse resolution model

is necessary. The advantage of using a coarse version is that the model can run in a shorter computational time compared with a higher resolution model and a variety of numerical experiments can be performed. In OCCAM 1 × 1 eddies need to be parametrized. Because the conventional parameterisation of momentum and tracers affects the representation of the large scale ocean circulation, as soon as the GM parameterisation was included in OCCAM 1 × 1 the effects of eddy mixing parameterization in the model was investigated. A comparison between OCCAM 1/4, OCCAM 1 × 1 using Gent P.R. and McWilliams J.C. (1990) parameterisation (here and after OCCAM GM) and OCCAM 1 × 1 using a standard eddy mixing parameterization (here and after OCCAM Am) is carried out in this chapter.

5.2 Sensitivity of the volume transport at the Drake Passage to the eddy mixing parameterization

The ACC volume transport at Drake Passage in OCCAM 1/4, OCCAM Am and OCCAM GM is shown in Figure 5.1. After 9 years integration OCCAM GM and OCCAM 1/4 volume transport are both between 144 and 158 Sv. OCCAM GM reaches an equilibrium state in the last 3 years. The mean volume transport from year 6 to year 9 is 150.8 Sv, a value comparable to the total transport at the Drake Passage in OCCAM 1/4 from year 8 to year 11 (152 Sv). OCCAM Am presents a decreasing trend in the ACC volume transport at the Drake Passage

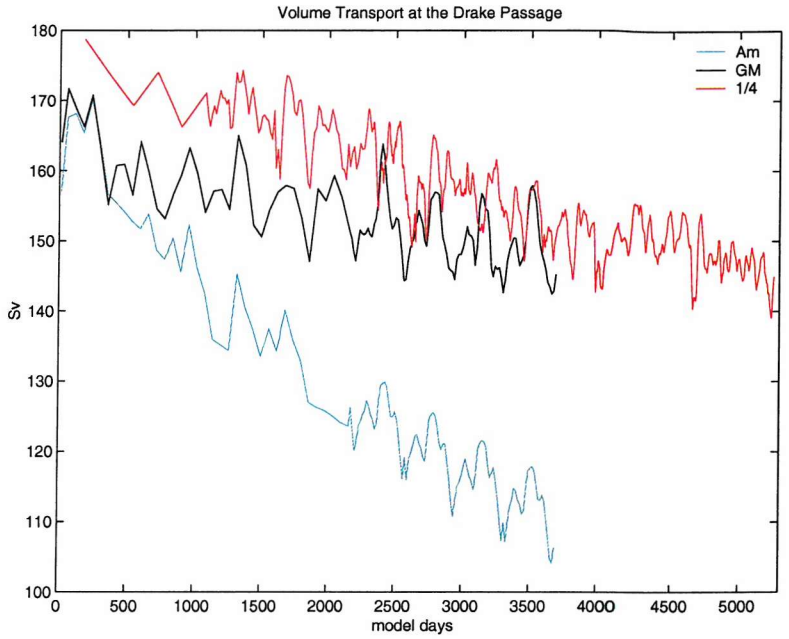

Figure 5.1: *Volume transport at the Drake Passage in OCCAM 1/4, OCCAM GM and OCCAM Am*

and there is no steady state after 10 years. Apart from the decreasing trend, in OCCAM Am a well repeated cycle can be recognised, due to the zonal wind stress field in the Southern Ocean. A maximum value of the volume transport occurs in spring (around September) and a peak occurs in autumn (around April). The lowest absolute transports are found in summer. OCCAM 1/4 volume transport and OCCAM GM do not present a similar cycle. Gent et al. (2001) and Gnanadesikan and Hallberg (2000) discussed how representation of eddies can set the ACC volume transport. The dominant effects of eddies is to mix warm water and cold water along isopycnal surfaces rather than horizontally. The effect of this mixing is a density transformation which induces changes in the meridional density gradients. As a result, changes in the vertical shear of zonal velocities and variation

of mass transport occur. This can explain why OCCAM 1/4 with the highest resolution does not follow any regular cycle.

OCCAM Am understimates the net transport through the Drake Passage. Danabasoglu et al. (1994) applied the standard eddy mixing parameterisation and the GM parameterization to a coarse resolution model, which was in an equilibrium state after 10,000 years. In their model the ACC volume transport was overestimated in the standard eddy mixing parameterisation than the GM parameterization. This decreasing trend in the ACC volume transport in OCCAM AM could be the incomplete adjustment of the baroclinic fields which involves a time longer than 10 years integration.

5.3 ACC flow in the Southern Ocean in coarse models

A global view of the ACC flow is given by the time mean vertically integrated mass transport streamfunctions in each version of OCCAM (Figure 5.2). They were calculated over 4 years of the model integration (from year 8 to 11 inclusive in OCCAM 1/4 and from year 6 to 9 inclusive in OCCAM AM and OCCAM GM). Those ranges of years have been considered the equilibrium state of OCCAM 1/4 and OCCAM GM and all comparisons between the time mean fields are made over this periods. The equilibrium state can be recognised observing the total kinetic energy (KE) of the model and the rate of change of the tracers (salinity and temperature) (Figure 5.3). The spin up phase of these runs is in the first year. The KE in OCCAM 1/4 is the highest in the set of OCCAM ver-

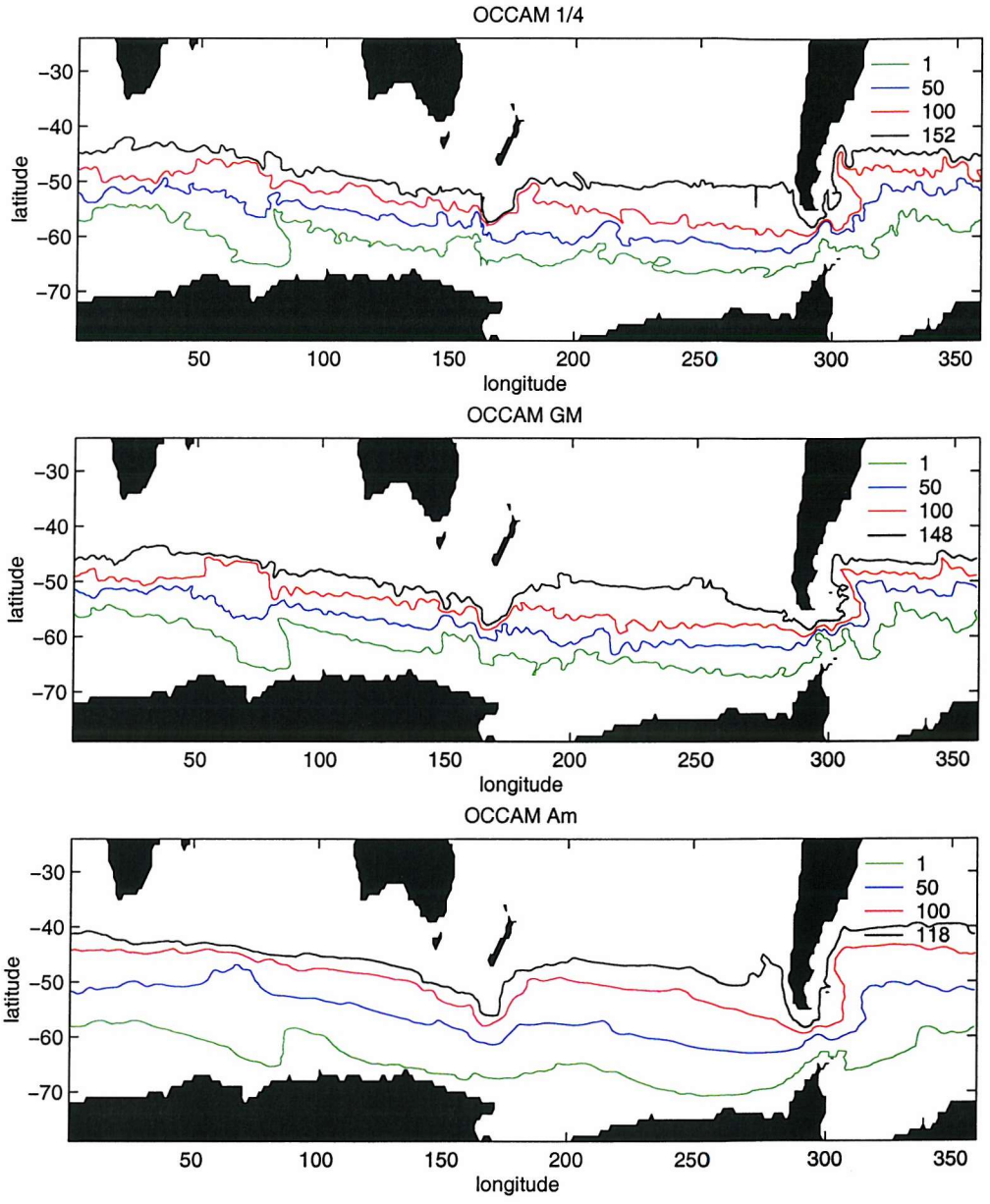

Figure 5.2: *Streamfunctions (Sv) in OCCAM 1/4, OCCAM GM and OCCAM Am*

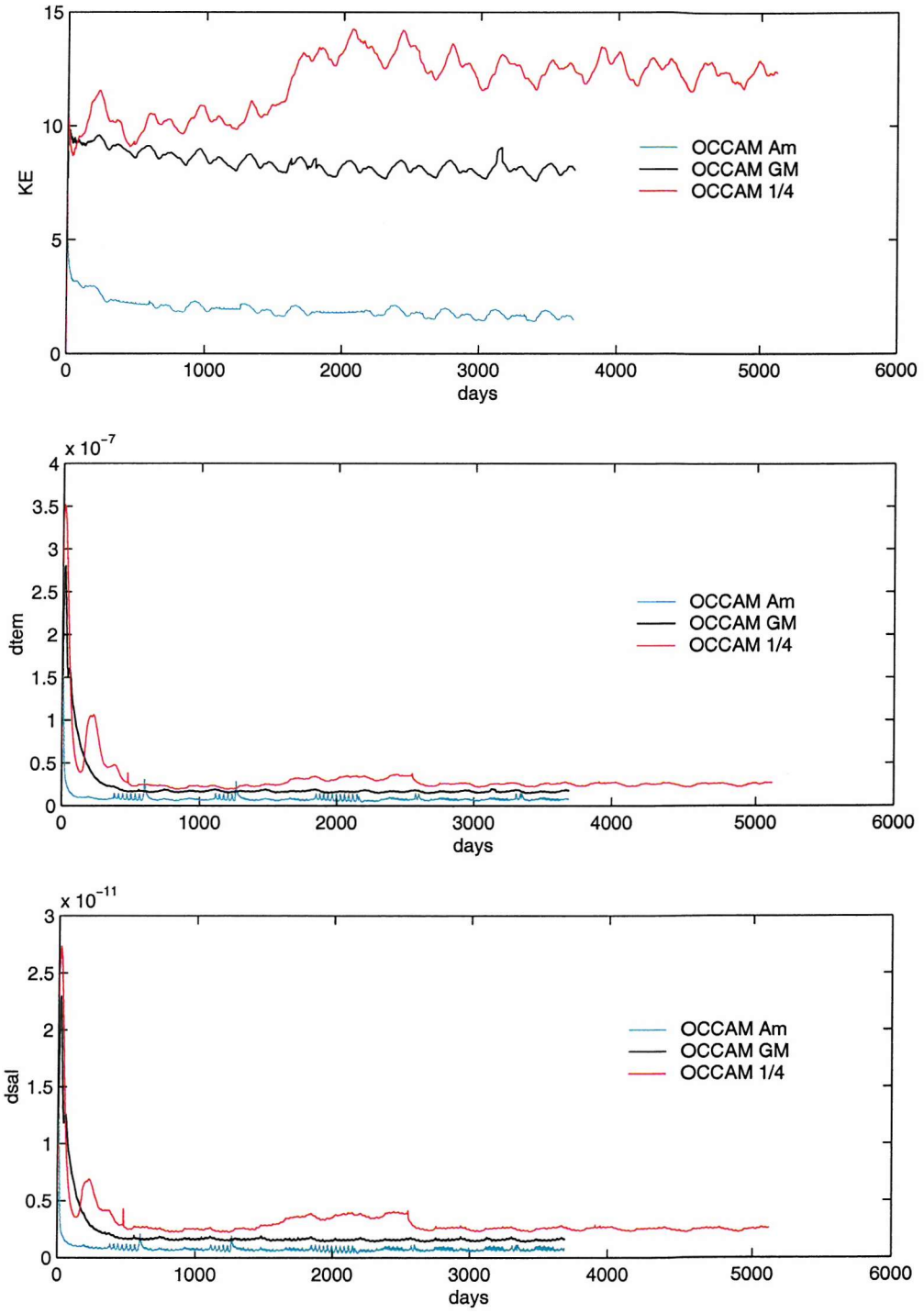

Figure 5.3: *Kinetic energy, rate of change of temperature and salinity in OCCAM 1/4, OCCAM GM and OCCAM Am*

sions because of the highest eddy activity of the model and OCCAM Am is the lowest due to the poor eddy activity. On the other hand, OCCAM GM presents significantly higher KE values compared to OCCAM Am and this is due to the Gent P.R. and McWilliams J.C. (1990) parameterisation. The divergence-free eddy-induced velocity in the GM parameterisation incorporates that aspect of baroclinic eddies representing the transfer of available potential energy to eddy kinetic energy Griffies (1998).

In the case of OCCAM Am the lack of eddy activity affects the ACCP, which is defined by the streamfunctions 1 Sv and 118 Sv. The ACCP is wider and smoother in OCCAM AM compared to OCCAM GM and OCCAM 1/4. The ACCP in OCCAM GM reproduces quite well the meandering of the ACCP and the major structures of the ACC as found in OCCAM 1/4. However, we can recognise some discrepancies between OCCAM GM and OCCAM 1/4 in the Drake Passage region, South of New Zealand and over Kerguelen Plateau, which are the regions with the highest eddy activity.

5.4 Momentum budgets and Vorticity budgets

5.4.1 Momentum budgets and Vorticity budgets in the ACCB

The time mean area averaged depth integrated momentum budgets were calculated in the ACCB in OCCAM Am and OCCAM GM. The time mean involves the last 4 years of the model integration. The main balance is between the wind

stress and the bottom form stress in all cases as it was for OCCAM 1/4 (Table 5.1). The time mean area averaged depth integrated vorticity budgets were

$\times 10e^{-3}Nm^{-2}$	**OCCAM GM**	**OCCAM Am**
Coriolis term	- 2.319	- 1.969
momentum flux divergence	0.206	0.126
bottom form stress	-110.907	-105.025
horizontal mixing	- 0.059	- 0.011
wind stress	113.359	113.359
bottom stress	- 0.434	- 0.199
RHSM	- 0.154	6.281

Table 5.1: *Time mean area averaged depth integrated momentum budget in OCCAM GM and OCCAM Am in the ACCB*

calculated in the ACCB in OCCAM Am and OCCAM GM and compared with OCCAM 1/4. The main balance is between the wind stress and the bottom form stress in all cases (Table 5.2). However non-linear advection term is reduced by one order in the coarse version OCCAM Am and by 40 % in OCCAM GM compared to OCCAM 1/4. This is consistent with the results of the previous chapter. In OCCAM GM the momentum and vorticity budgets do not include the eddy-induced transport velocity $\mathbf{u}*$. This velocity is necessary only for the advection of tracers in order to parameterize the eddy effects. These effects are present in the large scale flow through the density distribution and in the equations of motion through the horizontal pressure gradient terms.

$\times 10e^{-12}ms^{-2}$	OCCAM GM	OCCAM AM
planetary vorticity	2.133	2.254
non-linear advection	- 6.047	- 0.993
bottom pressure torque	133.753	124.900
lateral friction	0.285	0.051
wind curl	-130.281	-130.281
bottom friction	0.767	0.126
RHSV	0.610	- 3.943

Table 5.2: *Time mean area averaged depth integrated vorticity budget in OCCAM GM and OCCAM Am in the ACCB*

5.4.2 Vorticity budgets in the ACCP

In order to have a more complete analysis, vorticity budgets were calculated in the ACCP also, which is defined by the streamfunctions through the Drake Passage (Figure 5.2).

The main balance between wind curl and bottom pressure torque confirms the results of the previous section. In all numerical experiments the wind field applied was the monthly mean ECMWF, however Table 5.3 shows different values of wind curl in the ACCP. In OCCAM Am the calculation of the wind curl involves a different area compared to OCCAM GM because of the different path of the ACC. The rate of change of vorticity (RHSV) is one of the major terms indicating that over the last four years the flow is not in steady state. In the accumulations of the time mean area averaged depth integrated vorticity budgets the main balances are between bottom form stress, wind curl and planetary vorticity in the ACCB

$\times 10e^{-12}ms^{-2}$	OCCAM GM	OCCAM AM
planetary vorticity	- 0.136	- 0.774
non-linear advection	5.887	0.223
bottom pressure torque	59.138	37.985
lateral friction	- 1.357	- 0.396
wind curl	- 65.598	- 48.215
bottom friction	0.093	0.140
RHSV	- 1.973	- 11.037

Table 5.3: *Time mean area averaged depth integrated vorticity budget in OCCAM GM and OCCAM Am in the ACCP*

(Figure 5.4). A small contribution to the balance is from the non-linear advection in OCCAM GM. The most interesting term in the accumulated budgets is the bottom pressure torque. The bottom pressure torque is not a leading term in the OCCAM Am vorticity budget outside Drake Passage and a Sverdrup-like balance is held over the ACCP in the regions far from the Drake Passage and the Weddell Sea.

5.5 Meridional overturning streamfunction in the Southern Ocean in coarse models

The meridional overturning streamfunctions

$$\psi(\varphi, z) = \int_{-H}^{h} \int_{0}^{2\pi} v(\lambda, \varphi, z') R \cos\varphi d\lambda dz' \tag{5.1}$$

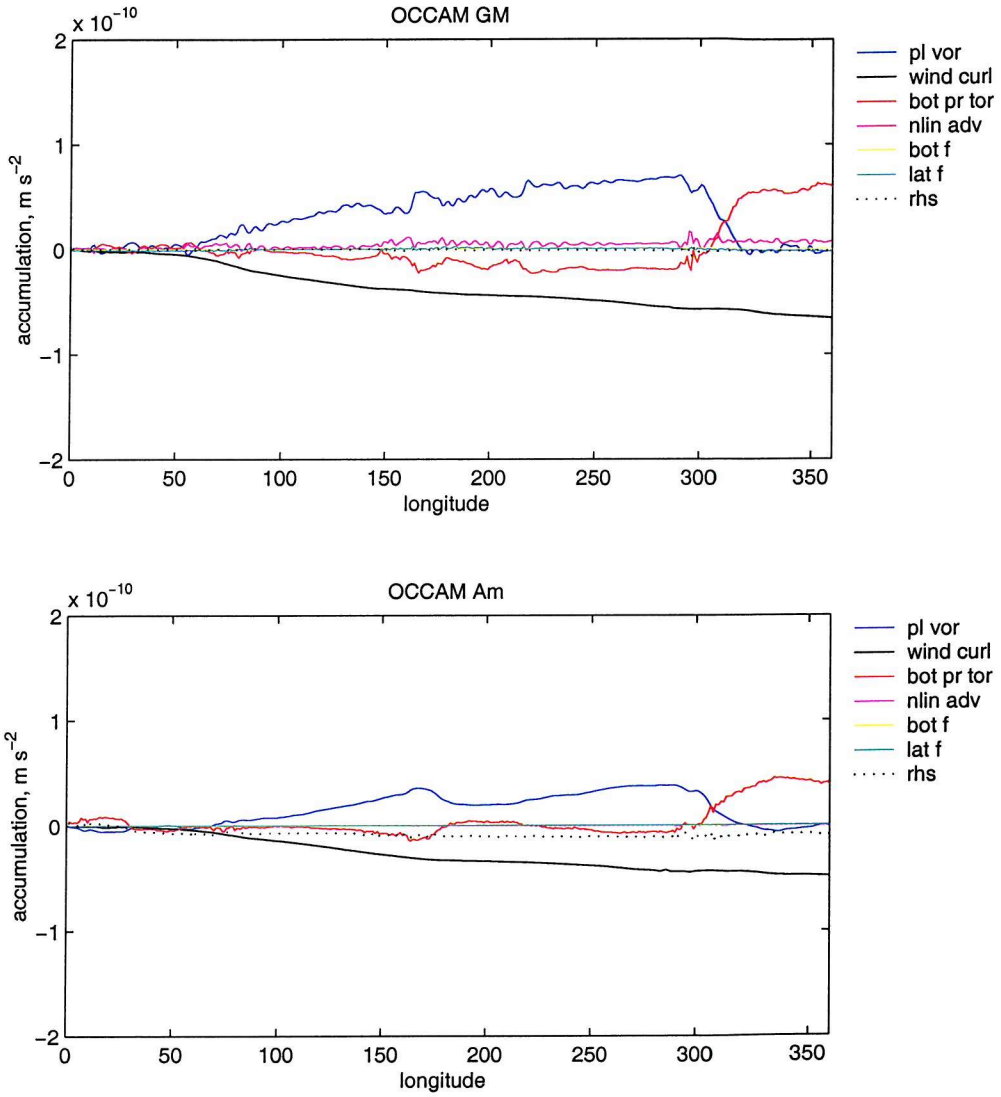

Figure 5.4: *Accumulated time mean area averaged depth integrated vorticity budget in the ACCP in OCCAM GM and OCCAM Am*

were calculated in OCCAM 1/4, OCCAM GM and OCCAM Am. They show the Sub-Tropical Cell in the upper levels between 24 S and 30 S, the Deacon Cell between 40 and 65 S in the upper 3500 m depth, the Sub-Polar Cell between 24 and 65 S in the range of depth 500 m and 3500 m and and the Deep Cell between 24 and 55 from 3500 m to 5000 m (Figure 5.5). The streamfunctions close the cells in the very superficial levels (not shown).

OCCAM GM reproduces those features even if the southward flow is weaker than OCCAM 1/4 in the deep levels and at 55 S. In OCCAM GM the overturning streamfunction from the meridional component of the eddy-induced transport velocity $v*$ (Figure 5.6) and the overturning streamfuction from the effective transport velocity $(v + v*)$ (Figure 5.7) were calculated. The meridional eddy-induced transport velocity produces a general weakening of the Deacon Cell in the Southern Ocean as also found by England and Rahmstorf (1999).

In OCCAM Am the Deacon Cell is even weaker than the one in OCCAM GM and OCCAM 1/4 and the southward Deep Cell spans between 1770 and 5000 m at 30 S. A southward flow of 4 Sv can be recognised at levels between 500 and 3500 m. Associated with this general strengthening of the southward flow there are the erosion and the lowering of the thermocline (Figure 5.8).

The general structure of the water masses and meridional flow in the Southern Ocean is deeply changed in the OCCAM Am version produced by the strong eddy viscosity. Similar results were recognised by Danabasoglu et al. (1994) who compared the case of conventional parameterization of tracers with the case of GM parameterization. In the first case they found an unrealistic extensive upwelling near 60 S that weakens the density stratification and enhances convection. In the second case the upwelling was weaker and there was much less convection. On

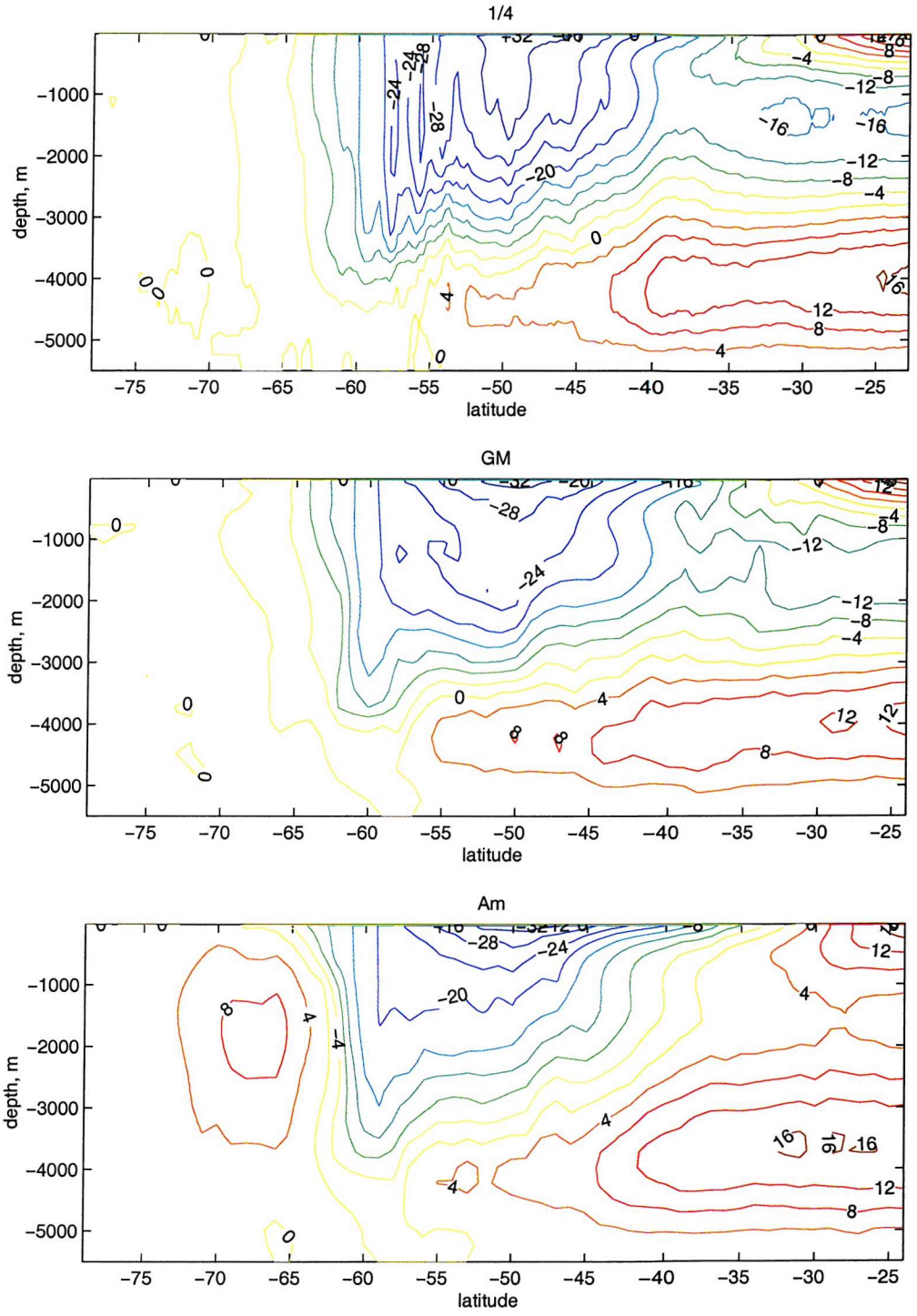

Figure 5.5: *Overturning stream function (Sv) in OCCAM 1/4, OCCAM GM and OCCAM Am*

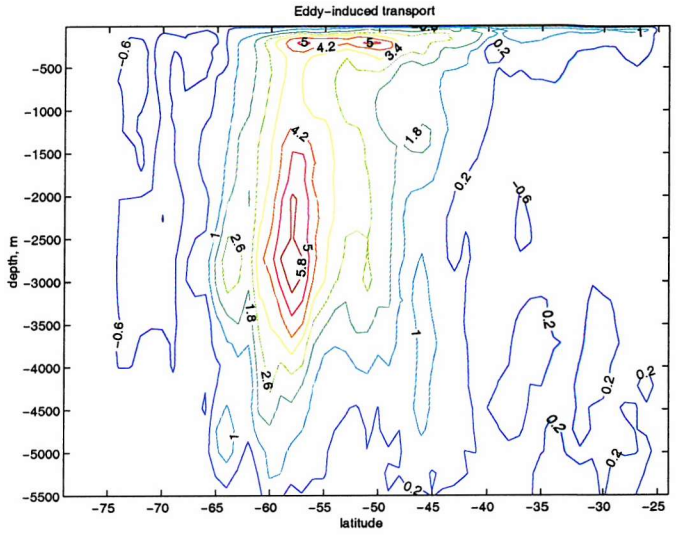

Figure 5.6: *Overturning stream function (Sv) from the eddy-induced transport velocity v* in OCCAM GM*

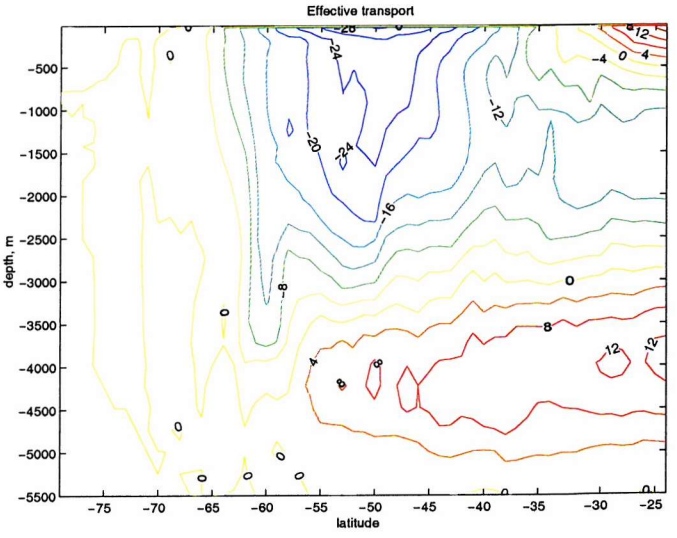

Figure 5.7: *Overturning stream function from the effective transport velocity* $(v + v*)$ *(Sv) in OCCAM GM*

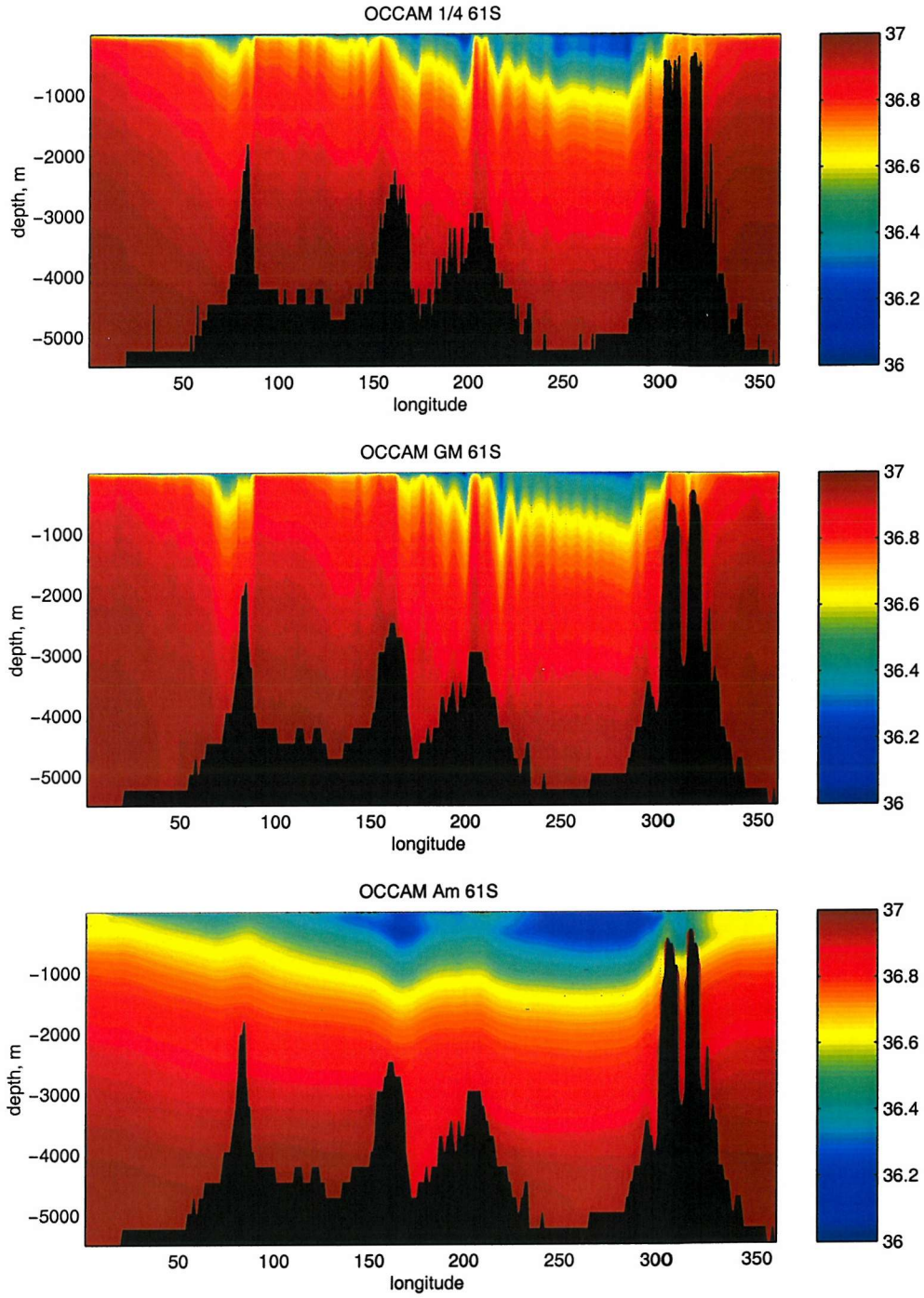

Figure 5.8: *Potential density in OCCAM 1/4, OCCAM GM and OCCAM Am (level of reference: about 2000 m)* (Kgm^{-3})

the other hand, in a recent paper Sorensen et al. (2001) pointed out that while the midlatitude convection is exaggerated in the standard parameterization it may be underestimated in the GM parameterisation. Figure 5.8 shows that levels between 300-600 m depth in OCCAM GM are denser than in OCCAM 1/4 in particular in the South Pacific Ocean (Table 5.4). Despite this discrepancy in the upper levels, the deeper levels in OCCAM GM present values consistent with OCCAM 1/4.

Kgm^{-3}	**OCCAM 1/4**	**OCCAM GM**	**OCCAM Am**
at 389 m	36.3030	36.4494	36.1935
at 3224 m	36.8926	36.8962	36.8699

Table 5.4: *Potential density in OCCAM 1/4, OCCAM GM and OCCAM Am (level of reference: about 2000 m)*

5.6 Summary

In this chapter the ACC dynamics in the ACCB and ACCP has been investigated in a coarse resolution model. The eddy resolution and the eddy parameterization affects the ACC volume transport through the Drake Passage. In the case of a standard eddy parameterization the ACC volume transport presents a decreasing trend and there is no equilibrium state. In the coarse resolution models the volume transport presents an annual cycle. This cycle is not present in the highest resolution version of OCCAM. Despite the different parameterizations all the models show a main balance between bottom pressure torque and wind curl. The

most important effects of the eddy mixing parameterization are in the vertical structure of the flow and water masses.

Chapter 6

Topographic effects on the ACC dynamics

6.1 Introduction

FRAM, OCCAM 1/4 and POP results pointed out the importance of topographic structures on the ACC flow in the ACCB. In order to investigate the role of topography in the Southern Ocean a set of experiments was performed. The ACC crosses Kerguelen Plateau, South-East Indian Ridge and Antarctic-Pacific Ridge and their depths are comparable to the Drake Passage depth. In particular the analysis is focused on topographic features upstream Drake Passage (Antarctic-Pacific Ridge), downstream Drake Passage (Kerguelen Plateau) and the Drake Passage itself. The study was accomplished using a low resolution version of OCCAM which includes GM parameterization. The advantage of using a 1×1 degree resolution OCCAM is that the model can run in a shorter computational time than OCCAM 1/4.

6.2 The set of numerical experiments

The investigation of topographic effects on the ACC dynamics was carried out modifying three of the most important topographic features in the Southern Ocean and analysing the response of the flow to these changes.

OCCAM GM is considered the control run. The control run was made using realistic topography and the other experiments were made by lowering the topography about 2000 m in the above mentioned regions. Each experiment involved one of the above mentioned regions and topography elsewhere was kept unchanged. When topography was removed the added grid boxes were filled using the interpolated temperature, salinity, baroclinic and barotropic velocities obtained from the surrounding points of the 15th model day. In the very deep levels in the Drake Passage region the surrounding points were land or topography and the new ocean boxes were filled using averaged values over those areas. In these experiments the volume of the ocean has been increased by 0.13% in the case of Kerguelen Plateau, 0.58% in the case of Antarctic-Pacific Ridge and 0.60% in the case of Drake Passage using pre-existent water masses. After about 6 months of integration the spin up phase of the global model was completed. The restarts files were stored with 1 day frequency from model day 15 to model day 45, with 60 days frequency until the 5th model year and then with 15-days frequency. Each experiment was 10 model years of integration and the wind field was ECMWF (years 1986-1988, monthly mean) as it was in the higher resolution OCCAM run. The set of performed experiments is:

• **Control run.** In the control run the topography is at the model resolution (Figure 6.1). The OCCAM 1 × 1 topography reproduces quite well the realistic topography. However, we can recognise in the Drake Passage region that the sill depth through the island arc is changed. The realistic sill which allows the northward ACC flow is at about 3000 m, in the control run this sill is shallower (about 2000 m) than the realistic one. Despite this discrepancy the ACC flow represents quite well the meandering of the ACC and the major structure of all the ACCP.

• **Kerguelen Plateau.** In this experiment the Kerguelen Plateau has been lowered by about 2000 m (the maximum depth in the Kerguelen Plateau region is 3224 m)(Figure 6.1). The importance of the Kerguelen Plateau as a second topographic barrier was recognised by Webb (1993).

• **Antarctic-Pacific Ridge.** In this case the topography was removed (Figure 6.1) and the whole region was at 5244 m. The Antarctic-Pacific Ridge is another region of large variations of bottom pressure torque and eddy activities (Grezio et al. (2001)). In this case observations show (Reid (1986)) that there is an intense meridional flow on the east side of the Antarctic-Pacific Ridge from the Antarctica to 60 S. However, there is a lack of numerical studies about the dynamics around the Antarctic-Pacific Ridge and the role of this meridional flow in the Southern Ocean.

• **Drake Passage Region.**The topography in the Drake Passage region is removed (bottom is at 5244 m). Moreover, in this case also the Scotia Arc and the Falkland Plateau were removed (Figure 6.1). This experiment is complementary to Gill and Bryan (1971)'s experiment. The intention here is to see the role of topography far from the Drake Passage and the effects of these changes on the ACC volume transport using a realistic model.

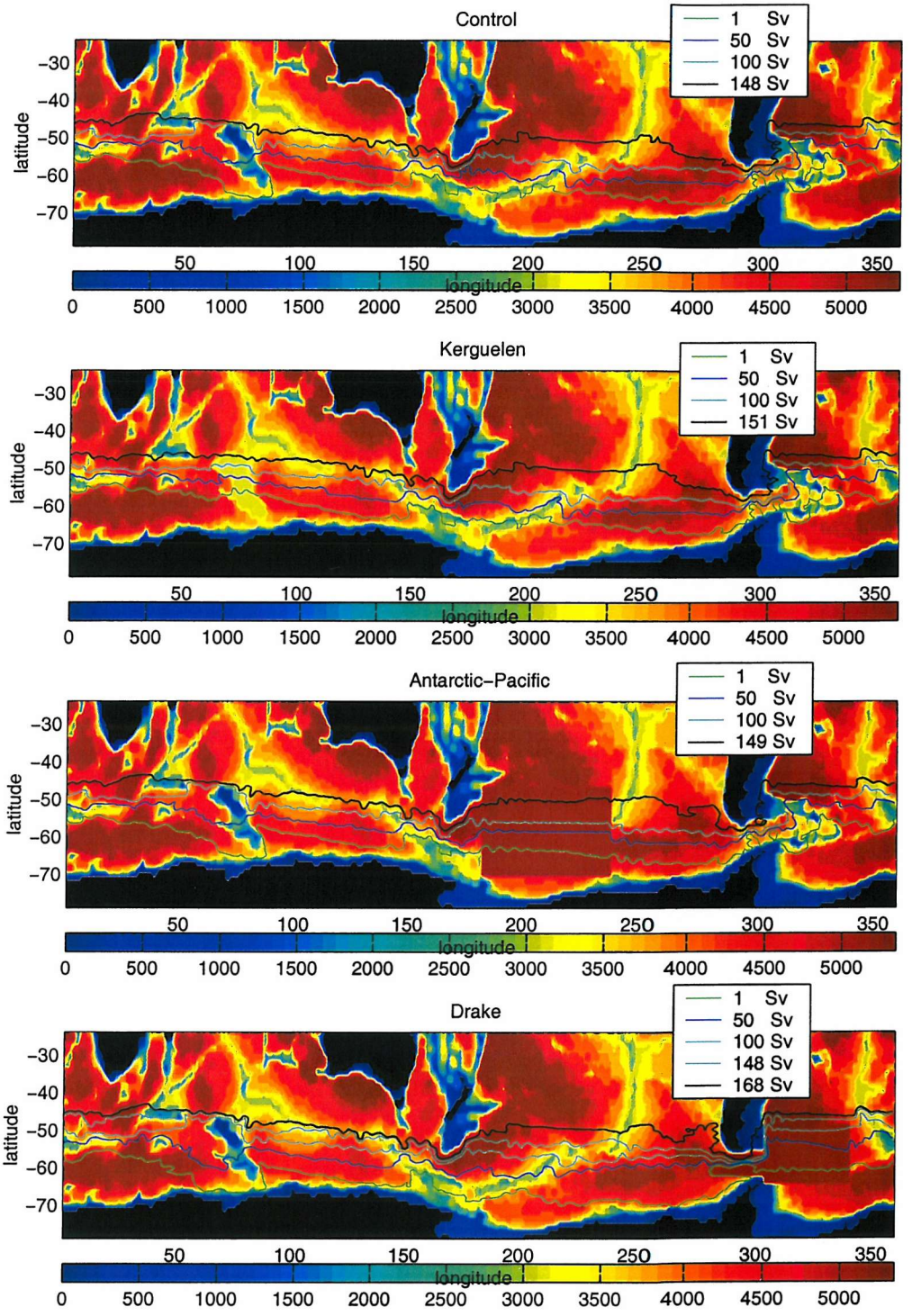

Figure 6.1: *Streamfunctions (Sv) in Control run, Kerguelen Plateau, Antarctic-Pacific Ridge and Drake Passage*

6.3 Spin up and Adjustment to the topographic changes

The model starts with a non-motion ocean and Levitus et al. (1994) initial conditions applied to the temperature and salinity fields. Restoring boundary conditions on heat and freshwater fluxes are applied at the surface with a time scale of 30 days. The spin up is completed in the time required for the Rossby wave to travel all the way across the ocean and in the case of OCCAM 1×1 it is about 6 months in all numerical experiments. The modification of the topography is applied after 15 days model run. Measurements of the ACC transport estimated that the barotropic response of the ACC to a disturbance is about 9 day (Whitworth (1983), Gille et al. (2001)). Models evaluated the barotropic response timescale less than 9 days in the ACC(Clarke (1982)). Then any barotropic response to a topographic change occurs during the spin up of the model. In order to analyse the barotropic response the outputs of the model were stored every day for 30 days. The analysis of the barotropic response to the topographic changes is made considering the model response after 1 day (model day 16), 10 days (model day 25) and 1 year (model day 360) of Kerguelen Plateau, Antarctic-Pacific Ridge and Drake Passage cases and they are compared with the control run case.

• **Spin up of the Control run**

In the *Control run* the ACC flow presents complex meandering after 15 days and a wave-like structure along the path (Figure 6.2). During the first month the flow adjusts and after about 1 year the ACCP develops very similarly to the ACCP found after 10 years.

In this first period the area averaged depth integrated momentum budget in the

ACCB shows that the main balance is between the rate of change of momentum (RHSM), the bottom form stress, the wind stress and the Coriolis term, whereas the momentum flux divergence, the bottom stress and the horizontal mixing are small (Figure 6.3). In this period the Coriolis term has the highest values of the all 10 years of model integration but after 41 days the Coriolis term is about 25% of the value after 15 days. The reduction of the Coriolis term indicates a reduction of the meandering of the flow and an increase of the eastward flow in the ACCB. The bottom form stress is the term in the budget which responds very quickly to the Coriolis term variations in order to retard the flow during the adjustment.

The area averaged and depth integrated vorticity budget in the first 45 days shows a main balance between the rate of change of vorticity (RHSV), bottom pressure torque and wind curl and the other terms in the budget are small (Figure 6.4). The RHSV term and the bottom pressure term are correlated in the spin up phase, showing that all the variation in time of vorticity are associated with the torque due to pressure gradients.

• **Effects of the topographic changes after 1 day**

After 1 day in all cases the ACCP shows the major responses to the topographic perturbations.

In *Kerguelen Plateau* case the ACCP shows a stronger northward propagation of the flow south-west of Australia compared to the control run (Figure 6.5). This is indicated also by the area averaged and depth integrated momentum and vorticity budgets in the ACCB. At this stage the main balance in the momentum equations occurs between Coriolis and pressure gradients at one particular snapshot and the stronger flow is due a stronger pressure gradients at that particular

day compared to the Control run.

Antarctic-Pacific Ridge case also presents a wider northward flow in the South Pacific Basin compared to the Control run (Figure 6.6).

In *Drake Passage* case the ACC flow starts to set the narrow western current in the South Atlantic (Figure 6.7).

• **Effects of the topographic changes after 10 days**

After 10 days the flow in *Kerguelen Plateau* case is less meandering than the Control run and the flow becomes more jet-like over the Kerguelen region compared to the Control run (Figure 6.5).

On the contrary, *Antarctic-Pacific Ridge* case shows complex meanders in the Pacific Basin south-west of South-America and west of the Antarctic Peninsula (Figure 6.6).

Drake Passage case presents a narrower and more intense flow in West South Atlantic Ocean with a persistent wave-like flow (Figure 6.7).

• **Effects of the topographic changes after 1 year**

After 1 year of integration in the all experiments (*Control run*, *Kerguelen Plateau* (Figure 6.5), *Antarctic-Pacific Ridge* (Figure 6.6), *Drake Passage* (Figure 6.7)) the adjustment phase is almost completed and the flow is very similar to the mean flow after 10 years of model integration.

In general, lowering or removing the topography in the Southern Ocean allowed the ACC flow to move northward. The modification of topography produced a flow which does not feel anymore the constraints of bathymetry. This characteristic of the flow appears in the early stage of the model integration and it is preserved also in the stable state in the following years.

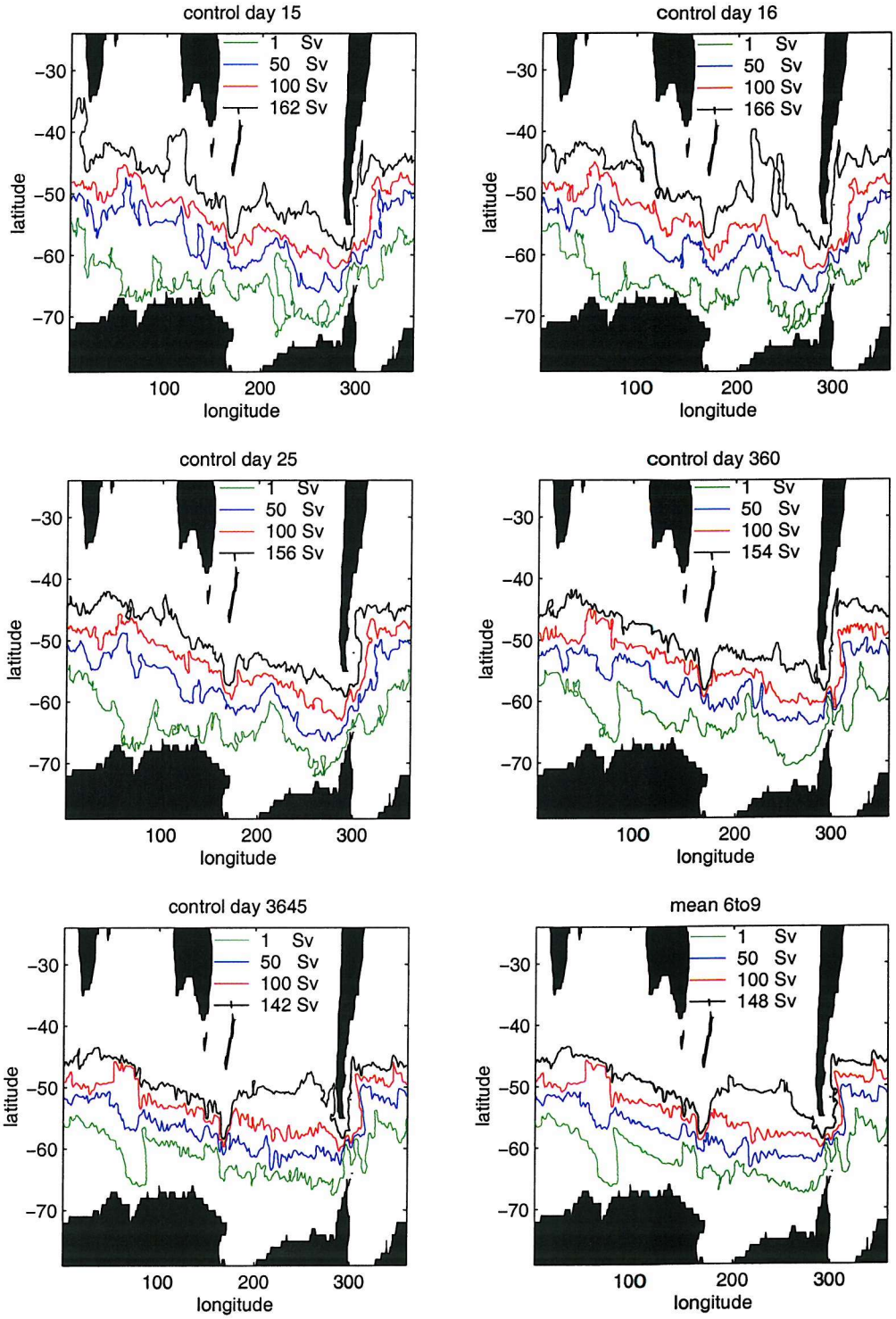

Figure 6.2: *Streamfunctions (Sv) in Control run at day 15, day 16, day 25, day 3645, and mean values from year 6 to year 9*

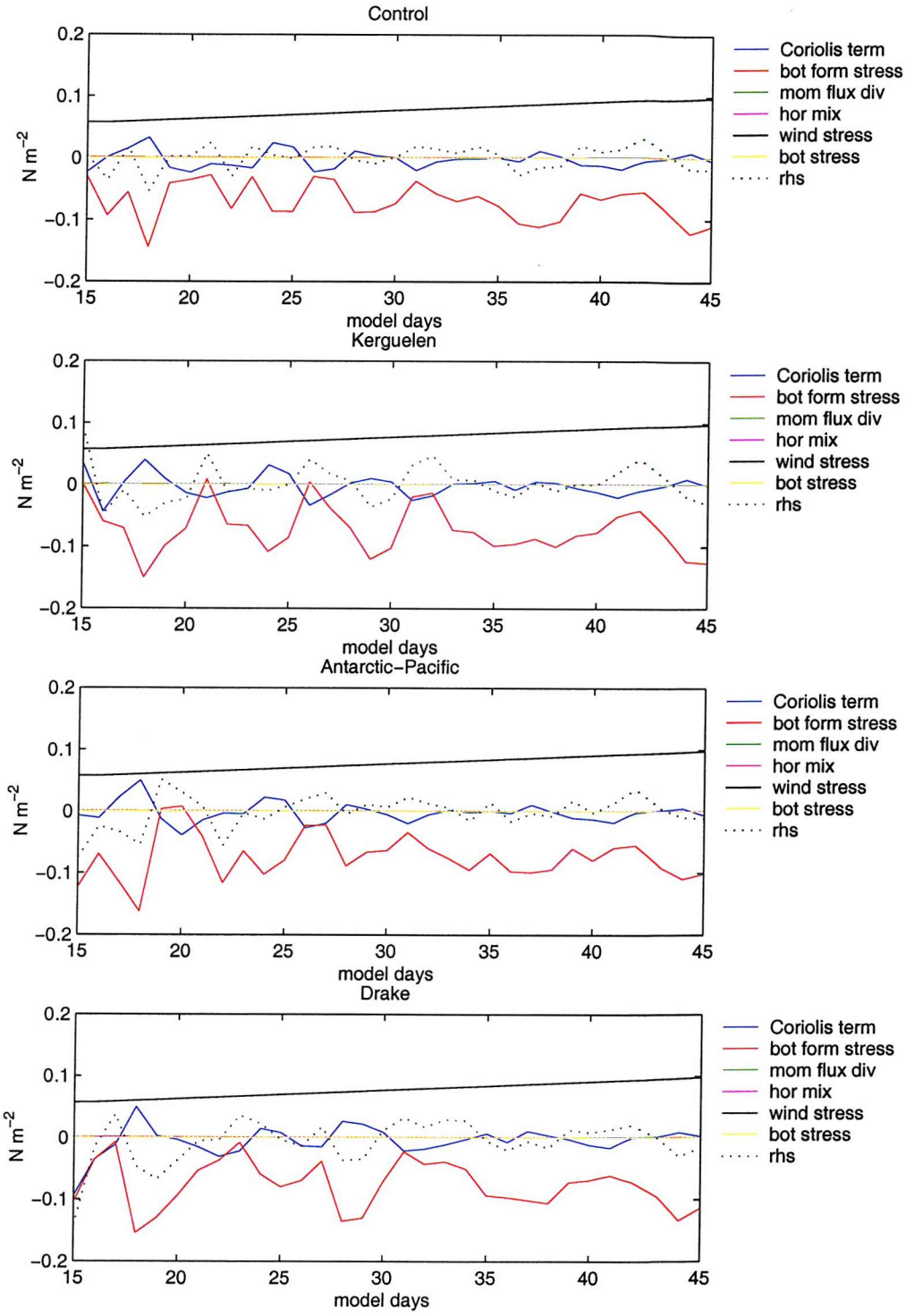

Figure 6.3: *Area averaged depth integrated momentum budget in OCCAM GM, Kerguelen Plateau, Antarctic-Pacific Ridge and Drake Passage in the ACCB*

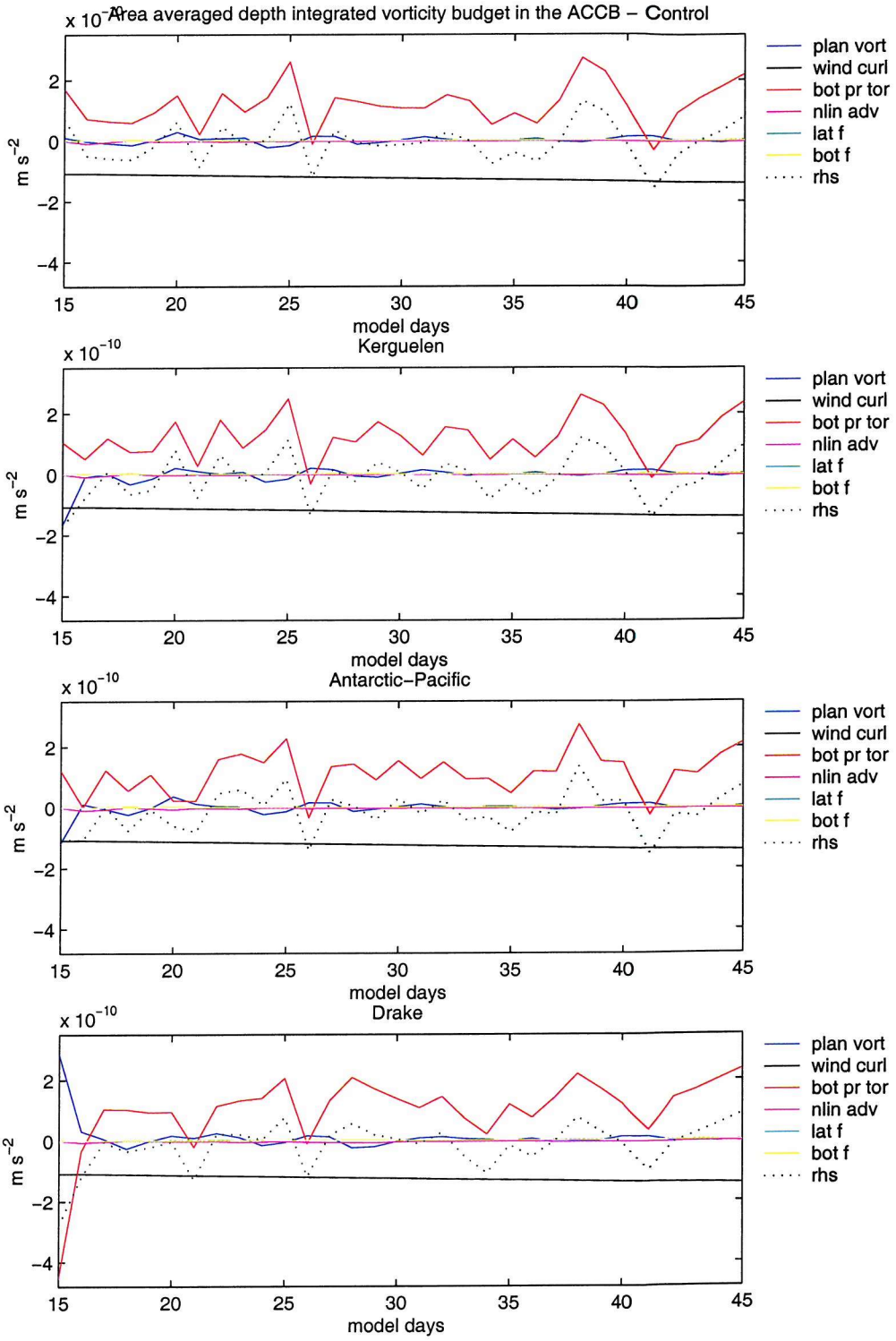

Figure 6.4: *Area averaged depth integrated vorticity budget in Control run, Kerguelen Plateau, Antarctic-Pacific Ridge and Drake Passage in the ACCB*

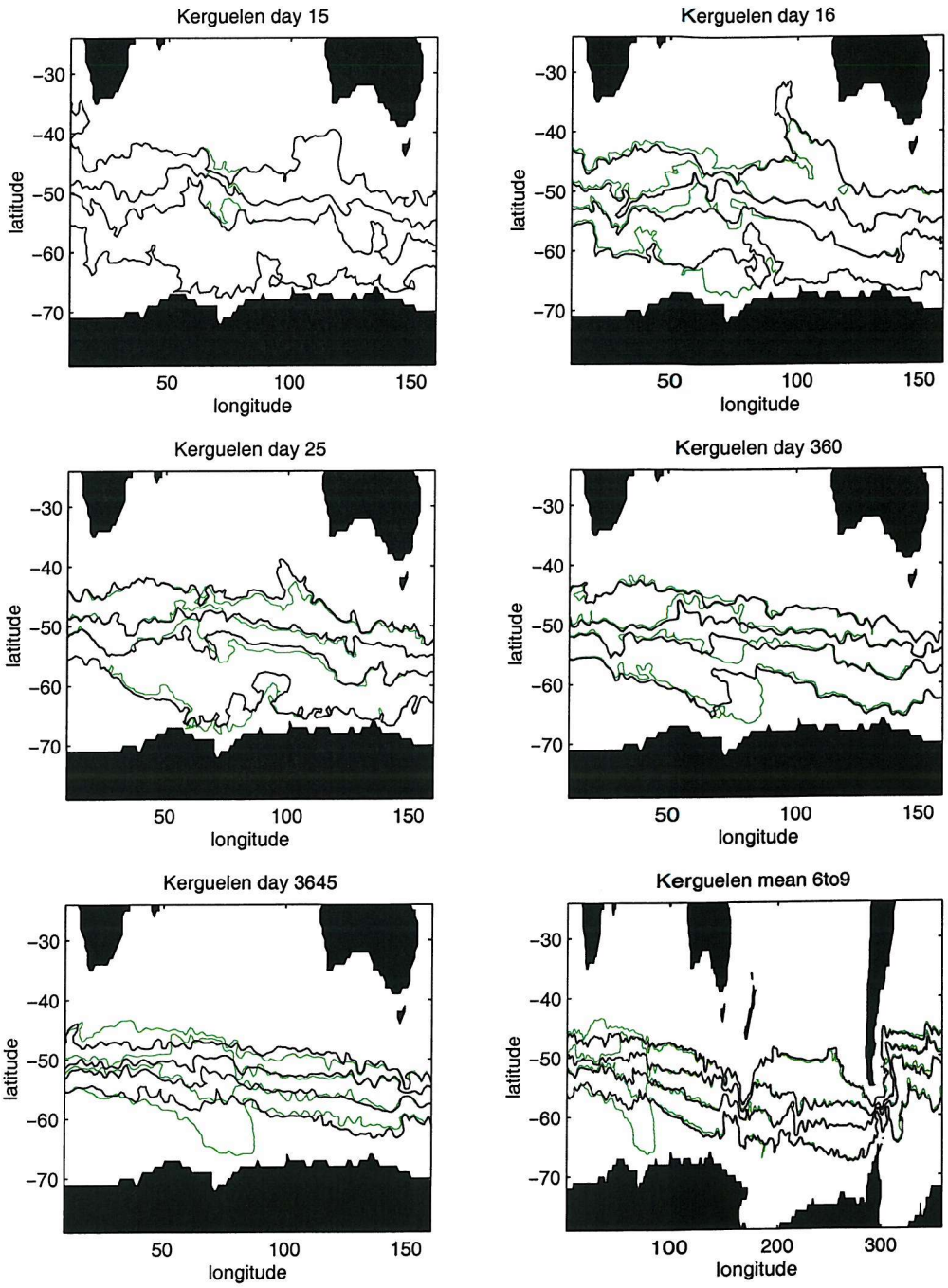

Figure 6.5: *Streamfunctions (Sv) in Kerguelen Plateau case at day 15, day 16, day 25, day 3645, and mean values from year 6 to year 9, green line is the Control run*

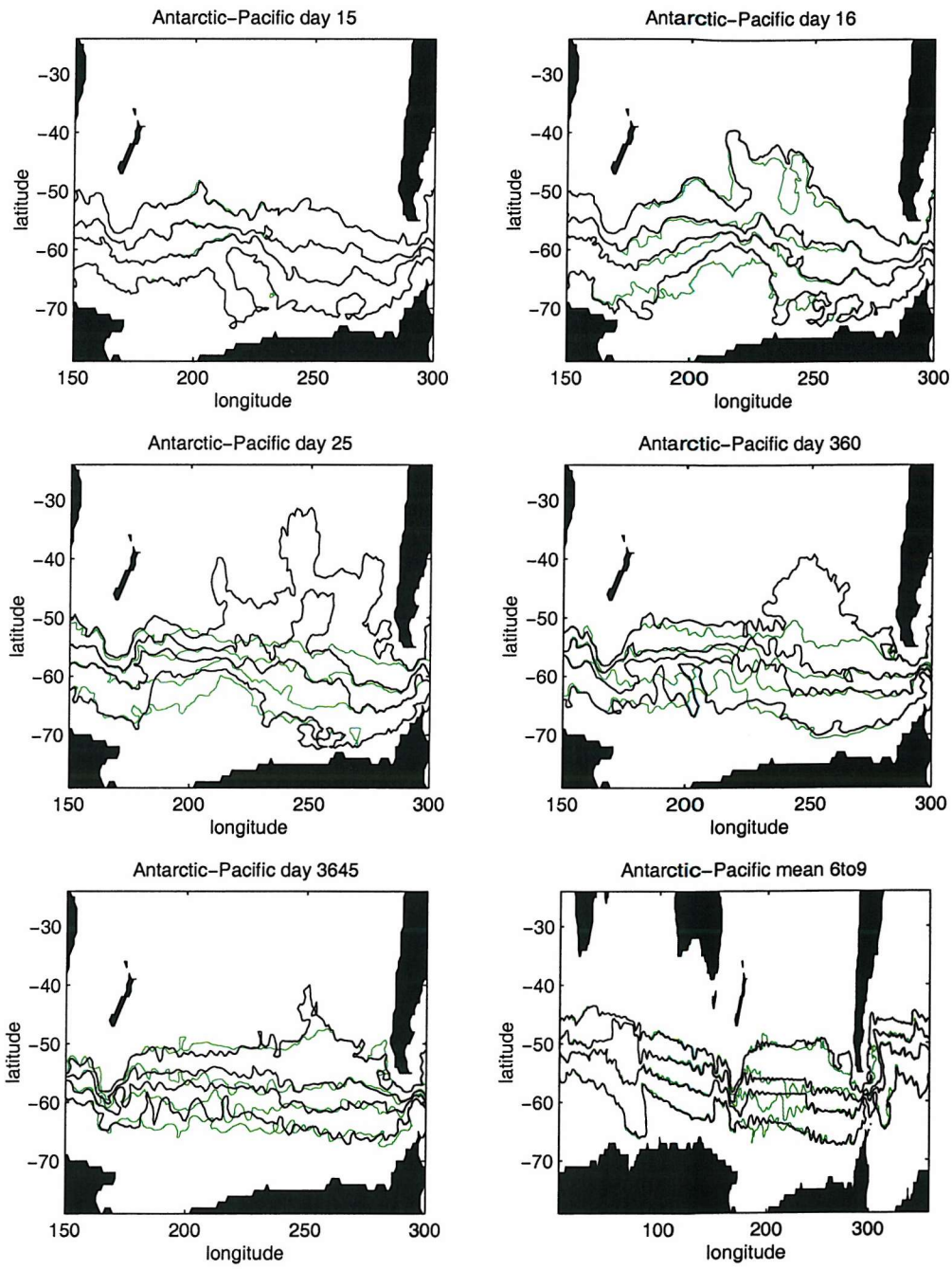

Figure 6.6: *Streamfunctions (Sv) in Antarctic-Pacific case at day 15, day 16, day 25, day 3645, and mean values from year 6 to year 9, green line is the Control run*

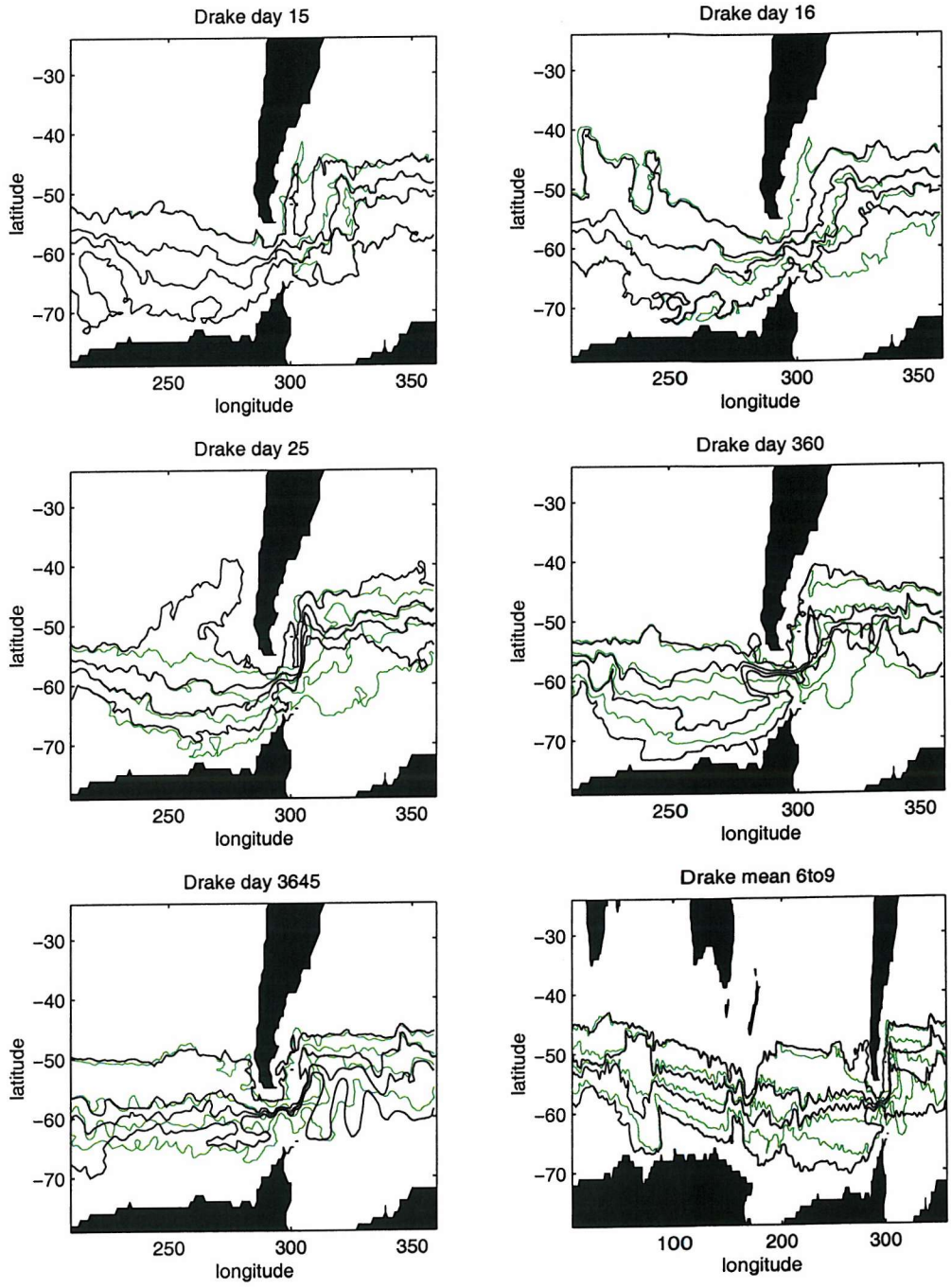

Figure 6.7: *Streamfunctions (Sv) in Drake Passage case at day 15, day 16, day 25, day 3645, and mean values from year 6 to year 9, green line is the Control run*

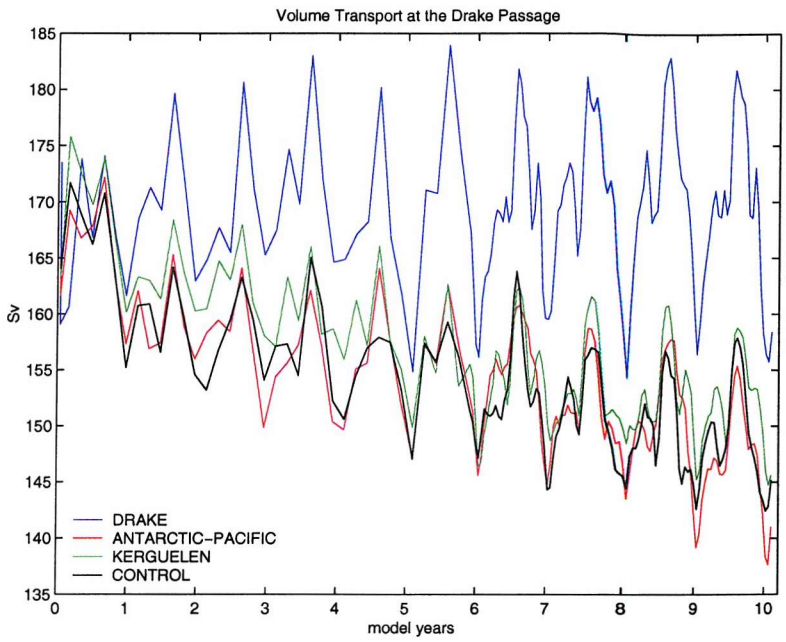

Figure 6.8: *Volume transport in Control run, Kerguelen Plateau, Antarctic-Pacific Ridge and Drake Passage*

6.4 Volume transport

One of the major effects of these topographic changes is the variation of the ACC volume transport at the Drake Passage. The ACC volume transport for each experiment has been calculated (Figure 6.8). In the first year all the cases presented a very similar volume transport, but from the second year on the volume transport presented a stable signal in the Drake Passage case and a decreasing trend in the cases of Control run, Kerguelen Plateau and Antarctic-Pacific Ridge. The control run reaches an equilibrium state in the last 3 years. The mean volume transport from year 6 to year 10 is 150.76 Sv, a value which is consistent with the recent reviews of the ACC volume transport at the Drake Passage (Cunningham

(2001)). In the Antarctic-Pacific Ridge case there is the decreasing trend, but the volume transport is very close to the control run (150.99 Sv in the last 4 years of the model integration). The volume transport calculated in the Kerguelen Plateau run also shows a decreasing trend and it is higher than the control run for almost all period of integration and it is 153.37 Sv in the last 4 years of the model run. These decreasing trends indicate that the model is not in the equilibrium state after 10 years of integration. The most interesting case is the Drake Passage Region. The volume transport reaches an equilibrium state earlier in the model run (4th year) compared to the other runs and average volume transport over the last four years is about 18 Sv higher than the control run. The interseasonal variations are stronger and the annual cycle is not well repeated. The interseasonal variations occur because of the seasonal variations of the wind field but in this case they are stronger than the control case because the intensity of the flow is not reduced by the topography. Unlike OCCAM 1/4 in this coarse resolution model eddies cannot be resolved but only parameterized. Then the significant differences in the annual cycles of the ACC volume transport in Drake Passage case could be due to a westward propagating planetary waves (which can be observed in the time dependent response analysis) or instabilities (baroclinic and barotropic).

6.5 Stable State and Time mean response to the topographic changes

6.5.1 Momentum Budgets in the ACCB

The time mean area averaged and depth integrated momentum budget was calculated for the zonal component of the motion in the ACCB (Appendix A.1). The time mean involves the last 4 years of the model integration for each numerical experiment. The main balance in all cases is between the wind stress and the bottom form stress and all other terms are two orders smaller than the main terms (Table 6.1). As expected, in this non eddy resolving version of OCCAM non-linear advection values are smaller compared to the ones calculated using OCCAM 1/4 version. The analysis of the zonal momentum is a standard analysis for the investigation of the zonal character of the ACC (McWilliams et al. (1978), Grezio et al. (2001)). There are negligible changes in the zonal momentum budgets when the major topographic feature are removed. In all experiments the model was forced by the same wind stress although there are differences in the value of the wind stress in the Drake Passage case. This can be explained considering that some islands were removed in that region so more grid points were involved in the calculations. In the case of Kerguelen Plateau removing the land did not affect the zonal averaged wind stress.

In the ACCB the ACC flow sets the pressure gradients in order to reach a balance between the bottom form stress and the zonal wind stress when a major structure disappears (Figure 6.9). In Figure 6.9 the accumulations of the time mean area averaged and depth integrated momentum budgets show how the leading terms

$\times 10e^{-3}Nm^{-2}$	**Control**	**Kerguelen**	**Antarctic-Pacific**	**Drake**
Coriolis term	- 2.319	- 2.353	- 2.277	- 2.332
momentum flux divergence	0.206	0.450	0.008	- 0.529
bottom form stress	-110.907	-111.072	-110.514	-110.051
horizontal mixing	- 0.059	- 0.047	- 0.086	- 0.021
wind stress	113.359	113.359	113.359	113.432
bottom stress	- 0.434	- 0.426	- 0.417	- 0.538
RHSM	- 0.154	- 0.089	0.073	- 0.039

Table 6.1: *Time mean area averaged depth integrated momentum budget in Control run, Kerguelen Plateau, Antarctic-Pacific Ridge and Drake Passage in the ACCB*

in the budgets are modified in the ACCB after the topographic changes. The retarding effects of the bottom form stress are negative correlated in all cases to the Coriolis term in the ACCB.

6.5.2 Vorticity Budgets in the ACCB and ACCP

The time mean area averaged and depth integrated vorticity budgets were calculated in the ACCB and ACCP for each numerical experiments.

The main balance is between wind curl and bottom pressure torque in the ACCB. In all numerical experiments the wind field applied was ECMWF, however Table 6.2 shows different values of wind curl in the ACCB. The calculation of the wind curl involves different grid points in the Drake Passage case and in Kerguelen Plateau case having removed some islands. In the Antarctic-Pacific case

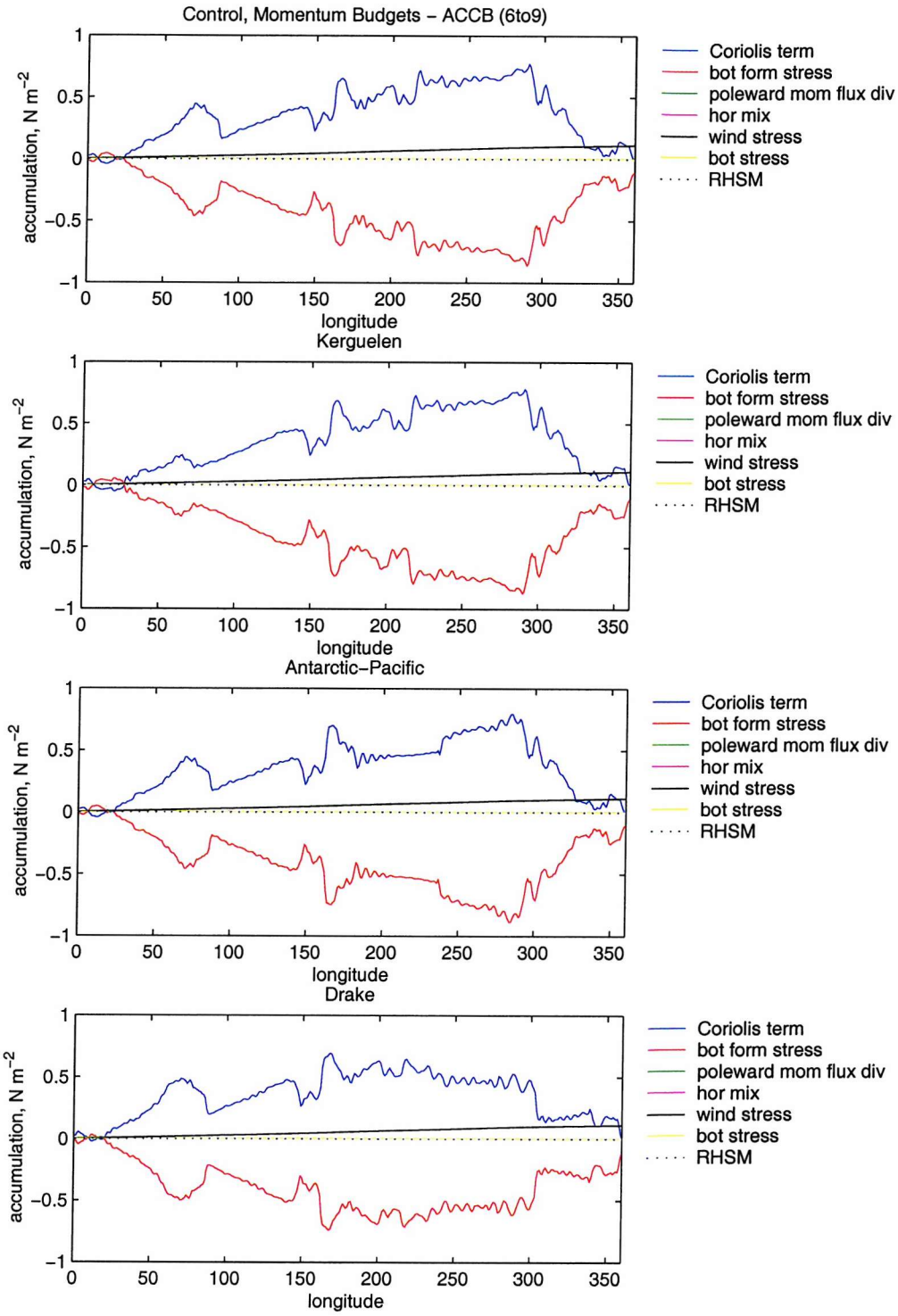

Figure 6.9: *Time mean area averaged depth integrated momentum budget in Control run, Kerguelen Plateau, Antarctic-Pacific Ridge and Drake Passage in the ACCB*

no island were removed and the sea surface area was kept constant respect to the control case. As expected, in this non eddy resolving version of OCCAM non-linear advection values are smaller compared to the ones calculated using OCCAM 1/4 version.

$\times 10e^{-12}ms^{-2}$	**Control**	**Kerguelen**	**Antarctic-Pacific**	**Drake**
planetary vorticity	2.133	2.161	2.087	1.999
non-linear advection	- 6.047	- 6.160	- 3.669	- 0.587
bottom pressure torque	133.753	134.803	130.680	127.770
lateral friction	0.285	- 0.059	0.520	0.070
wind curl	-130.281	-130.294	-130.281	-130.940
bottom friction	0.767	0.616	0.629	0.919
RHSV	0.610	1.067	- 0.034	- 0.769

Table 6.2: *Time mean area averaged depth integrated vorticity budget in Control run, Kerguelen Plateau, Antarctic-Pacific Ridge and Drake Passage in the ACCB*

In the accumulations of the time mean area averaged and depth integrated vorticity budgets the main balances are between bottom form stress, wind curl and planetary vorticity in the ACCB. In all cases the effect of topography is small and produces localised changes of the planetary vorticity and bottom pressure torque. The Kerguelen Plateau case, the Antarctic-Pacific case and the Drake Passage case show that the effect of topography is local in the belt. The ACC has a zonal character, but is not completely a zonal current. There is a shift of the ACC flow of about 10 degrees northward in the south-west Atlantic Ocean,

a decreasing trend in the flow over all the basins and another northward shift of the flow of about 5 degree at about 200 E. In order to have a more complete analysis, vorticity budgets were calculated in the ACCP (Table 6.3).

$\times 10e^{-12}ms^{-2}$	**Control**	**Kerguelen**	**Antarctic-Pacific**	**Drake**
planetary vorticity	- 0.136	- 9.415	- 2.185	- 17.078
non-linear advection	5.887	5.129	7.634	5.659
bottom pressure torque	59.138	64.254	54.869	86.078
lateral friction	- 1.357	- 0.611	- 1.003	1.435
wind curl	- 65.598	- 62.807	- 62.488	- 77.559
bottom friction	0.093	0.044	0.088	0.328
RHSV	- 1.973	- 3.406	- 3.085	- 1.137

Table 6.3: *Time mean area averaged depth integrated vorticity budget in Control run, Kerguelen Plateau, Antarctic-Pacific Ridge and Drake Passage in the ACCP*

The main balance in the time mean area averaged and depth integrated vorticity budget in the ACCP is between bottom pressure torque and wind curl. However, in the Drake Passage case the planetary vorticity presents the highest values in the all cases indicating a strong poleward flow through the ACCP. In a separate analysis (not shown here) it has been demonstrated that a negative value of planetary vorticity indicates a southward volume transport.

Regarding the accumulation of the time mean area averaged and depth integrated vorticity budget in the ACCP, there are local effects of the topographic changes in the Kerguelen Plateau case and Antarctic-Pacific case (Figure 6.10). The most

interesting case is the Drake Passage case. When the Drake Passage was removed the vorticity budgets presented higher values of bottom pressure torque which are mainly positive along the ACCP.

6.5.3 Meridional overturning streamfunction and water masses

The time mean meridional overturning stream function has been calculated for each numerical experiment

$$\psi(\varphi, z) = \int_0^{2\varpi} v(\varphi, \lambda) a cos(\varphi) d\varphi \tag{6.1}$$

In the *Control run* the meridional overturning streamfunction OCCAM 1 × 1 reproduces the Sub-tropical Cell, the Deacon Cell, the Sub-polar Cell and the Deep Cell (Figure 6.11 and Figure 6.12).

Kerguelan Plateau presents two major areas where the overturning circulation is modified. The maximum intensification (6 Sv) of northward flow is reached at about 3500 m depth at 55 S but the increasing of the flow spans between 2000 m and 4500 m in that area. In this case the presence of the southern part of Kerguelen Plateau induces the ACC to flow southward. When the Plateau is removed the jet-like flow produces a northward shift of the mean flow. This is associated with a deepening of the Deacon Cell and a squeezing of the Deep Cell. The water mass going northward between 62 S and 45 S is denser compared to the water mass at that depth in the control case (Figure 6.13). At about 4000 m depth in that range of latitude the density is higher in the Kerguelen case than the Control case. We can recognise that the flow going northward is denser at 2000 m and the flow going southward at 4000 m is fresher. Removing Kerguelen Plateau

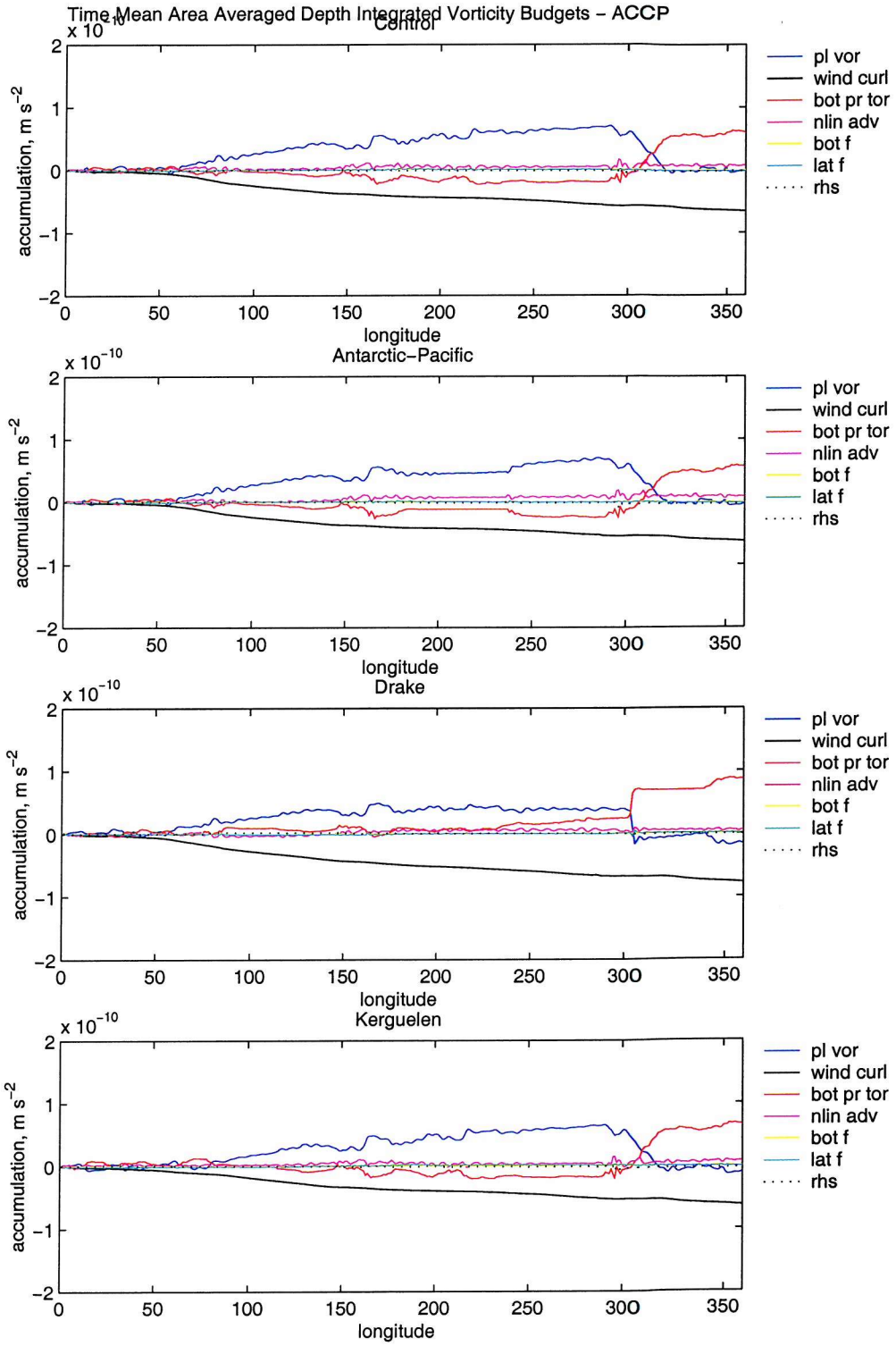

Figure 6.10: *Time mean area averaged depth integrated vorticity budget in Control run, Kerguelen Plateau, Antarctic-Pacific Ridge and Drake Passage in the ACCP*

allowed a stronger meridional circulation of deep water. The water is colder and saltier over the Plateau and south of the Plateau. Because of the jet-like flow there is no split of the two branches and the Polar Front and the Sub-Polar Front are moved northward.

In the *Antarctic-Pacific Ridge* case there is a deepening of the southern branch of the Sub-Polar Cell and the northward flow increases by about 1.8 Sv (Figure 6.12). The northern flow of the Deacon cell is reduced. Denser water is going south between 40 S and 55 S and fresher water is going north between 78 S and 55 S. The fronts are moved northward and the Sub-Antarctic Zone and Sub-Tropical Zone are wider.

The most interesting modifications of the Circumpolar Cells occur in the *Drake Passage* case. In the southern part of the Sub-Polar Cell (south of 60 S) a strong flow is driven northward from the surface to the bottom with a maximum value of 6 Sv at 3000 m at 60 S (Figure 6.12). Between 60 S and 40 S there is an increasing of the flow going southward which makes the Deep Cell weaker and the Sub-polar Cell stronger compared to the Control run. The fronts are moved northward and there are stronger pressure gradients. At 2500 m denser water goes north while more fresher Atlantic water goes south.

6.6 Time dependent response to the topographic changes

Figure 6.6 and Figure 6.7 present a wave structure of the streamfunctions after 1 year. This characteristic of the flow is investigated considering the accumulations of the Coriolis term during the all period of integration (3690 model days).

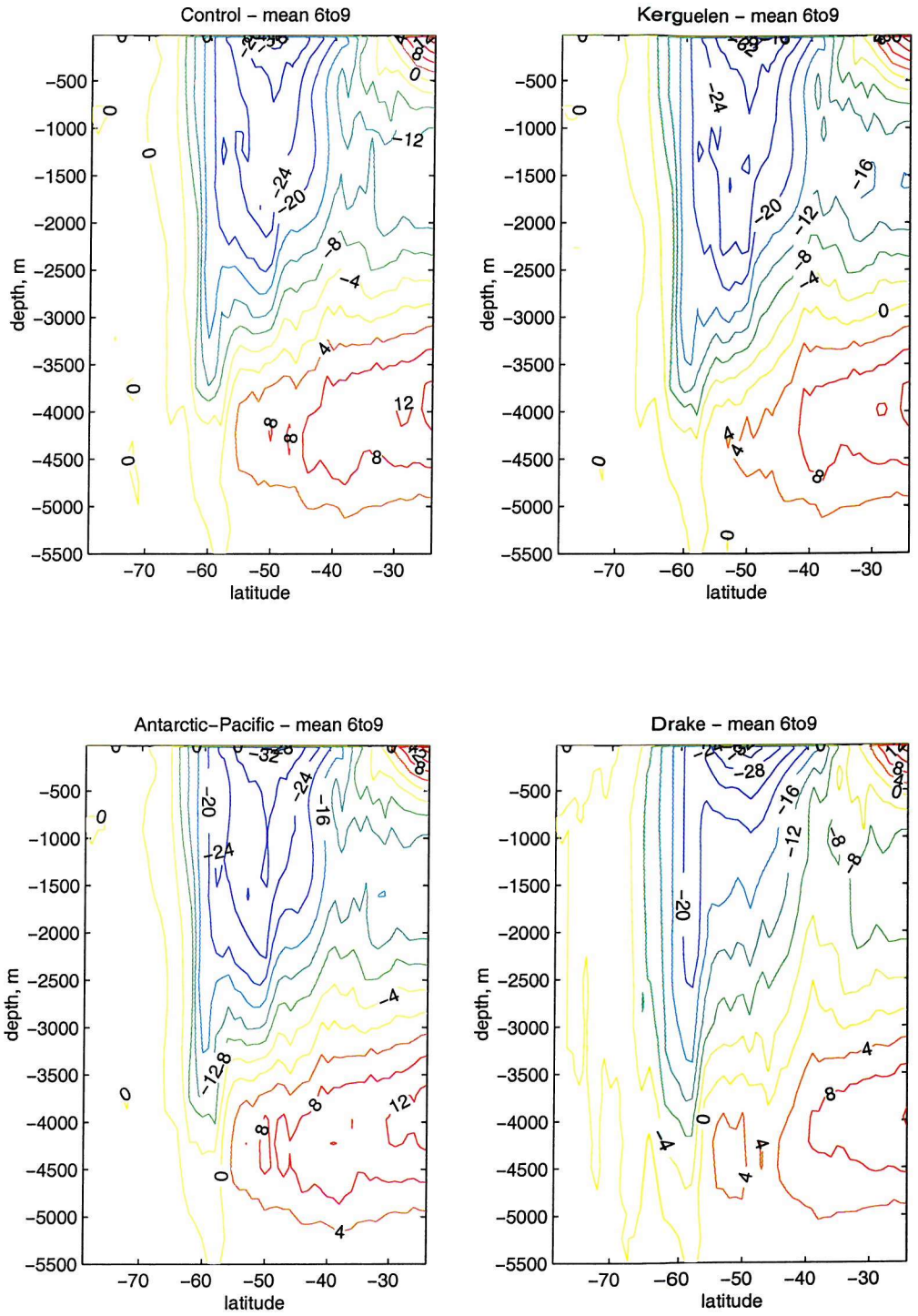

Figure 6.11: *Time mean area averaged overturning streamfunctions (Sv) in Control run, Kerguelen Plateau, Antarctic-Pacific Ridge and Drake Passage in the ACCP*

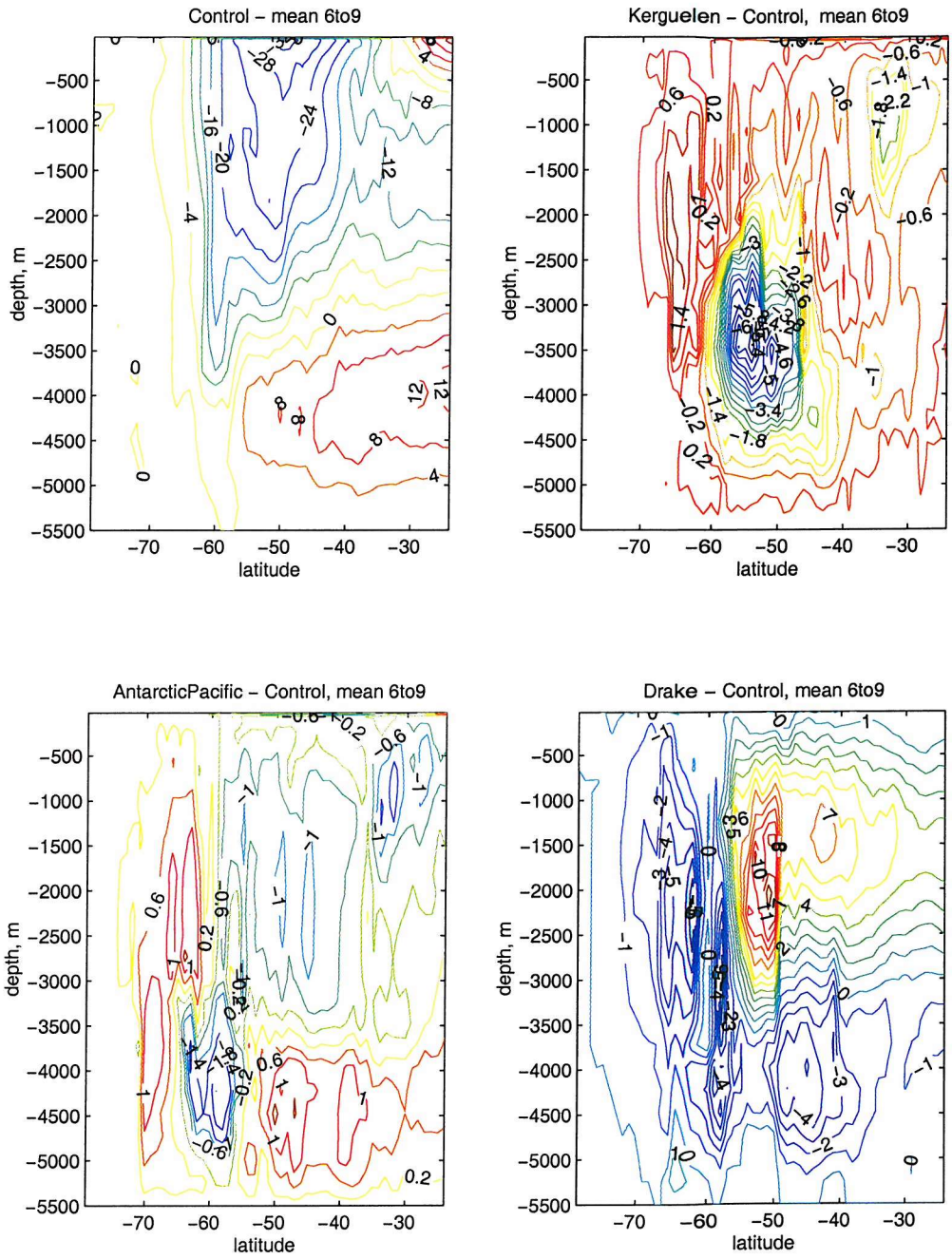

Figure 6.12: *Time mean area averaged overturning streamfunctions (Sv) in Control run and differences between OCCAM GM and Kerguelen Plateau, Antarctic-Pacific Ridge and Drake Passage in the ACCP*

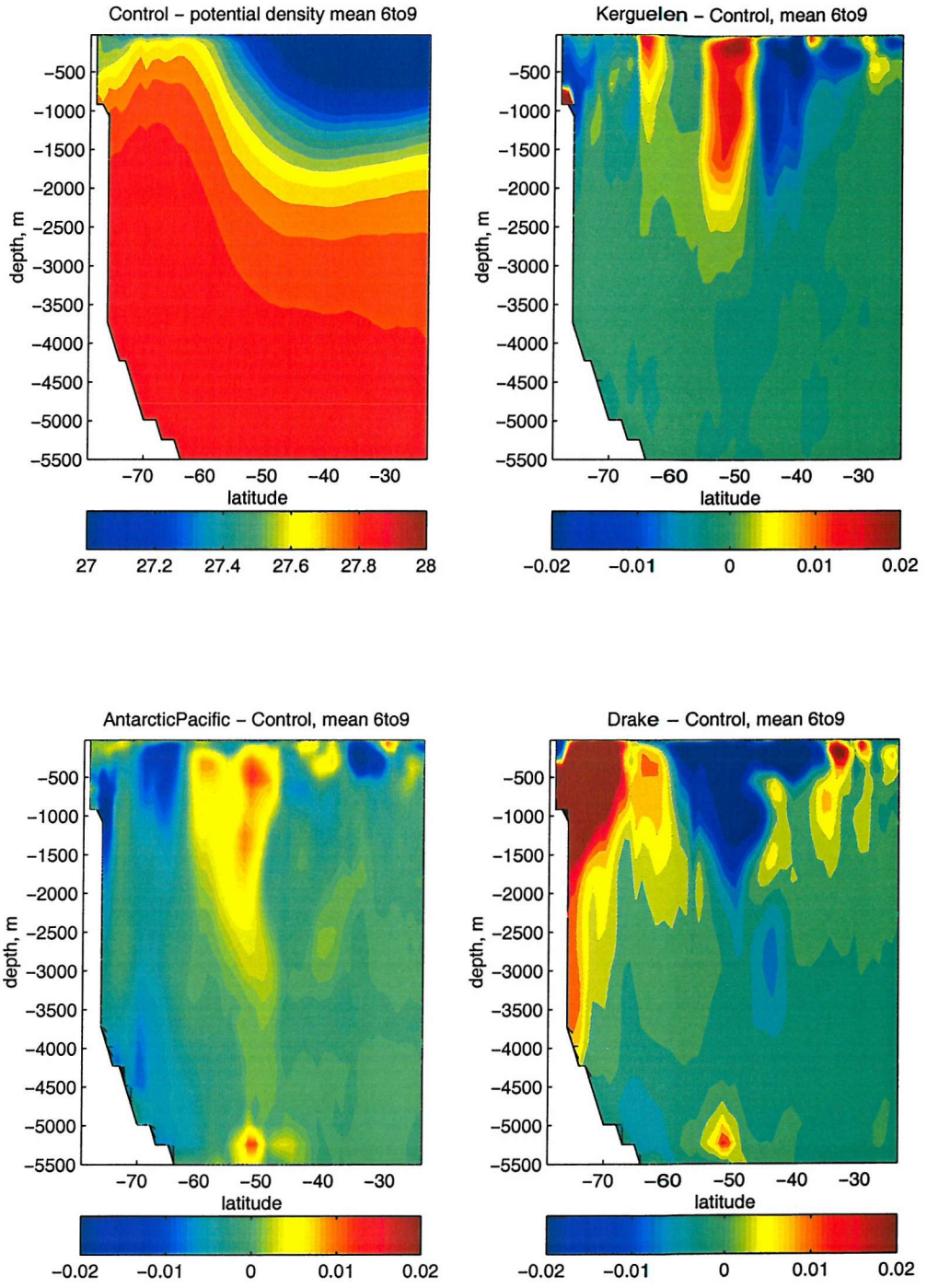

Figure 6.13: *Time mean area averaged potential density in Control run and differences between Control run and Kerguelen Plateau, Antarctic-Pacific Ridge and Drake Passage in the ACCP (level of reference: surface)* (Kgm^{-3})

The analysis of the Coriolis terms show that term is modified in the ACCB in time (Figure 6.14). The Hovmöller diagram displays the evolution of a westward propagation signal through the ACCB in all cases.

In the *Kerguelen Plateau case* there is a reduction of the accumulated positive contributions in time between 60 E and 75 E, and an increase of the accumulated negative contributions between 80 E and 100 E. The decreasing of positive (negative) contributions indicates that the southward (northward) flow decreases (increases). The flow is not steered south by topography and then steered north by the topography as it is in the Control run. This is consistent with the view that the flow crosses the lowered plateau as a jet-like current.

In the *Antarctic-Pacific case* the accumulation in the region of the Antarctic-Pacific Ridge presents a clear seasonal increasing (winter) and decreasing (summer) of the accumulated Coriolis term as the fronts in the South Pacific Basin are moved north or south.

In the *Drake Passage case* the Coriolis term decreases with the time and the decreasing trend follows a wave-like westward propagation from 340 E at the beginning of the run to 170 E after 10 years. From model day 2160, there is a change of regime in the westward propagation, this an aliasing effect due to the frequency of storage of the data. In fact before day 2160 the restart files were stored with a 60 days frequency, instead of 15 days. The region affected by propagation is the Drake Passage region, however the values in the South Pacific Basin decrease in time.

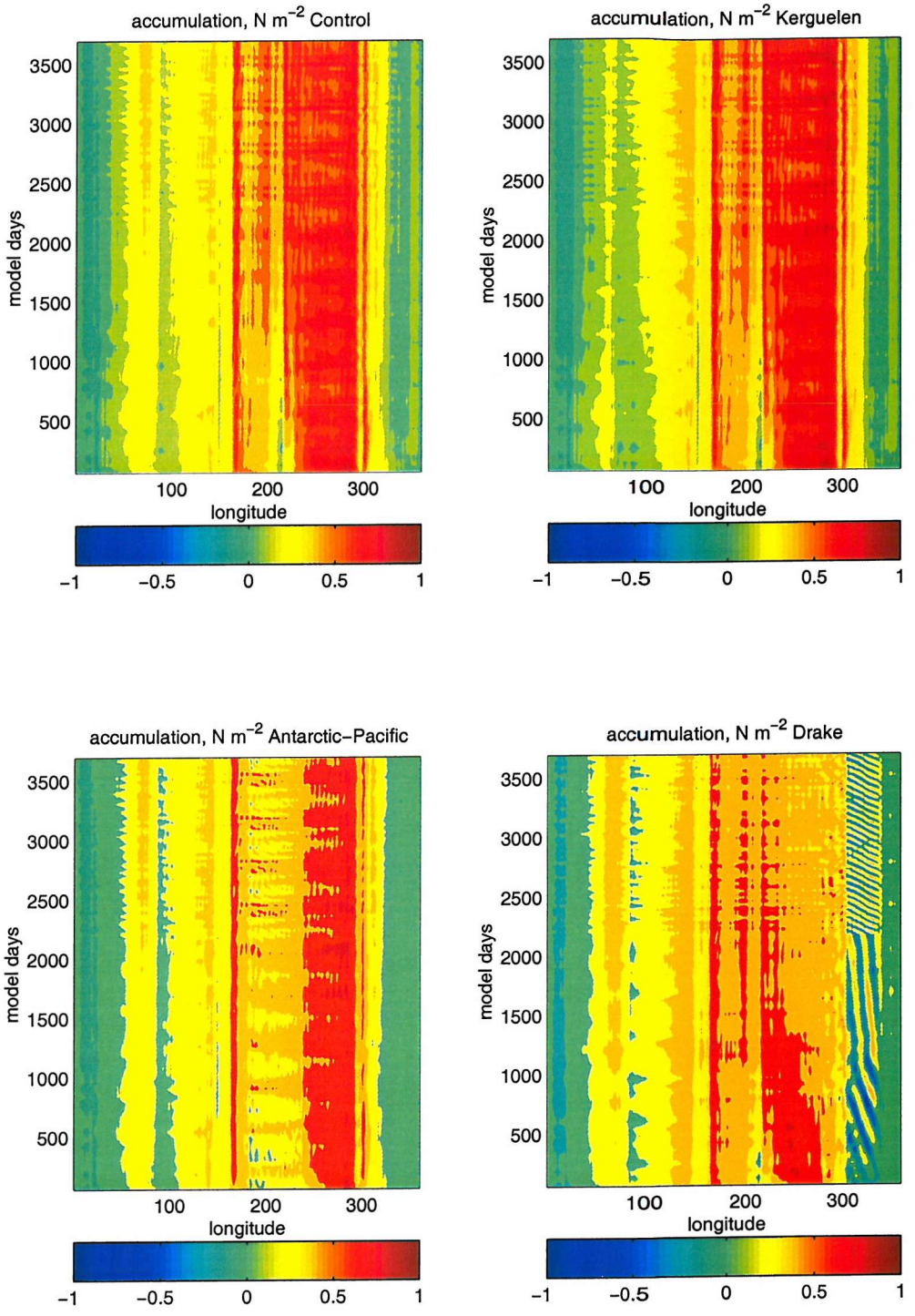

Figure 6.14: *Time mean area averaged depth integrated Coriolis term in Control run, Kerguelen Plateau, Antarctic-Pacific Ridge and Drake Passage in the ACCP*

6.7 Summary

Three numerical experiments changing topography have been performed using a low resolution version of OCCAM model. The Kerguelen Plateau, the Antarctic-Pacific Ridge and the Drake Passage region were lowered about 2000 m. The barotropic response of the flow occur during the first 10 days after the topographic changes are introduced. The volume transport indicates that the model is not in an equilibrium state after 10 years integration in all the numerical experiments, except in the Drake Passage case which is in an equilibrium state after 4 years. The momentum and the vorticity budgets in the ACCB indicate that each topographic feature has a local effect on the ACC dynamics. However, the momentum and vorticity budgets in the ACCP indicate that the Drake Passage plays a key role in the dynamics of the Southern Ocean.

Chapter 7

Discussion

7.1 Introduction

In this chapter the results are summarised and discussed. The analysis of three eddy-permitting models and their comparison emphasised the role of eddies and the importance of topography in the ACCB. However, for a complete analysis on the ACCP dynamics a set of numerical experiments was performed using a coarse resolution model. The effect of the major topographic features on the ACC flow was investigated.

7.2 The ACC dynamics in the ACCB

The comparison of three different OGCMs allows the investigation of the role of eddies and of the effect of resolution on the flow in the ACCB, which is the continental-free region of the ACC. FRAM, OCCAM 1/4 and POP are able

to display eddies and they are different not only because of resolution but also because of forcing and topography. Consequently, they represent differently the ACC flow and the ACC volume transport.

The hypothesis proposed by Munk and Palmén (1951) has been investigated using FRAM, OCCAM 1/4 and POP models. Munk and Palmén (1951) calculated that an eastward wind stress of 0.2 Nm^{-2} would require a northward Ekman flow of 35.7 Sv. They considered that a return flow should occur between 1000 m and 4000 m. The southward flow would be accelerated eastward by the Coriolis force and then the flow would be retarded by pressure forces acting against the submarine ridges balancing the surface wind stress.

The standard analysis on the depth integrated zonal momentum budgets showed that the zonal wind stress applied at the surface is dissipated at the bottom by the bottom form stress in the ACCB in OGCMs, confirming the Munk and Palmén (1951)'s hypothesis. A small role is played by bottom stress. This result is consistent with previous studies using QG models in a zonal channel on a β-plane (McWilliams et al. (1978), Treguier and McWilliams (1990),Wolff et al. (1991), Olbers (1998)). However, QG models tend to overestimate the bottom stress at the bottom.

Bottom form stress is the main sink of momentum and decreases northward as the wind stress increases through the ACCB showing that an increase of the wind stress increases the bottom form stress. Moreover, the bottom form stress presents oscillations which are anticorrelated to the momentum flux divergence showing that the retarding effect on the flow due to the bottom form stress is affected by eddy activity. Momentum flux divergence is the only term at intermediate depth which is in balance with the Coriolis term below the Ekman layer and above the

levels where the topography start to obstruct the flow.

QG models and FRAM (McWilliams et al. (1978), Stevens and Ivchenko (1997)) demonstrated that the vertical penetration of momentum is achieved through the action of the interfacial form stress, which is provided by eddies. The role of eddies is investigated using OCCAM 1/4 and POP models. OCCAM 1/4 and POP, as it is in FRAM, confirm that standing eddies mainly decelerate the flow in the ACCB. However, transient eddies behave differently in the three models. In the upper levels transient eddies accelerate the flow in POP model, as it was in FRAM, a result which is consistent with the observations made by Morrow et al. (1992). On the other hand OCCAM 1/4 is showing that the transient eddies decelerate the flow in the upper levels in the ACCB, confirming the Hughes and Ash (2001) 's analysis. The transient components of the momentum flux divergence are different in the ACCB because of the geographical representation of the momentum flux in the two models especially in the South Pacific Basin and in the Drake Passage Region. In OCCAM 1/4 and POP standing eddies act to accelerate the flow at the surface. Moreover, the upper levels acceleration is not held throughout the water column in the ACCB in OCCAM 1/4 and POP. The model intercomparison also highlights large differences in the way OCCAM 1/4 and POP represent transient and standing eddies at intermediate levels. In fact, below the Ekman layer OCCAM 1/4 presents a strong standing eddy activity which decelerates the flow. POP standing eddies start to decelerate the flow below 2200 m. We deduce that where the input of momentum is very strong standing eddies start to decelerate the flow also at intermediate depths. This is supported also by Hallberg and Gnanadesikan (2001), who demonstrated that

the standing eddies are sensitive to the strength of the forcing. The main result is that in the higher resolution models eddies exhibit a dragging effect on the flow at the levels where the topography starts to obstruct the flow (2737m in OCCAM 1/4 and 2200m in POP).

In order to explore the non-sverdrup character of the ACC flow the vorticity budgets were calculated. The ACCB is the only zonal channel in the ocean and the traditional Sverdrup dynamics fails. Stommel (1957) suggested that the ACC has a sverdrupian character in the Southern Ocean except in the Drake Passage Region. Baker (1982) using satellite measurements found that the flow through the Drake Passage is equal to the flow going southward at 55 S on the portion of parallel which does not include the Drake Passage Region. Recently, satellite measurements (Gille et al. (2001)) and models studies (Gnanadesikan and Hallberg (2000) and Gent et al. (2001)) indicated that the ACC volume transport is not set by the curl of the wind stress but by the zonal wind stress, by eddies and by thermodynamical processes. In this research we investigated the depth integrated vorticity budgets using FRAM, OCCAM 1/4 and POP. The leading terms in the vorticity budgets are wind curl and bottom pressure torque in all of the three models in the ACCB. Non-linear advection is a leading term only in the highest resolution model (POP). Bottom friction and lateral friction are small compared to the main terms. In FRAM the accumulation of each term in the vorticity budgets showed that the balance is mainly between the beta term, wind curl and bottom pressure torque. A main balance between wind curl and beta term (Sverdrup balance) is reached almost everywhere except in the Drake Passage region. In OCCAM 1/4 the eastern part of the Weddell Sea (40-80 E) is

the only region where the planetary vorticity and the wind curl balance. Except for this region, a Sverdrup-like balance is never reached. Conversely to FRAM and OCCAM 1/4, in POP non-linear advection is one of the leading terms in the accumulated balance, in particular downstream of the Drake Passage and above the Maquarie Ridge and South Pacific Ridge. In the ACCB the regions of northward flow are associated with positive pressure torque, and regions with southward flow are associated with negative pressure torque. In this study we demonstrated that the region with highest bottom pressure torque is the Drake Passage. However, there are other regions where bottom pressure torque contributes to the balance. In fact, apart from the Drake Passage, the ACC crosses Kerguelen Plateau, South-East Indian Ridge and South Pacific Ridge. In these regions the bottom pressure torque and the non-linear advection terms provide the strongest contribution to the budgets. OGCMs indicated that the flow is driven northward in the Ekman layer in the ACCB and a return southward flow occurs in the deep layers. In the intermediate layers (below the Ekman layer and above the topography) the flow is ageostrophic and the main balance is between momentum flux divergence and the Coriolis term.

In the coarse version of OCCAM the main terms in the vorticity budgets confirm that bottom pressure torque and wind curl are in balance. The leading terms in the budgets presented negligible changes when one important topographic feature was removed. We can conclude that one topographic feature does not determine the dynamical budgets in the ACCB, but all the topography in the ACCB contributes to the final values of the bottom form stress.

7.3 The ACC dynamics in the ACCP

The topographic steering (Gordon et al. (1978), Marshall (1995), Hughes et al. (1999)) and bottom form stress and bottom pressure torque (Wells and de Cuevas (1995), Ivchenko et al. (1999), Grezio et al. (2001)) are well recognised in the Southern Ocean. The topographic structures of the Drake Passage region, Kerguelen Plateau and Antarctic-Pacific Ridge affect all the ACC flow. The investigation of the role of these topographic structures both in the ACCB and in the ACCP requires a set of numerical experiments. The major problem in this case is the realistic representation of the ACC dynamics in a coarse resolution model. The model used is a coarser version of OCCAM. Either OCCAM Am and OCCAM GM do not resolve eddies but parameterize their effects. The conventional parameterization of momentum and tracers affects the representation of large scale circulation and the general structure of the water masses is not reproduced. On the other hand, the GM eddy parameterization can underestimate the convection processes (England (1995)). Despite these limitations, both coarse versions of OCCAM conserve the major balances in the momentum and the vorticity budgets in the ACCB and ACCP. However, the more realistic parameterization of eddies is necessary in order to determine the non-linearity in vorticity budgets.

The traditional Sverdrup theory is not held in the ACCB because of the lack of continents, as it has been demonstrated in the comparison between FRAM, OCCAM and POP models. If there are no continental boundaries there are no western boundary currents that we can identify. In the ACCB the torque on the flow due to the pressure gradients across topography increases the planetary vorticity

inducing the flow to go northward over the Kerguelen Plateau, the South-East Indian Ridge, the Antarctic-Pacific Ridge and the Drake Passage. Between the major topographic structures the flow moves southward. In the other basins the ageostrophy is mainly concentrated in the western boundary currents but in the ACCB it is distributed over the belt. This is quite evident in the eddy-permitting models with higher horizontal resolution and more realistic representation of topography, whereas in the FRAM case the ageostrophic processes are confined to the Drake Passage region.

In the ACCB the Sverdrup Balance does not hold even far from the Drake Passage Region mainly because of the bottom pressure torque associated with the topographic features. Those features affect the ACC dynamics also in the regions where the flow is not zonal. Then analysis of the dynamics in the Southern Ocean is focused on the ACCP.

Lowering the Kerguelen Plateau and removing the Drake Passage and the Antarctic-Pacific Ridge is an effective methodology for the investigatation of the short time scale effects of topography. The attempts to explain the ACC dynamics far from the Drake Passage can be summarised in three major approaches: Stommel's model, Webb's model and Hughes' model. The first used the wind curl to determine the ACC transport and was proposed by Stommel (1957). The second one used the wind stress to determine the ACC transport and was proposed by Webb (1993). The third model applies the Island Rule of Godfrey (1989).

Stommel's model. Stommel (1957)'s model is the first attempt to explain the complex circumpolar current in the Southern Ocean using the Sverdrup theory. This model suggestes that the ACC is frictionless except in a narrow region after the flow passes through Drake Passage, where all the dissipation of energy, any

instabilities and higher order process occur. In this region the water turns northward, as a western boundary current, there is a sharp deflection of 10 degree of the latitude before flowing to the east again near 40 S. In Stommel's models the viscous dissipation takes place in the western boundary current that exists along land boundary of the South America coast and a Sverdrup balance would hold in the ACC far from the Drake Passage region. In his simple model the ACC volume transport is proportional to the wind stress curl and the maximum Ekman transport (about 20 Sv) occurs at about 55 S. The northward volume transport in the Ekman layer returns southward in the deep layers below topography (between 1000 and 4000 m) as a western boundary current. However, his theory is not complete, as Stommel recognized, because it does not explain how the flow goes from the east of the Antarctica peninsula to the west near South America.

Webb's model. Webb's model is the first explanation of the dynamics in the Southern Ocean that considers topography. In this model a barrier (the Kerguelen Plateau) occludes a periodic zonal channel (the ACCB). A sink and a source represent the effects of the northward Ekman transport due to the eastward wind stress and the southward flow below the Ekman layer. This model produces an east-west current which turns north-south at the east side of the barrier. Then the flow moves eastward again. A pressure gradient between the east of South America (source) and the south of Kerguelen Plateau (sink) and a western boundary current east of South America need to be added to the original version of this models in order to produce the necessary meridional pressure gradient.

Hughes' model. The necessary modifications to Webb's model are presented by Hughes (2002) applying the Island Rule of Godfrey (1989) to Webb's model, where the island is the Antarctica. In Hughes (2002)'s study Stommel's model

and Webb's model are special cases of a general model. This general model consideres the ACC flow at the Drake Passage latitude blocked by a submerged topography connecting the Antarctica Peninsula to the South America by the Scotia Arc. Hughes (2002)'s model does not parameterize or resolve eddies as it is in Stommel's and Webb's models.

In this study we have not tested Stommel's model by changing the wind stress curl. However, from the comparison between the three eddy-permitting models we can show that a stronger wind stress curl does not produce a higher volume transport throughout the Drake Passage if eddies are involved. In this study the numerical experiments in the Southern Ocean demonstrate that the most important topographic feature in the Southern Ocean is the Drake Passage. The effects of Kerguelen Plateau and Antarctic-Pacific Ridge on the ACC dynamics appear to be local. Lowering the Drake Passage Region supports Hughes (2002)'s explanation. In Hughes (2002)'s general model the strength of a western boundary current adjacent to South America is predicted by the Sverdrup balance plus a term related to the pressure gradients.

The vorticity budgets calculated in the ACCP show that the balances changed when the Drake Passage was removed. The topographic structure of the Drake Passage region affects all of the ACC flow. The accumulated bottom pressure torque becomes small far from the Drake Passage. Removing Drake Passage reduces the contribution of the bottom pressure torque to the vorticity balance. In this case the region of Sverdrup balance in the ACCP is extended from about 150 E to about 250 E. It means that in the real ocean the great part of the non-sverdrup flow is in the Drake Passage Region.

The numerical experiment with low Kerguelen Plateau and flat Antarctic-Pacific

Ridge show no significant changes in the results compared to the Control run indicating that the key role for the all Southern Ocean is played by the Drake Passage but not by other topographic features.

7.4 The role of Kerguelen Plateau, Antarctic-Pacific Ridge and Drake Passage Region

Removing topography changes the flow and the formation of water masses and also the dynamical and thermodynamical balances in the Southern Ocean. Moreover, after a long integration the model will show the effects of those topographic changes on the global thermohaline circulation. In order to explore the baroclinic response to these changes the time integration of the model should be order 100 years (or 1000 years). This time scale is necessary for the baroclinic adjustment. However, 10 years of model integration allow us to understand the effects of the topography on the barotropic flow. After 10 years model run we can start to see the slow baroclinic response but we can only speculate about the processes involving the thermohaline circulation.

Kerguelen Plateau. The first effect observed was an eastward intensification of the flow at the depth where the Plateau is removed. The Sub-Antarctic Front and the Polar Front advance northward moving water masses at the surface and at intermediate depths. This has an effect on the thermohaline circulation. In fact, this northward volume transport in the surface and upper layers makes the flow denser. Increasing dense water induces there a slower incoming of NADW towards the Antarctica. The changes of density are simply due to the low Ker-

guelen Plateau. In the real ocean the Kerguelen Plateau induces the flow to split, one branch goes southward and another goes northward. The Southern branch is forced to cross the gap between the plateau and Antarctica. This is due to the fact that the flow is driven by the difference in pressure gradients west the plateau (dense water) and east the Plateau (less dense water). The eastward flow of this southern branch reduces the northward propagation of CDW which is forced to flow zonally. Webb (1993) showed that if a zonal channel is occluded by a barrier then a meridional flow and a strong eastward jet occurs. The meridional flow is a deep western boundary current. This is the case of the Southern Ocean where the Kerguelen Plateau rises to 1000 m depth and occludes the ACC path. In his paper he could not refer to observations in order to validate his simple model because there were no observations available in that region. Donohue et al. (1999) recognised a deep western boundary current from acoustic Doppler current profiler data in the Australian-Antarctic Basin (east the Kerguelen Plateau). The deep flow is north-westward and is supplied by westward flow along the Antarctic Continental slope and by eastward flow of Weddell Basin Water. These observations support Webb (1993)'s theory regarding the deep western boundary current in the Kerguelen Plateau region.

Antarctic-Pacific Ridge. In the Antarctic-Pacific case when topography is removed the ACC flow appears to be jet-like in the South-Pacific Ocean. The fronts are moving northward when there are no abstacles. In the real ocean it is well known that the ACC follows the f/H contours and with or without topography the flow in the Antarctic-Pacific follows these contours.

Drake Passage Region. The Drake Passage Region plays a key role in the Southern Ocean. Denser water moves northward at the surface and the bottom

whereas the NADW moves farther south when this region is flattened. There is no northward shift of the fronts due to the Scotia Arc and the fronts are parallel throughout the Drake Passage during the numerical experiment. This jet like structure in the Drake Passage reduces also the Weddell gyre extension.

In all the numerical experiments we have not changed the wind stress. The increasing of denser/fresher water masses occurs because of mixing. This mixing is induced by the removing the topography. When the topography is removed the flow is not constrained to follow f/H contours and water masses can mix. The topography in the Southern Ocean retards and reduces this mixing and the flow is forced to flow zonally and recirculate.

Chapter 8

Conclusions

The ACCB (63.5 S - 55 S) is the region of the Southern Ocean where the ACC flows with no continental barriers and it is the unique channel connecting three oceans in the world. In this research we have made a comparison between three eddy-permitting models (FRAM, OCCAM 1/4 and POP) in order to understand the ACC dynamics in the ACCB, where eddies and topography play a crucial role.

In FRAM, OCCAM 1/4 and POP models transient eddies behave differently in the ACCB. In the upper levels transient eddies accelerate the flow in POP model, as in FRAM, a result which is consistent with the observations made by Morrow et al. (1992). On the other hand OCCAM 1/4 is showing that the transient eddies decelerate the flow in the upper levels, confirming the Hughes and Ash (2001)'s satellite altimeter analysis. Moreover, the upper level acceleration does not hold throughout the whole water column in the ACCB in OCCAM 1/4 and POP. Standing eddies mainly decelerate the flow in the ACCB. The main result is that in both models eddies exhibit a dragging effect on the flow at the levels

where the topography starts to obstruct the flow (2737 m in OCCAM and 2200 m in POP).

FRAM, OCCAM 1/4 and POP momentum budgets show that the main balance occurs between wind stress and bottom form stress, which confirms previous studies. Bottom form stress is the main sink of momentum and decreases northward as the wind stress increases through the ACCB. Momentum flux divergence is not a leading term in the momentum budgets in FRAM, OCCAM 1/4 and POP. However, below the Ekman layer and above the topography this is the only term balancing the Coriolis term. FRAM, OCCAM 1/4 and POP vorticity budgets show a main balance between bottom pressure torque and wind curl. When horizontal resolution is higher (POP case) the non-linear advection is one of the leading terms in the vorticity budget and redistributes vorticity in order to balance the planetary vorticity.

Apart from the Drake Passage, the ACC crosses Kerguelen Plateau, South-East Indian Ridge and South Pacific Ridge. In these regions the bottom pressure torque and the non-linear advection terms present the strongest contribution to the budgets.

The large effect of topography in the Southern Ocean is investigated by carrying out a set of numerical experiments. The Kerguelen Plateau is lowered and the Drake Passage and the Antarctic-Pacific Ridge are removed. Regarding the ACCB the changing of topography presented a local effect on the dynamics in all cases.

A complete investigation of the ACC dynamics needs to consider the ACC flow in the ACCP. Because the ACCB dynamics is a special case it is not representative

of the flow in the Southern Ocean. In fact, the ACC connects all oceans but it is not a completely zonal current.

The vorticity budgets were calculated in the ACCP. This analysis shows that when the Drake Passage was removed the balances changed and the topographic structure of the Drake Passage region affects all of the ACC flow. Removing Drake Passage reduces the contribution of the bottom pressure torque to the vorticity balance and the region of Sverdrup balance is extended from about 150 E to about 250 E. It means that in the real ocean the great part of non-sverdrup behaviour is in the Drake Passage Region. The key role for the all Southern Ocean is played by the Drake Passage but not for other topographic features.

The effects of Kerguelen Plateau and Antarctic-Pacific Ridge on the ACC dynamics appear to be local in the ACCP.

Chapter 9

Further work

One of the main limitations in the OGCMs used in this research was the fact that they are not eddy-resolving models. They do not fully resolve the internal Rossby radius and therefore the eddies. A new generation of global models should improve horizontal and vertical resolutions in order to reach a better representation of non-linear processes. An increased resolution would give a realistic representation of the ACC flow in the Southern Ocean. Furthermore, the contradictions and the different behaviours of the OGCMs could disappear and models results should converge.

The flow in the ACCB is a portion of the ACC flow in the Southern Ocean. There are other regions with high eddy KE in the Southern Ocean and the investigation of the ACC dynamical budgets could be extended to the ACCP using also OCCAM 1/4 and POP.

The effect of topography on the ACC dynamics was explored and the barotropic response to this changes was analysed. However, the effect of topography and topographic changes, on the thermohaline circulation and the baroclinic response

cannot be speculated. An extension of the time integrations (order 100 years) would give a clear view of the global effects of the topography on the Southern Ocean circulation. Morover, the combined effects of topography and wind stress variations could give more understanding on the effects of the role of the ACC in global ocean circulation.

We can indicate the region south of Australia as another region in the Southern Ocean which plays an important role in the ACC dynamics. Whereas long term in situ measuraments of velocity and temperature have been concentrated in the Drake Passage, efforts have been only recently focused on the ACC flow south of Australia. However there is a lack of numerical investigations in this region regarding interaction between ACC flow, eddy variability, density field and topography. Numerical experiments could be performed in order to investigate the effects of topography on the ACC flow south of Australia.

Appendix A

A.1 Momentum Budgets

A.1.1 Depth integrated momentum budget in OCCAM and POP

The eastward component of the momentum budget is

$$\underbrace{\rho_0 \int_{-H}^{h} \frac{\partial u}{\partial t}}_{LHSM} = - \underbrace{\rho_0 \int_{-H}^{h} \frac{1}{a\cos\varphi}\frac{\partial uu}{\partial \lambda} dz}_{EastwardMomentumFluxDivergence} - \underbrace{\rho_0 \int_{-H}^{h} \frac{1}{a\cos\varphi}\frac{\partial uv\cos\varphi}{\partial \varphi} dz}_{PolewardMomentumFluxDivergence}$$
$$- \underbrace{\rho_0 \int_{-H}^{h} \frac{\partial uw}{\partial z} dz}_{VerticalMomentumFluxDivergence} + \underbrace{\rho_0 \int_{-H}^{h} fv dz}_{CoriolisTerm} - \underbrace{\int_{-H}^{h} \frac{1}{a\cos\varphi}\frac{\partial p}{\partial \lambda} dz}_{BottomFormStress} + \underbrace{\rho_0 \int_{-H}^{h} d^{\lambda} dz}_{HorizontalMixing}$$
$$+ \underbrace{\tau_s^u}_{WindStress} - \underbrace{\tau_b^u}_{BottomStress} \quad \text{(A.1)}$$

where d^{λ} is the eastward component of $\mathbf{d_u} = (d^{\lambda}, d^{\varphi})$.

In OCCAM

$d^{\lambda} = A_m(\nabla^2 u + (1 - \tan^2\varphi)u/a^2 - 2v_{\lambda}\tan\varphi/a^2\cos\varphi)$

and

$d^{\phi} = A_m(\nabla^2 v + (1 - \tan^2\varphi)v/a^2 + 2u_{\lambda}\tan\varphi/a^2\cos\varphi).$

In POP

$d^\lambda = A_m(\nabla^2 u + (1 - \tan^2\varphi)u/a^2 - 2v_\lambda \tan\varphi/a^2\cos\varphi) - B_m\nabla^4 u$

and

$d^\phi = A_m(\nabla^2 v + (1 - \tan^2\varphi)v/a^2 + 2u_\lambda \tan\varphi/a^2\cos\varphi) - B_m\nabla^4 v.$

A.1.2 Momentum budget level by level in OCCAM

The momentum budget level by level

$$\underbrace{\rho_0 \int_{zk+1}^{zk} \frac{\partial u}{\partial t}}_{LHSM} = - \underbrace{\rho_0 \int_{zk+1}^{zk} \frac{1}{a\cos\varphi}\frac{\partial uu}{\partial\lambda} dz}_{EastwardMomentumFluxDivergence} - \underbrace{\rho_0 \int_{zk+1}^{zk} \frac{1}{a\cos\varphi}\frac{\partial uv\cos\varphi}{\partial\varphi} dz}_{PolewardMomentumFluxDivergence}$$
$$- \underbrace{\rho_0 \int_{zk+1}^{zk} \frac{\partial uw}{\partial z} dz}_{VerticalMomentumFluxDivergence} + \underbrace{\rho_0 \int_{zk+1}^{zk} fv dz}_{CoriolisTerm} - \underbrace{\int_{zk+1}^{zk} \frac{1}{a\cos\varphi}\frac{\partial p}{\partial\lambda} dz}_{FormStress}$$
$$+ \underbrace{\rho_0 \int_{zk+1}^{zk} d^\lambda dz}_{HorizontalMixing} + \underbrace{\rho_0 \int_{zk+1}^{zk} f^\lambda d\not{z}}_{VerticalMixing} \quad \text{(A.2)}$$

where f^λ is the eastward component of $\mathbf{f_u} = (f^\lambda, f^\varphi)$.

In OCCAM

$f^\lambda = K_m \frac{\partial^2 u}{\partial z^2}$ and $f^\varphi = K_m \frac{\partial^2 v}{\partial z^2}$.

A.2 Vorticity Budgets

A.2.1 Depth integrated vorticity budget in FRAM

In FRAM because of the rigid lid condition, the vertically integrated velocity field is non-divergent and it is possible to define a stream function $\nabla\Psi = \int_{-H}^{0} \mathbf{k} \times \mathbf{u} dz$. Then the time mean depth integrated vorticity budget is

$$\underbrace{\frac{\partial \nabla\Psi^2}{\partial t}}_{LHSV} = -\underbrace{\mathbf{k}\cdot\nabla\times f\nabla\Psi}_{Beta} - \underbrace{\mathbf{k}\cdot\nabla\times\mathbf{N}}_{Non-linear Advection} - \underbrace{\mathbf{k}\cdot\nabla\times\int_{-H}^{h}\frac{1}{\rho}\nabla p dz}_{BottomPressureTorque} + \underbrace{\mathbf{k}\cdot\nabla\times\mathbf{D_u}}_{LateralFriction} + \underbrace{\mathbf{k}\cdot\nabla\times\frac{\tau_s}{\rho_0}}_{WindCurl} - \underbrace{\mathbf{k}\cdot\nabla\times\frac{\tau_b}{\rho_0}}_{BottomFriction} \quad \text{(A.3)}$$

where $\mathbf{N}$ and $\mathbf{D_u}$ are

$\mathbf{N} = -\int_{-H}^{0} \rho_0(\mathbf{V}\cdot\nabla\mathbf{V} + w\frac{\partial \mathbf{V}}{\partial z} + \dot{\lambda}\sin\varphi\times\mathbf{V})dz$

$\mathbf{D_u} = \int_{-H}^{0} \rho_0 \mathbf{G} dz$

$\mathbf{G} = (G^{\lambda}, G^{\varphi})$ is a horizontal body force due to horizontal mixing:

$G^{\lambda} = A_m(\nabla^2 u + (1-\tan^2\varphi)u/a^2 - 2v_{\lambda}\tan\varphi/a^2\cos\varphi) - B_m\nabla^4 u$

$G^{\varphi} = A_m(\nabla^2 v + (1-\tan^2\varphi)v/a^2 + 2u_{\lambda}\tan\varphi/a^2\cos\varphi) - B_m\nabla^4 v$

A.2.2 Depth integrated vorticity budget in OCCAM and POP

The depth integrated vorticity budget in the free-surface models is

$$\underbrace{\mathbf{k}\cdot\nabla\times\int_{-H}^{h}\frac{\partial \mathbf{u}}{\partial t}dz}_{LHSV} = -\underbrace{\mathbf{k}\cdot\nabla\times\int_{-H}^{h} f\mathbf{k}\times\mathbf{u}dz}_{PlanetaryVorticity} - \underbrace{\mathbf{k}\cdot\nabla\times\int_{-H}^{h}[(\mathbf{u}\cdot\nabla)\mathbf{u} + w\frac{\partial \mathbf{w}}{\partial z}]dz}_{Non-linear Advection}$$

$$\underbrace{-\mathbf{k}\cdot\nabla\times\int_{-H}^{h}\frac{1}{\rho}\nabla p dz}_{BottomPressureTorque}+\underbrace{\mathbf{k}\cdot\nabla\times\int_{-H}^{h}\mathbf{d_u}dz}_{LateralFriction}+\underbrace{\mathbf{k}\cdot\nabla\times\frac{\tau_s}{\rho_0}}_{WindCurl}-\underbrace{\mathbf{k}\cdot\nabla\times\frac{\tau_b}{\rho_0}}_{BottomFriction} \quad \text{(A.4)}$$

A.2.3 Vorticity budget level by level in OCCAM

The vorticity budget was also calculated level by level.

$$\underbrace{\mathbf{k}\cdot\nabla\times\int_{zk+1}^{zk}\frac{\partial\mathbf{u}}{\partial t}dz}_{LHSV}=\underbrace{-\mathbf{k}\cdot\nabla\times\int_{zk+1}^{zk}f\mathbf{k}\times\mathbf{u}dz}_{PlanetaryVorticity}\underbrace{-\mathbf{k}\cdot\nabla\times\int_{zk+1}^{zk}[(\mathbf{u}\cdot\nabla)\mathbf{u}+w\frac{\partial\mathbf{w}}{\partial z}]dz}_{Non-linearAdvection}$$
$$\underbrace{-\mathbf{k}\cdot\nabla\times\int_{zk+1}^{zk}\frac{1}{\rho}\nabla p dz}_{PressureTorque}+\underbrace{\mathbf{k}\cdot\nabla\times\int_{zk+1}^{zk}\mathbf{d}_u dz}_{LateralFriction}+\underbrace{\mathbf{k}\cdot\nabla\times\int_{zk+1}^{zk}\mathbf{f}_u dz}_{VerticalMixing} \quad \text{(A.5)}$$

Bibliography

Baker, D. (1982). A note on Sverdrup balance in the Southern Ocean. *Journal of Marine Research*, 40 Suppl.:pp.21–26.

Barnier, B., L.Siefrid, and Marchesiello, P. (1995). Thermal forcing for a global ocean circulation model using a three-year climatology of ECMWF analyses. *Journal of Marine Systems*, 6:pp.363–380.

Beckmann, A., Boning, C., Koberle, C., and Willebrand, J. (1994). Effect of increased horizontal resolution in a simulation of the North Atlantic Ocean. *Journal of Physical Oceanography*, 24:pp.326–344.

Best, S., Ivchenko, V., Richards, K., Smith, R., and Malone, R. (1999). Eddies in numerical models of the Antarctic Circumpolar Current and their influence on the mean flow. *Journal of Physical Oceanography*, 29:pp.328–350.

Boning, C. and Budich, R. (1992). Eddy dynamics in a Primitive Equation model: Sensitivity to horizontal resolution and friction. *Journal of Physical Oceanography*, 22:pp.361–381.

Boning, C., Holland, W., Bryan, F., Danabasoglu, G., and McWilliams, J. (1995). An overlooked problem in model simulations of the thermohaline circulation and heat transport in the atlantic ocean. *Journal of Climate*, 8:pp. 515–523.

Bryan, F., Smith, R., Maldtrud, M., and Hecht, M. (1998). Modelling the north atlantic circulation: from eddy-permitting to eddy-resolving. *WOCE Conference, Halifax*, page poster.

Bryan, K. (1969). A numerical method for the study of the circulation of the world ocean. *Journal of Computational Physics*, 4:pp.347–376.

Bryan, K., Manabe, S., and Pacanowski, R. (1975). A global ocean–atmosphere climate model. part ii. the oceanic Circulation. *Journal of Physical Oceanography*, 5:pp.30–46.

Bryden, H. and Heath, R. (1985). Energetic eddies at the northern edge of the Antarctic Circumpolar Current in the Southwest Pacific. *Progress in Oceanography*, 14:pp.65–87.

Clarke, A. (1982). The dynamics of large scale, wind driven variations in the Antarctic Circumpolar Current. *Journal of Physical Oceanography*, 12:pp.1092–1105.

Cox, M. (1984). A primitive equation, 3-dimensional model of the ocean. *NOAA, GFDL Ocean Group Technical Report n1.*

Cunningham, S. (2001). Net transport and variability of the Antarctic Circumpolar Current through Drake Passage: A review of the international Southern Ocean studies. *Submitted to WOCE Newsletter.*

Danabasoglu, G. and McWilliams, J. (1995). Sensitivity of the Global Ocean Circulation to parameterizations of mesoscale tracer transports. *Journal of Climate*, 8:pp.2967–2987.

Danabasoglu, G., McWilliams, J., and Gent, P. (1994). The role of mesoscale tracer transport in the global ocean circulation. *Science*, 264:pp. 1123–1126.

Donohue, K., Hufford, G., and McCartney, M. (1999). Sources and transport of deep western boundary current east of the Kerguelen Plateau. *Geophysical Research Letters*, 26 n7:pp.851–854.

Dukowicz, J. and Smith, R. (1994). Implicit free-surface method for the Bryan-Cox-Semtener ocean model. *Journal of Geophysical Research*, 99 C4:pp.7991–8014.

England, M. (1995). Using chlorpfluorocarbons to assess ocean climate models. *Geophysical Research Letters*, 22:pp. 3051–3054.

England, M. and Rahmstorf, S. (1999). Sensitivity of ventilation rates and radiocarbon uptake to subgrid-scale mixing in ocean models. *Journal of Physical Oceanography*, 29:pp. 2802–2827.

FRAM-Group (1991). An eddy-resolving model of the Southern Ocean. *EOS*, 72(15):pp.169–175.

Gent, P., Large, W., and Bryan, F. (2001). What sets the mean transport through Drake Passage? *Journal of Geophysical Research*, 106 C2:pp.2683–2712.

Gent P.R. and McWilliams J.C. (1990). Isopycnal mixing in Ocean Circulation models. *Journal of Physical Oceanography*, 20:pp.150–155.

Gill, A. (1968). A linear model of the Antarctic Circumpolar Current. *Journal of Fluid Mechanics*, 32:pp.465–488.

Gill, A. and Bryan, K. (1971). Effects of geometry on the circulation of a three-dimensional Southern-Hemisphere ocean model. *Deep-Sea Research*, 18(pp.685–721).

Gille, S., Stevens, D., Tokmakian, R., and Heywood, K. (2001). Antarctic Circumpolar Response to zonally averaged winds. *Journal of Geophysical Research*, 106 C2:pp.2743–2759.

Glowienka-Hense, R., Hense, A., and Volker, C. (1992). ECMWF versus Hellermann and Rosenstein stress climatology of the Southern Ocean. *Antarctic Science*, 4(1):pp 111–117.

Gnanadesikan, A. and Hallberg, R. (2000). On the relationship of the Circumpolar Current to Southern Hemisphere winds in coarse-resolution ocean models. *Journal of Physical Oceanography*, 30:pp.2013–2034.

Godfrey, J. (1989). A Sverdrup model of the depth-integrated flow for the world ocean allowing for island circulations. *Geophysics and Astrophysics Fluid Dynamics*, 45:pp.89–112.

Gordon, A., Molinelli, E., and Baker, T. (1978). Large scale relative dynamic topography of Southern Ocean. *Journal of Geophysical Research*, 83 C6:pp.3023–3032.

Grezio, A., Wells, N., Ivchenko, V., and de Cuevas, B. (2001). The dynamical controls on the antarctic circumpolar current. *Journal of Marine Research*, submitted.

Griffies, S. M. (1998). The gent and mcwilliams skew flux. *Journal of Physical Oceanography*, 28:pp.831–841.

Grose, T., Johnson, J., and Bigg, G. (1995). A comparison between the FRAM (Fine Resolution Antarctic Model) results and observations in the Drake Passage. *Deep-Sea Research*, 42:pp.365–388.

Hallberg, R. and Gnanadesikan, A. (2001). An exploration of the role of transient eddies in determining the transport of a zonally reetrant current. *Journal of Physical Oceanography*, 31:pp.3312–3330.

Hellerman, S. and Rosenstein, M. (1983). Normal monthly wind stress over the world ocean with error estimates. *Journal of Physical Oceanography*, 13:pp.1093–1104.

Hidaka, K. and Tsuchiya, M. (1953). On the Antarctic Circumpolar Current. *Journal of Marine Research*, 12:pp.214–222.

Hughes, C. (1997). On the obscurantist physics of form drag in theorizing about the Circumpolar Current: Comments. *Journal of Physical Oceanography*, 27:pp.210–211.

Hughes, C. (2002). Sverdrup-like theories of the Antarctic Circumpolar Current. *Journal of Marine Research*, 60:pp.1–17.

Hughes, C. and Ash, E. (2001). Eddy forcing of the mean flow in the Southern Ocean. *Journal of Geophysical Research*, 106 C2:pp.2713–2722.

Hughes, C., Meredith, M., and Heywood, K. (1999). Wind driven transport fluctuations through drake passage: a southern mode. *Journal of Physical Oceanography*, 29:pp.1971–1992.

Ivchenko, V., Krupitsky, A., Kamenkovich, V., and Wells, N. (1999). Modeling the Antarctic Circumpolar Current: A comparison of FRAM and Equivalent Barotropic model results. *Journal of Marine Research*, 57:pp.29–45.

Ivchenko, V., Richards, K., and Stevens, D. (1996). The dynamics of the Antarctic Circumpolar Current. *Journal of Physical Oceanography*, 26:pp.753–774.

Ivchenko, V., Treguier, A., and Best, S. (1997). A kinetic energy budget and internal instabilities in the Fine-Resolution Antarctic Model. *Journal of Physical Oceanography*, 27:pp.5–27.

Johnson, J. and Bryden, H. (1989). On the size of the Antarctic Circumpolar Current. *Deep-Sea Research*, 36:pp.39–53.

Killworth, P. (1992). An Equivalent-barotropic mode in the Fine-Resolution Antarctic Model. *Journal of Physical Oceanography*, 22:pp.1379–1387.

Killworth, P. (1996). The interpolation of forcing fields in ocean models. *Journal of Physical Oceanography*, 21:pp.136–143.

Killworth, P. and Nanneh, N. (1994). Isopycnal momentum budget of the Antarctic Circumpolar Current in the Fine Resolution Antarctic Model. *Journal of Physical Oceanography*, 24:pp.1201–1223.

Klinck, J. (1986). Vorticity dynamics of seasonal variations of the Antarctic Circumpolar Current from a modelling study. *Journal of Physical Oceanography*, 21:pp.1515–1533.

Krupitsky, A. and Cane, M. (1994). On topographic pressure drag in a zonal channel. *Journal of Marine Research*, 52:pp.1–23.

Levitus, S. (1982). Climatological atlas of the world oceans. *NOAA professiona Paper, US Governament Printing Office, Washington*, pages pp 1–173.

Levitus, S., Burgett, R., and Boyer, T. (1994). World ocean atlas 1994. *NOAA Atlas NESDIS*.

Maltrud, M., Smith, R., Semtner, A., and Malone, R. (1998). Global eddy-resolving ocean simulations driven by 1985–1995 atmosferic winds. *Journal of Geophysical Research*, 103 C13:pp.30825–30853.

Marshall, D. (1995). Influence of topography on the large scale circulation. *Journal of Physical Oceanography*, 25:pp.1622–1635.

Marshall, J., Olbers, D., Ross, H., and Wolf-Gladrow, D. (1993). Potential vorticity constraints on the dynamics and hydrography of the Southern Ocean. *Journal of Physical Oceanography*, 23:pp.465–487.

McWilliams, J. and Chow, J. (1981). Equilibrium geostrophic turbulence i: A reference solution in a β -plane channel. *Journal of Physical Oceanography*, 11:pp.921–949.

McWilliams, J., Holland, W., and Chow, J. (1978). A descriptionm of numerical Antarctic Circumpolar Currents. *Dynamics of Atmospheres and Oceans*, 2:pp.213–291.

Morrow, R., Church, J., Coleman, R., Chelton, D., and White, N. (1992). Eddy momentum flux and its contribution to the Southern Ocean momentum balance. *Nature*, 357:pp.482–484.

Munk, W. (1950). On the wind-driven ocean circulation. *Journal of Meteorology*, 7:pp.79–93.

Munk, W. and Palmén, E. (1951). Note on the dynamics of the Antarctic Circumpolar Current. *Tellus*, 3:pp.55–53.

Olbers, D. (1998). On the obscurantist physics of form drag in theorizing about the Circumpolar Current: Comments. *Journal of Physical Oceanography*, 28:pp.1647–1654.

Olbers, D. and Wubber, C. (1991). *The role of wind and buoyancy forcing of the Antarctic Circumpolar Current.* Strategies for future cimate research Ed. M. Latif Max-Planck Institute fur Meteorologie, Hamburg,Germany.

Pacanowski, R. and Philander, S. (1981). Parameterization of vertical mixing in numerical models of Tropical Oceans. *Journal of Physical Oceanography*, 11:pp.1443–1451.

Patterson, S. (1985). Surface Circulation and kinetic energy distributions in the Southern hemisphere oceans from fgge drifting buoys. *Journal of Physical Oceanography*, 15:pp. 865–884.

Reid, J. (1986). *On the total geostrophic circulation of the South Pacific Ocean: Flow Patterns, Tracers and Transports*, volume 16. Prog. Oceanog. Pergamon Press Ltd.

Semtner, A. (1974). *An oceanic general circulation model with bottom topography.* Numerical simulation of Weather ad Climate, Tech. Rep. vol. 50, University of California, Los Angeles.

Semtner, A. and Chervin, R. (1988). A simulation of the global ocean circulation with resolved eddies. *Journal of Geophysical Research*, 93 C12:pp.15502–15522.

Semtner, A. and Chervin, R. (1992). Ocean general Circulation from a global eddy-resolving model. *Journal of Geophysical Research*, 97 C12:pp.15502–15522.

Siefridt, L. and Barnier, B. (1993). Banque de donnees aviso vent/flux: climatologie des analyses de surface du cepmmt. *Report*, 91:pp. 1–43.

Smith, R., Dukowicz, J., and Malone, R. (1992). Parallel ocean general circulation modelling. *Physica D*, 60:pp.30–61.

Smith, R., Dukowicz, J., and Malone, R. (1993). A reformulation and implementation of the Bryan-Cox-Semtner ocean model on the connection machine. *Journal of Atmospheric and Oceanic Technology*, 10:pp.196–208.

Sorensen, J., Ribbe, J., and Shaffer, G. (2001). Antarctic intermediate water mass formation in ocean general circulation models. *Journal of Physical Oceanography*, 31:pp.3295–3311.

Stevens, D. (1990). On open boundary conditions for three dimensional primitive equation ocean circulation models. *Geophysics And Astrophysics Fluid Dynamics*, 51:pp.103–133.

Stevens, D. (1991). The open boundary condition in the United Kingdom Fine-Resolution Antarctic Model. *jpo*, 21:pp.1494–1499.

Stevens, D. and Ivchenko, V. (1997). The zonal momentum balance in an eddy-resolving general-circulation model of the Southern Ocean. *Quarterly Journal Meteorological Society*, 123:929–951.

Stevens, D. and Killworth, P. (1992). The distribution of kinetic energy in the Southern Ocean: A comparison between observations and an eddy resolving general circulation model. *Philosophical Transactions of the Royal Society of London, B*, 338:pp.251–257.

Stevens, I. and Stevens, D. (1999). Passive tracers in a general circulation models of the Southern Ocean. *Annales Geophysicae*, 17:pp.971–982.

Stommel, H. (1957). A survey of ocean current theory. *Deep-Sea Research*, 4:pp.149–184.

Taylor, H. (1978). Some large-scale aspects of the southern ocean and its enviroment. *Ph.D thesis, Columbia University, New York.*

Thompson, S. (1995). Sills of the global ocean: a compilation. *Ocean Modelling*, 109:pp. 7–9.

Treguier, A. and McWilliams, J. (1990). Topographic influences on wind-driven, stratified flow in a β -plane channel: An idealized model for the Antarctic Circumpolar Current. *Journal of Physical Oceanography*, 20:pp.321–343.

Wang, L. and Huang, R. (1995). A linear homogeneous model of wind driven circulation in a β -plane channel. *Journal of Physical Oceanography*, 25:pp.587–603.

Warren, B., LaCasce, J., and Robbins, P. (1996). On the obscurantist physics of form drag in theorizing about the Circumpolar Current. *Journal of Physical Oceanography*, 26:pp.2297–2301.

Warren, B., LaCasce, J., and Robbins, P. (1997). On the obscurantist physics of form drag in theorizing about the Circumpolar Current: Reply. *Journal of Physical Oceanography*, 27:pp.211–212.

Warren, B., LaCasce, J., and Robbins, P. (1998). On the obscurantist physics of form drag in theorizing about the Circumpolar Current: Reply. *Journal of Physical Oceanography*, 28:pp.1655–1658.

Wearn, R. and Baker, D. (1980). Bottom pressure measurements across the antarctic circumpolar current and their relation to the wind. *Deep-Sea Research*, 27A:pp.875–888.

Webb, D. (1993). A simple model of the effect of the kerguelan plateau on the strength of the Antarctic Circumpolar Current. *Geophys. Astrophys. Fluid Dynamics*, 70:pp.57–84.

Webb, D., Coward, A., de Cuevas, B., and Gwilliam, C. (1997). A multiprocessor ocean general Circulation model using message passing. *Journal of Atmospheric and Oceanic Technology*, 14:pp.175–183.

Wells, N. and de Cuevas, B. (1995). Depth-integrated vorticity budget of the Southern Ocean from a general circulation model. *Journal of Physical Oceanography*, 25:pp.2569–2582.

Whitworth, T. (1980). Zonation and geostrophic flow of the Antarctic Circumpolar Current at the Drake Passage. *Deep-Sea Research*, 27:pp.497–507.

Whitworth, T. (1983). Monitoring the transport of the Antarctic Circumpolar Current at the Drake Passage. *Journal of Physical Oceanography*, 13:pp.2045–2057.

Whitworth, T. and Peterson, R. (1985). Volume transport of the Antarctic Circumpolar Current from bottom pressure measurements. *Journal of Physical Oceanography*, 15:pp.810–816.

Wolff, J., Ivchenko, V., Klepikov, A., and Olbers, D. (1992). The effect of bottom topography on the dynamics of zonal flows in the ocean. *Scripta Technica*, pages pp. 323–326.

Wolff, J., Maier-Reimer, E., and Olbers, D. (1991). Wind driven flow over topography in a zonal β -plane channel: A quasi-geostrophic model of the Antarctic Circumpolar Current. *Journal of Physical Oceanography*, 21:pp.236–264.

Wolff, J. and Olbers, D. (1989). *The Dynamical Balance Of The Antarctic Circumpolar Current Studied with an Eddy Resolving Quasi-Geostrophic Model.* Ed. Mesoscale/Synoptic Coherent Structures In Geostrophical Turbulence, vol. 50, Nihoul And Jamart.